ULTRASOUND CAVITATION EROSION OF LIMESCALE ON METAL SURFACES

Boštjan Pečnik

Doctoral Dissertation
Jožef Stefan International Postgraduate School
Ljubljana, Slovenia

Supervisor: Prof. Dr. Branko Širok, University of Ljubljana, Faculty of Mechanical Engineering, Aškerčeva 6, 1000 Ljubljana, Slovenia
Co-Supervisor: Assoc. Prof. Dr. Marko Hočevar, University of Ljubljana, Faculty of Mechanical Engineering, Aškerčeva 6, 1000 Ljubljana, Slovenia

Evaluation Board:
Prof. Dr. Milena Horvat, Chair, Jožef Stefan International Postgraduate School and Jožef Stefan Institute, Jamova 39, 1000 Ljubljana, Slovenia
Prof. Dr. Ester Heath, Member, Jožef Stefan International Postgraduate School and Jožef Stefan Institute, Jamova 39, 1000 Ljubljana, Slovenia
Prof. Dr. Matjaž Hriberšek, Member, University of Maribor, Faculty of Mechanical Engineering, Smetanova ulica 17, 2000 Maribor, Slovenia

MEDNARODNA PODIPLOMSKA ŠOLA JOŽEFA STEFANA
JOŽEF STEFAN INTERNATIONAL POSTGRADUATE SCHOOL



Boštjan Pečnik

ULTRASOUND CAVITATION EROSION OF LIMESCALE ON METAL SURFACES

Doctoral Dissertation

ULTRAZVOČNA KAVITACIJSKA EROZIJA VODNEGA KAMNA NA KOVINSKIH POVRŠINAH

Doktorska disertacija

Supervisor: Prof. Dr. Branko Širok

Co-Supervisor: Assoc. Prof. Dr. Marko Hočevar

Ljubljana, Slovenia, August 2016

Acknowledgments

First of all, I would like to sincerely thank my supervisor Professor Brane Širok. Apart from being my supervisor, he was my main motivator and advisor, and as such the key person in my completion of this thesis.

I would also like to thank my co-supervisor Professor Marko Hočevar, especially for his contribution in planning and conducting the experimental part of my studies.

Besides, I would also like to thank Dr. Benjamin Bizjan, Professor Matevž Dular and Aleš Malneršič from the Laboratory for water and turbine machines (LVTS) at the Faculty of mechanical engineering in Ljubljana.

I am especially grateful to Professor Aleksandra Kornhauser, who eagerly followed my study process and was able to encourage, direct and motivate me in the most critical moments.

I would also like to thank my company, Gorenje d.d., which financially supported my studies. A number of my coworkers offered to assist me in preparation and conduction of experiments, for which I am very thankful.

At last, I want to thank my partner Irena for help and advice during my studies, and for the double role she made in our large family.

Abstract

The build-up of $CaCO_3$ (lime) scale is an operational problem which affects a range of industrial processes including membrane filtration (desalination), drilling and especially those that involve heat transfer. In heat exchangers the effects are twofold: firstly, even a thin scale coating can significantly reduce heat transfer efficiency and secondly, by acting as an insulator, it may cause heating elements to internally overheat, leading to component failure. Consequently, this leads to increased operating and maintenance costs, as well as a larger negative impact on the environment.

Currently, the most effective method of scaling prevention is by using different chemicals. However, such chemicals are costly and can cause a negative environmental impact. Ultrasonic cavitation is one of the possible alternative approaches. It is a hydrodynamic process of rapid formation, oscillation, growth and collapse of cavitation bubbles as a result of excitation of the liquid by ultrasonic acoustic waves. In this thesis, we have further examined the effect of cavitation on limescale coated surfaces.

Experimental measurements of ultrasonically induced cavitation below the sonotrode were carried out in a transparent chamber filled with distilled water. Using the high-speed imaging data, pressure fluctuations were calculated by a computer-aided algorithm based on the Brennen's theory of cavitation cloud kinematics and a modified version of the Rayleigh-Plesset equation. Reference measurements of the pressure pulsations were conducted by a hydrophone installed at the bottom of the chamber. The analysis of cavitation structure dynamics was complemented by calculation of velocity fields from the imaging data. The results indicate a strong correlation between the fields of velocity and pressure fluctuations during the growth and collapse of cavitation structures. A comparison of pressure time series and power spectra demonstrates that our cavitation analysis method is in a good agreement with results of reference measurement methods. This way, an experimental tool was formed for prediction of pressure fluctuations in the region near the limescale deposit, with possible applications to other engineering problems.

By developing an experimental method for monitoring of cavitation phenomena, we were able to study the mechanism of scale deposit destruction on exposed metallic surfaces. For the purpose of our study, specimens were prepared in form of round-shaped steel substrates with different surface roughness, to which limescale was deposited under controlled conditions. Scale deposition was performed on a specially designed experimental set-up under operating conditions which resembled those in real industrial appliances prone to scale build-up. In the second phase of the experiment, the specimens were exposed to ultrasonic cavitation, induced by oscillations of an ultrasonic probe (sonotrode). The sonotrode, which resonated at a constant frequency, was operated at different power levels – excitation amplitudes. The progress of scale erosion was monitored by macro photography of specimens and by measurement of pressure fluctuations in the near field. During the phase of experimental data postprocessing, phenomenological relations between the sonotrode excitation power and pressure pulsation intensity in the region near the deposited scale layer were investigated, and a strong correlation between these two parameters was determined. A correct sample preparation and knowledge of the local pressure pulsations near the specimen surface meant the conditions were met for conduction of the experiment, which resulted in an assessment of scale deposit cavitation erosion.

The results have shown the intensity of cavitation erosion to be proportional to the sonotrode voltage, and consequently to the intensity of pressure fluctuations. The cavitation erosion also depends on the surface roughness of steel substrate surfaces, to which the scale was deposited. By performing an additional experiment, it was found that the descaling process can be intensified by reducing the substrate surface roughness. The scale destruction mechanism was found to largely depend on the microstructure of the scale

deposit, as local inhomogeneities may intensify the erosion rate by affecting the scale adhesion on the micro and macro scale. The overall durability of limescale deposits depends on the scale surface hardness, the presence of local inhomogeneities in scale microstructure, and the substrate surface finish. These factors determine the mechanism of scale removal, which can occur either as layer by layer erosion, or by breakage of larger areas. A typical parameter to describe the topography of partly and fully eroded scale deposits is the edge length-to-area ratio of descaled surfaces. In all of the observed cases, this ratio decreases with cavitation time, leading to a gradual reduction in descaling efficiency.

The above-mentioned research results have been published in four papers in scientific journals with a good impact factor. Since the doctoral thesis has dealt with limescale accumulation and removal, which is a relevant and significant industrial problem, a wide range of industries may benefit from the new knowledge about this process. For the same reason, there is also a strong incentive to continue with the research work, especially in the field of scaling prevention methods.

Povzetek

Nabiranje kalcijevega karbonata ($CaCO_3$) v obliki vodnega kamna je operativni problem, ki vpliva na vrsto industrijskih procesov, kot so membranska filtracija (razsoljevanje), vrtanje in še zlasti na tiste, ki vključujejo prenos toplote. Pri prenosnikih toplote sta prisotna dva učinka: prvi, kjer je že pri majhnih debelinah oblog vodnega kamna značilno zmanjšan prenos toplote in drugi, kjer deluje vodni kamen kot toplotni izolator, ki povzroča pregrevanje grelnih elementov in posledično njihove okvare. Posledice navedenih značilnosti so višji obratovalni in vzdrževalni stroški ter povečano obremenjevanje okolja.

Trenutno je najbolj učinkovit način za preprečevanje oblog uporaba različnih kemikalij, ki pa so pogosto drage in imajo vprašljiv vpliv na okolje. Ultrazvočna kavitacija je ena od alternativnih metod, pri kateri gre za hidrodinamski proces tlačnega oscilirajočega formiranja kavitacijskih struktur, sestavljenih iz rasti in kolapsov kavitacijskih mehurčkov kot posledice vzbujanja kapljevine z ultrazvočnimi akustičnimi valovi. Pri našem delu smo podrobneje proučevali vpliv kavitacije na z vodnim kamnom prevlečene površine.

Eksperimentalne meritve ultrazvočno generirane kavitacije pod ultrazvočno sondo smo izvedli v prosojni posodi, napolnjeni z destilirano vodo. Na osnovi slik, posnetih s hitro kamero, smo tlačne pulzacije izračunali z računalniško podprtimi algoritmi, temelječimi na Brennenovi teoriji kinematike kavitacijskega oblaka kot modificirani verziji Rayleigh-Plessetove enačbe. Referenčne meritve tlačnih pulzacij so bile izmerjene s hidrofonom, nameščenim na dnu posode. Analizo dinamike kavitacijskih struktur pa smo dopolnili z izračunom hitrostnih polj na osnovi slikovnih podatkov. Rezultati kažejo na močno povezavo med hitrostnim poljem in tlačnimi pulzacijami v času rasti in kolapsa kavitacijskih struktur. Primerjava tlačnih časovnih vrst in močnostnih spektrov dokazuje, da se naša metoda analize kavitacije dobro ujema z rezultati referenčnih merilnih metod. Na ta način smo oblikovali eksperimentalno orodje za napoved tlačnih fluktuacij v področju nanesenega vodnega kamna, ki pa se lahko aplicira tudi na drugačne inženirske probleme.

S tem, ko smo razvili eksperimentalno metodo za spremljanje kavitacijskih pojavov, je bila odprta pot študiji mehanizma destrukcije vodnega kamna, naloženega na izpostavljenih kovinskih površinah. Za namen študije smo pripravili vzorce za nanos vodnega kamna, ki so bili v obliki okroglih jeklenih ploščic različnih hrapavosti in na katere je bil pod kontroliranimi pogoji nanesen vodni kamen. Nanos vodnega kamna je bil izveden na posebej za ta namen izdelani eksperimentalni postaji v pogojih, ki so bili podobni realnim obratovalnim pogojem naprav, v katerih se nalaga vodni kamen. V drugi fazi eksperimenta so bili vzorci izpostavljeni ultrazvočni kavitaciji, povzročeni z nihanjem ultrazvočne sonde (sonotrode). Sonotroda, ki je resonirala pri konstantni frekvenci, je obratovala pri različnih močeh - amplitudah vzbujanja. Potek erozije smo spremljali z makro fotografiranjem vzorcev in z merjenjem tlačnih pulzacij v bližini vzorcev. V fazi obdelave pridobljenih eksperimentalnih podatkov so bile preučevane fenomenološke relacije med močjo vzbujanja sonotrode in intenzivnostjo tlačnih pulzacij v področju površine nanesenega vodnega kamna, pri čemer je bila ugotovljena močna korelacija med navedenima parametroma. Ob korektni pripravi vzorcev in poznavanju lokalnih tlačnih pulzacij ob površini vzorcev so bili izpolnjeni pogoji za izvedbo eksperimenta, ki je pripeljal do ocene kavitacijske erozije na površini nanosa vodnega kamna.

Rezultati so pokazali, da je intenzivnost kavitacijske erozije proporcionalna napetosti na sonotrodi, odnosno intenzivnosti tlačnih pulzacij, in je obenem odvisna od hrapavosti površine kovinskih ploščic - vzorcev, na katere je bil nanesen vodni kamen. Z dodatnim eksperimentom smo ugotovili, da se lahko odstranjevanje vodnega kamna intenzivira z zmanjšanjem hrapavosti kovinske površine. Mehanizem destrukcije vodnega kamna na vzorcih je v veliki meri odvisen od mikrostrukture nanesene obloge, saj lahko lokalne nehomogenosti intenzivirajo stopnjo erozije v odvisnosti od oprijema vodnega kamna na mikro ali makro nivoju. Obstojnost obloge vodnega kamna je odvisna od trdote njene

površine, prisotnosti lokalnih nehomogenosti v mikrostrukturi in površinske obdelave vzorca. Glede na te dejavnike je lahko obloga erodirana sloj za slojem, ali pa pride do odkrušenja večjih področij. Značilno za topografijo meje med erodirano in še ne popolnoma odstranjeno površino vodnega kamna je razmerje med dolžino roba erodirane površine in njeno površino. To razmerje se v vseh opazovanih primerih s časom delovanja kavitacije zmanjšuje, kar navaja na postopno zmanjševanje učinkovitosti odstranjevanja.

Zgoraj omenjeni raziskovalni rezultati so bili objavljeni v štirih člankih v revijah z visokim faktorjem vpliva. Ker se doktorska naloga ukvarja z nalaganjem in odstranjevanjem vodnega kamna – realnim industrijskim problemom, obstaja veliko različnih industrijskih panog, ki bi jim nova znanja lahko koristila. Isti razlog pomeni tudi močno spodbudo za nadaljnje raziskovalno delo, še posebej na področju metod za preprečevanje nastanka vodnega kamna.

Contents

Acknowledgments vii

Abstract ix

Povzetek xi

Contents xiii

List of Figures xv

1 Introduction 1
1.1 Description of the Problem 1
1.2 Purpose and Goals of the Dissertation 1
1.3 Organization of the Experimental Work 2

2 The Use of the Cavitation Effect in the Mitigation of $CaCO_3$ Deposits 5

3 Non-Contact Method for Analysis of Cavitating Flows 19

4 Cavitation Erosion of the Calcium Carbonate Deposits 35

5 Scale Deposit Removal by Means of Ultrasonic Cavitation 55

6 Conclusions 65
6.1 Future Perspectives 65

References 67

Bibliography 69
Publications Related to the Thesis 69
Journal Articles 69
Conference Paper 69

Biography 71

List of Figures

Figure 1: Flow chart describing the arrangement of the chapters.....4
Figure 2**:** Scanning electron micrographs of $CaCO_3$ scale deposits showing the characteristic a) calcite and b) aragonite. Adapted from (Andritsos et al., 1997).....5
Figure 3**:** A generalised view of bubble dynamics in an ultrasonic field.....5
Figure 4**:** Pressure fluctuations spectra for 40% sonicator power level.....19
Figure 5: Specimen 7 with deposited scale (a) before cavitation and (b) after cavitation (π=0,547(-), ε=0,238(-)).....35
Figure 6: Model of cavitation cloud dynamics and different basic material (Ra for metal and Ra* for enamel).....35
Figure 7: Specimen macro photos. Horizontal axis: specimens No. 1-14, vertical axis: time from the start of cavitation.....55
Figure 8: Multiple regression model for λ.....56

1 Introduction

1.1 Description of the Problem

The build-up of calcium carbonate ($CaCO_3$) scale (also known as limescale) on surfaces of functional assemblies is a major operational problem which affects a range of industrial processes including membrane filtration (desalination), drilling and especially those that involve heat transfer. In heat exchangers the effects are twofold: firstly, even a thin scale coating can significantly reduce heat transfer efficiency and secondly, by acting as an insulator, it may cause heating elements to internally overheat, leading to component failure. Scale can also drastically reduce flow in pipes. Heating elements of household appliances exposed to hard water (e.g. boilers, washing machines and solar collectors) are prone to scale build-up when water is heated, thus suffering from reduced operating efficiency. Consequently, this leads to increased operating and maintenance costs, as well as a larger negative impact on the environment.

According to the literature, the most efficient method to prevent scaling is by using chemical inhibitors or descalers. However, such chemicals have a questionable environmental impact. Ultrasonic cavitation is one of the possible alternatives, but its scaling prevention and removal mechanism is still not very well understood. Major open questions are linked to cavitation erosion as a mechanism of scale removal, as well as generation of pressure pulses which are the cause of the erosion. Even more unclear is the possible field of application of cavitation erosion in concrete technical applications. For these reasons, our thesis will be focused on research of cavitation erosion and its useful applications to the process of limescale removal.

1.2 Purpose and Goals of the Dissertation

The purpose of this thesis was to study the effect of cavitation on surfaces coated by limescale deposits. In vicinity of hard surfaces, cavitation causes local pressure impulses, which are a consequence of cavitation cloud collapses. Due to pressure pulsations, tension occurs in the solid scale layer structure, locally exceeding the strength of the scale crystalline structure. This condition can be referred to as destruction (crushing) of the material, namely cavitation erosion. Erosion intensity depends on cavitation process characteristics as well as the structure and mechanical properties of the material deposited on a solid wall. A proper understanding of the limescale cavitation erosion for various types of metallic substrates and scale crystalline structure allows for a proper selection of materials, to which the scale is deposited, and their surface treatment. Also, this way the knowledge about the cavitation mechanism is improved, so that recommendations can be made to improve the cavitation efficiency.

Based on the results of the study, phenomenological models of cavitation erosion can be formed, linking the cavitation intensity to the erosion effects on scaled surfaces. Also, it is important to note that the expansion of existing cavitation erosion models to mineral structures of calcium carbonate present a great challenge, as the constitutional relations of the force impulse transfer from the pressure field of the cavitation collapse to the solid scale structure are practically unknown. Experimental methods planned for application in this thesis will enable to research the influence of cavitation collapses of known intensity to the destruction of solid surfaces, which will be evaluated by topological parameters of the eroded surface. Having that said, the main purpose of this thesis – to research the cavitation erosion mechanism on the limescale surface – can be expanded to practical application of scale removal from the surfaces of heating elements, which presents the engineering challenge of the thesis.

The goals of the doctoral thesis have been as follows:

- Development of an experimental method for generation of controlled cavitation, which contains formation of a group of embryonic bubbles – a cavitation cloud,

controlled cavitation cloud dynamics, cloud collapse and the monitoring thereof in the final phase above the metallic wall, to which the limescale layer is adhered. The developed method will allow prediction of pressure pulsations depending on the cloud cavitation dynamics, which is observed by a visualization method. Model results are compared to simultaneously measured pressure pulsations on the metallic substrate surface, which was formed identically to the surfaces, to which the scale is to be deposited in the later part of this thesis. In the following part of the thesis, the model results are used as values, which predict the intensity of pressure pulsations.

- Determination of the effect of cavitation bubble collapse near the metallic wall on formation of cavitation damage in form of broken-off limescale surfaces, the topological structure of which is a consequence of cavitation collapses.
- On a macro scale, under conditions of ultrasonically induced cavitation, our study is focused on development of a multiple regression model linking the ultrasonic excitation parameters to the cavitation erosion parameters. In this step, the relation between cavitation cloud collapses and corresponding pressure fluctuations and cavitation erosion is investigated on the model including both the time and length scale.

Limescale removal by cavitation is based on mechanical action of the fluid upon the solid surface. The scale deposited to the surface in form of attached coatings is fractured and detached from the metallic substrate. Cavitation bubble collapse near the surface causes the formation of locally isolated damage on the scale deposit. The damage occurs in form of local material destruction such as individual cavities and cracks, which develop into larger damage structures in form of caverns with complex topologies. The cavitation erosion descaling process is complex and has not yet been properly investigated on surfaces, coated with limescale. It depends on the scale structure, its adhesion to the metallic substrate, as well as on the cloud cavitation dynamics in the collapse phase, and consequently on the propagation of pressure waves, which are the cause of solid surface destruction.

Based upon the stated purpose and goals, a hypothesis of our doctoral thesis can be formulated:

"Cavitation erosion as a consequence of cavitation cloud collapses and subsequently generated pressure waves near solid walls causes mechanical loads, which result in destruction of the solid wall structure – in the case of this thesis, the thin limescale layer adhered to a flat metallic surface.

The intensity of the limescale erosion depends on: the parameters of the limescale deposit to a metallic surface, metallic surface properties and the parameters of the cavitation generation process on the macro and micro scale."

1.3 Organization of the Experimental Work

The methodology of the research work has been divided into five main segments:

1) Overview of relevant achievements.
   In the field of limescale formation and cleaning the scale formation mechanisms and known existing descaling methodologies were reviewed. In this segment, we have reviewed the literature for the basic properties of limescale, the conditions for formation of different crystalline structures and the mechanism for scale layer deposition on a solid surface. Also reviewed has been the literature in the field of cavitation erosion, with a special emphasis of researching the known solid surface destruction mechanisms by means of cavitation cloud implosions. Based upon the review of the current state of the art the basic guidelines for preparation of this doctoral thesis were formed.

2) Specimen preparation.

In preparation of specimen substrates – steel sheet metal, special attention was dedicated to the surface treatment of specimens. The materials selected for this purpose are commonly used in manufacturing of heat transfers of heating bodies in household appliances. The specimens were processed by different methods of surface treatment, including cutting, grinding, brushing and enameling. Parameters varied in this process were the surface roughness R_a and specimen texture. In production of specimens, a special attention was given to repeatability of integral parameters. The size and shape of specimens were chosen so that homogeneous conditions for scale deposition were attained, and that cavitation erosion could later be applied.

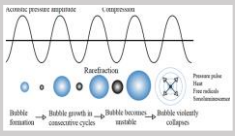
3) Construction of measurement set-ups.
The measurement set-up for limescale deposition on metallic specimens allowed maintaining the conditions, under which a growth of the scale layer can occur continuously on the surfaces of heating elements. A part of the measurement set-up was intended for preparation of water and maintaining its chemical properties constant. It was possible to change specimens, vary the water flow through the chamber with the water bath for specimens, and maintain the desired water bath temperature.

The measurement set-up for the ultrasound cavitation of specimens allowed varying the power of pressure fluctuations and thus cavitation intensity. The chamber with a built-in sonotrode, and the system for the mounting of individual specimens assured that the pressure cavitation field above the specimen was axissymmetric and homogeneous as much as possible. During the experiments, a special attention was given to maintaining the conditions for the mounting of specimens, in order to assure a good repeatability of the process. All of the relevant integral parameters were controlled: sonotrode oscillation intensity, bath temperature and sonotrode tip position relatively to the specimen. It was thus possible to make a comparison of erosion effects for different specimens.

4) Conduction of measurements.
The measurements were conducted as follows. In the first phase, limescale coatings were applied to all specimens using the measurement set-up for controlled scale deposition. This assured that the conditions for the scale layer formation were identical for all specimens. The second phase of the experiment was carried out in a cavitation vessel were sonotrode cavitation was performed on one specimen at a time and for selected integral conditions (sonotrode cavitation intensity and duration, water temperature). During the experiment, cavitation structures above the specimen mounted on the vessel's floor were visualized. Output data was in form of macro photographs of eroded specimens, and corresponding high-speed imaging sequences of cavitation cloud structures for selected integral experimental parameters.

5) Analysis of measurement results.
Cavitating fluid flow images recorded by a high-speed camera were analyzed by our computer-aided method (implemented in the software *ADMflow*). By using this method, velocity and pressure fields within the flow were calculated in order to analyze the dynamics of ultrasonic cavitation. On an integral level and on longer time scales, the analysis was carried out by postprocessing of macro photographs of scale-coated specimens, which were taken in selected time intervals during the erosion process. The rate and final efficiency of the scale removal process was calculated, in addition to the edge-to-length ratio of descaled surfaces as a parameter for geometric characterization of erosion. Based on these results, multiple regression models were formed to link the ultrasonic excitation parameters to the cavitation erosion parameters.

A schematic flow chart (Figure 1) shows the chapter structure of the doctoral thesis as well as provides their purpose and findings, which have been reported in published or under-review manuscripts as the results of studies performed for the purpose of this thesis.

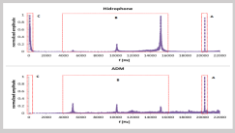


Chapter 2: "The Use of the Cavitation Effect in the Mitigation of $CaCO_3$ Deposits"

Heath, D., Širok, B., Hočevar, M., Pečnik, B.

Strojniški vestnik - Journal of Mechanical Engineering 59(2013)4, 203-215.

• Review of the literature on cavitation erosion of brittle crystalline materials

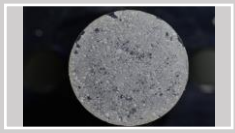


Chapter 3: "Non-contact Method for Analysis of Cavitating Flows"

Biluš, I., Lešnik, L., Bizjan, B., Širok, B., Dular, M., Pečnik, B.

Ultrasonics, 2016, under review

• Study of velocity fields and pressure fluctuations in phase of growth and collapse of cavitation structures

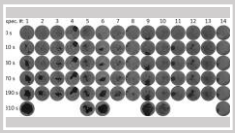


Chapter 4: "Cavitation erosion of the calcium carbonate deposits"

Pečnik, B., Šturm, R., Hočevar, M., Dular, M., Širok, B.

Int. J. Microstructure and Materials Properties, Vol. 10, Nos. 5/6, 2015

• Study of erosion effects caused by acoustic cavitation on metallic and enamelled specimens coated with calcium carbonate, simultaneously with the monitoring of cavitation the destruction of scale on the surface was analysed



Chapter 5: "Scale deposit removal by means of ultrasonic cavitation"

Pečnik, B., Hočevar, M., Širok, B., Bizjan, B.

Wear 356-357 (2016) 45-52

• Study of the mechanism of acoustic cavitation-generated erosion on metallic specimens coated with calcium carbonate (scale)

Figure 1: Flow chart describing the arrangement of the chapters.

2 The Use of the Cavitation Effect in the Mitigation of $CaCO_3$ Deposits

In this chapter, the paper entitled "The Use of the Cavitation Effect in the Mitigation of $CaCO_3$ Deposits" by David Heath, Brane Širok, Marko Hočevar and Boštjan Pečnik (Heath et al., 2013) is presented.

The purpose of this paper was to review the existing literature on cavitation erosion of brittle crystalline materials in an attempt to better understand the relationship between the material properties of calcium carbonate ($CaCO_3$) scale deposits and its removal mechanism by cavitation.

The literature study shows scale formation and cavitation erosion to be complex phenomena dependent on many factors. The study finds that from a material perspective cavitation erosion is closely linked to both material's bulk properties and its microstructure. The density, hardness and tenacity of the scale will depend on its depositional environment. In the case of $CaCO_3$, this will affect the material and surface properties of the resultant scale layer. Among the different mechanisms of cavitation, bubble cloud collapse and the splashing effect following jet formation are considered to be the most important. The type and structure of scale deposits formed will affect how it is removed by cavitation.

The graphical abstract of the paper is shown in Figures 2 and 3.

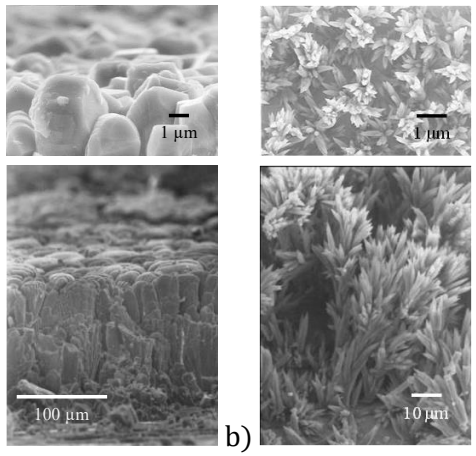


Figure 2: Scanning electron micrographs of $CaCO_3$ scale deposits showing the characteristic a) calcite and b) aragonite. Adapted from (Andritsos et al., 1997).

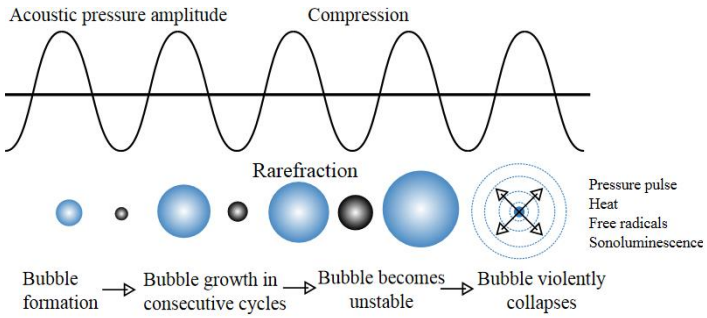


Figure 3: A generalised view of bubble dynamics in an ultrasonic field.

Strojniški vestnik - Journal of Mechanical Engineering 59(2013)4, 203-215
DOI:10.5545/sv-jme.2012.732
(1.02) Review Scientific Paper
Received for review: 2012-08-13
Received revised form: 2013-01-11
Accepted for publication: 2013-02-12
© 2013 Journal of Mechanical Engineering. All rights reserved.

The Use of the Cavitation Effect in the Mitigation of $CaCO_3$ Deposits

David Heath[1] – Brane Širok[2] – Marko Hočevar[2,*] – Boštjan Pečnik[1,3]
[1] MPŠ Jožef Stefan International Postgraduate School, Slovenia
[2] University of Ljubljana, Faculty of Mechanical Engineering, Slovenia
[3]Gorenje d.d., Slovenia

Hard mineral scale fouling results in significant economic losses both industrially and domestically. Recently, attempts have been made to use ultrasound to mitigate scale formation and its removal based on the phenomena of cavitation. Cavitation erosion is the removal of material from a solid surface by pressure shock waves associated with the formation and collapse of bubbles. This paper reviews the literature on cavitation erosion of brittle crystalline materials in an attempt to better understand the relationship between the material properties of $CaCO_3$ scale deposits and its potential removal by cavitation. The study finds that from a materials perspective cavitation erosion is intimately associated with both a material's bulk properties and importantly to its microstructure. The situation is further complicated because the macro and micro-properties of $CaCO_3$ scale are dependent on many factors relating to its depositional environment. The type of scale formed will affect how it is removed by cavitation.

Keywords: cavitation, cavitation erosion, ultrasound, scale, calcium carbonate

0 INTRODUCTION

The build-up of $CaCO_3$ (lime) scale is a major operational headache that affects a range of industrial processes including membrane filtration (desalination), drilling, and especially those that involve heat transfer. In a heat exchanger the effects are twofold: first, even a small coating of scale can significantly reduce heat transfer efficiency and second, by acting as an insulator, it will cause a heating element to get much hotter internally leading to component failure. Scale can also drastically reduce the flow in pipes. In the domestic setting, in areas affected by hard water, home appliances like boilers, washing machines, and solar collectors are prone to scale build-up and, just as in industry, it can reduce performance and working life. Additional consequences are increased service charges, frequent equipment replacement, and higher energy bills - up to 25% more [1]. The costs incurred in preventing and remedying scale both industrially and domestically are considerable. According to Müller-Steinhagen et al. [2], the total annual cost due to fouling for highly industrialized countries, such as the United States or the United Kingdom are about 0.25% of their Gross National Product (GNP). These figures may only be indicative, but they underline the significant impact that scale has on global energy efficiency [3]. The percentage of energy losses due to fouling is at least 2% globally. Another way of estimating the size of the problem is by looking at how much is spent on preventing scale. Scale inhibitors are the third largest product segment of the water treatment chemicals market (corrosion inhibitor market being the largest) and by 2016 will be worth an estimated $ 3.6 billion [4].

Scale management ideally is about the prevention of scale and currently the most efficient way to prevent scaling is by using chemical inhibitors or descalers. Chemicals, however, are costly and their environmental impact is questionable, which has led to the search for both cheaper and "greener" alternatives [5]. They include "natural" chemical agents, surface treatments including coatings, and magnetic and electronic conditioning, all of which show varying degrees of efficacy (Table 1). Once formed, the removal of a tenacious scale involves either chemical (acid) treatment to dissolve the scale or some form of mechanical removal [6]. The main benefit of using a mechanical method is that it avoids the use of chemicals, but where this has to be done by hand, it can be time consuming and costly. An alternative approach is the possible use of ultrasound. Ultrasonic cleaning is a well-established and efficient technology particularly for dislodging solid residues and removal of biological fouling. It is also the best-known application of acoustic cavitation. Cavitation is the phenomena of the rapid formation and implosion of bubbles in an area of low-pressure in liquids by means of mechanical forces [7] and [8].

The aim of this paper is to present a literature review in relation to existing studies involving ultrasonically induced cavitation for the mitigation and, importantly, the removal of tenacious $CaCO_3$ deposits. Fortunately, a large corpus of literature now exists on both scale formation and cavitation

*Corr. Author's Address: University of Ljubljana, Faculty of Mechanical Engineering, Aškerčeva 6, 1000 Ljubljana, Slovenia, marko.hocevar@fs.uni-lj.si

Strojniški vestnik - Journal of Mechanical Engineering 59(2013)4, 203-215

phenomena including mechanisms of cavitation erosion. From an initial survey of the literature it becomes readily apparent that cavitation erosion is intimately associated with material bulk properties and microstructure and therefore this topic is best researched from a materials science perspective. It is essential to review published studies that develop our understanding of the bulk macro- and micro-structural surface properties of scale and the cavitation erosion of brittle crystalline materials.

Table 1. The effectiveness of different scale treatments. Adapted from [9]

Scale treatment	Effectiveness (% reduction)
Ion exchange	100
Acid dosing	100
Chemical inhibitors	100
Metal ions	80
Magnetic conditioners	80
Electronic conditioners	80
Electrolytic	40
Ultrasound	30
Surface modifications	90

1 SCALE FORMATION

Calcium carbonate is atypical in that it is a reverse solubility salt, i.e. solubility decreases with increasing temperatures and hence is a fouling nuisance in heating equipment in areas of high water hardness. Generally, exceeding the solubility of a particular salt will initiate scale formation, albeit the actual process is complex and depends on many factors including supersaturation level, fluid composition, temperature, flow regime, and surface properties like surface energy and roughness [9] and [10]. When CO_2 dissolves in water, it forms a weak carbonic acid, which dissociates into hydrogen carbonate, hydrogen, and carbonate ions. Calcium ions then react with the bicarbonate to form calcium carbonate. The overall reaction can be written as follows:

$$Ca^{2+} + 2HCO_3^- \rightarrow CaCO_{3(s)} + CO_{2(g)} + H_2O$$

The physical process involves ion clustering, nucleation, crystal growth, agglomeration, and deposition. Initially there is an incubation or induction period, where seed crystals form. Briefly, cationic and anionic species collide to produce ion pairs in solution. These pairs then go on to create micro-aggregates or unstable clusters, which become nucleation centres or seed crystals in a process known as homogenous nucleation. Alternatively, a liquid/surface boundary or the presence of particles can also promote crystal growth particularly if there are surface defects and areas of turbulent flow. This is known as heterogeneous nucleation [11]. As the micro-crystals continue to grow, they fuse to form adherent macro-crystals. Growth then continues via the further adsorption of scaling ions to eventually form a uniform coating with subsequent deposition covering the rough scaled surface [12].

Of significance to this study is that calcium carbonate precipitates in different polymorphic crystalline forms, which, albeit chemically identical, have different crystal lattice structures and macro- and micro-structural properties. Three anhydrous crystalline polymorphs occur: vaterite, aragonite, and calcite and three hydrated phases, including amorphous calcium carbonate (ACC), monohydrate calcium carbonate (MCC; monohydrocalcite) and hexahydrate calcium carbonate (HCC; ikaite) [13]. The hydrated forms are unstable and most studies focus on the three anhydrous crystalline forms, of which calcite is the most stable, aragonite is metastable, and vaterite is the least stable form. Calcite and aragonite are the most common polymorphs (Fig.1).

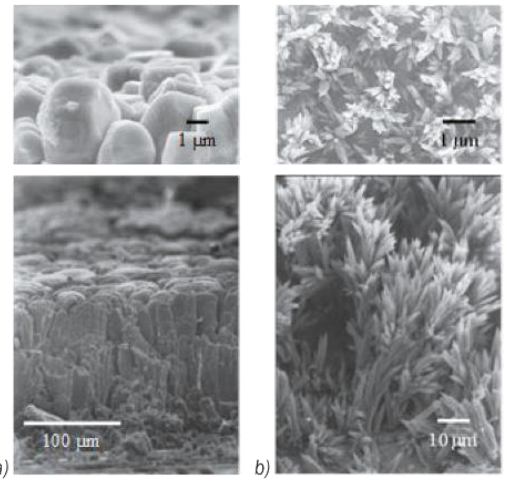


Fig. 1. *Scanning electron micrographs of $CaCO_3$ scale deposits showing the characteristic a) calcite (5 hrs, T = 18 °C, u =2 m/s, pH = 10.5, S = 15.5) and b) aragonite (60 min, T = 45 °C, u = 0.41 m/s, pH = 9.5, S = 12). Reprinted with permission from [14]. Copyright 1997 American Chemical Society*

Factors affecting the rate of scale deposition and the type of polymorph include pH, temperature, flow dynamics, surface properties, presence of other ions, and time. The higher the pH, the greater is the tendency for scale to form. According to Andritsos and Karabelas [15], an increase in the pH from 8.8 to

Strojniški vestnik - Journal of Mechanical Engineering 59(2013)4, 203-215

10 over a 2 hour period, will increase scale deposition from 2 to 12 mg/cm^2. Aragonite content also increases with increasing pH.

As stated, $CaCO_3$ shows reverse solubility and, as water temperature increases, carbon dioxide is removed, which causes a shift in the equilibrium to the right. This results in an increase in pH and the precipitation of $CaCO_3$. Additionally, Xia et al. [16] find that at lower temperatures, $CaCO_3$ scale is denser and adheres more strongly to the substrate, while at higher temperatures it exhibits a characteristic dendritic crystal structure. This is explained by the fact that below 30 °C, calcite is essentially the only polymorph present and is mainly in a prismatic form, while above 35 °C, aragonite is stable and creates dendrite formations (Fig. 2).

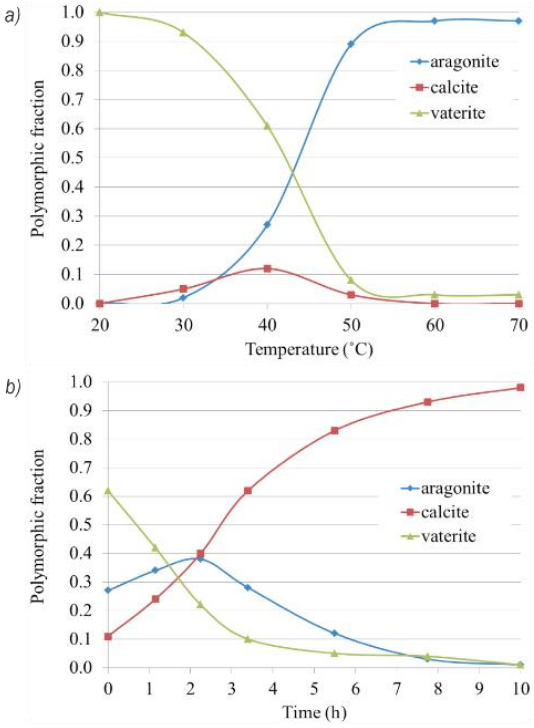


Fig. 2. *The relative concentrations of calcite, aragonite and vaterite with a) temperature and b) time. Adapted from [17]*

Vaterite can also be present at higher temperatures but it rapidly converts to calcite. The induction period increases with decreasing initial temperature because of the slower growth rate of $CaCO_3$, which favours formation of calcite. During the post-induction period the rate of $CaCO_3$ crystal growth is higher and favours the formation of aragonite [18] and [19].

Under low flow conditions a less dense scale will typically prevail, whereas higher flows result in a smoother surface. This is because the low density, poor coherence, and lower tenacity of aragonite mean it will be more easily removed. Scale properties are also influenced by the substrate surface in terms of size and crystal arrangement. For example, Malayeri et al. [3] find that highly alloyed austenitic stainless steel produces larger thicker harder and more adherent scale crystals. Time is also an important factor and with age the relative amount of calcite will increase.

It has long been known that the presence of other ions can affect scale formation from supersaturated solutions. Magnesium ions show the most pronounced affect [20] and [21]. Their presence not only delays and inhibits bulk precipitation and surface deposition processes, but also, to a different degree, favours the formation of the aragonite polymorph [20] and [21]. Low concentrations of magnesium ions in solution favour calcite formation, while aragonite is formed at high magnesium concentrations. It is the (Mg^{2+}):(Ca^{2+}) ratio and the initial ionic product of carbonate in solution that controls the time of nucleation and the mineralogy of the precipitate when Mg^{2+} ions are present [20]. The exact mechanism is not fully understood but it is thought that Mg^{2+} ions poison calcite crystal growth by becoming incorporated into the $CaCO_3$ lattice at Ca sites thus affecting its morphology and growth [21] and [22].

2 ULTRASONIC SCALE REMOVAL

Ultrasonic cleaning is a technology that uses high frequency sound waves and combines the phenomenon of cavitation, which dislodges contaminants, and agitation (micro-streaming), which accelerates the dissolution of contaminants by supplying fresh solution to the surface being cleaned. Cavitation describes the life-cycle of a transient cavity or bubble from formation via inception and nucleation, its expansion, and its eventual implosion. The result is extremely high pressure shock-waves (Table 2) and temperatures (approx. 5,000 K). Its observable effect, when near a solid boundary, is material damage known as cavitation erosion. Acoustically driven cavitation is the most important source of the cavitation effect for practical purposes, although it is also possible to utilise hydrodynamic cavitation in scale prevention [23]. Cavitation occurs as an acoustic wave (20 to 100 kHz) passes through a fluid. This then creates oscillating pressure with resultant phases of compression and rarefaction. During rarefaction, molecules are increasingly pulled

Strojniški vestnik - Journal of Mechanical Engineering 59(2013)4, 203-215

apart, eventually forming a cavity or void [24]. Fig. 3 shows how a bubble grows and collapses in an ultrasonic field. In reality, pre-existing nucleation sites require less energy to develop into bubbles. These sites are typically micro-heterogeneities, such as tiny gas bubbles, gas bubbles trapped in pockets and in crevices, trace impurities, and solid particles [25]. In most situations ample nuclei exist for bubble formation [26]. Two distinct types of bubble oscillations exist. The first are "stable" bubbles that oscillate for many periods of the sound field, while the second are "transient" (inertial) unstable bubbles that exist for less than a single compression half-cycle and increase in size 2 to 3 times their resonant size before imploding [27]. This transformation of a low energy density sound wave into a high energy density one means that a collapsing bubble will concentrate the energy into very small volumes producing extreme pressures (shock waves), temperatures, and even light in a process known as sonoluminescence [26]. Fig. 3 gives an overview of ultrasonic cavitation.

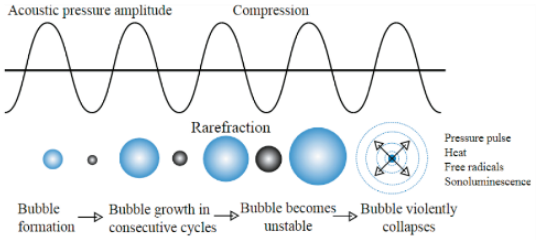


Fig. 3. *A generalised view of bubble dynamics in an ultrasonic field*

In terms of pressure as a damage mechanism, the forces impacting a surface are a result of spherical bubble collapse, impact of micro-jets [28], splash effect following the impact of a jet [29] and the combined effect of multi-bubble systems known as "clouds" [30]. The interaction of these shock waves subjects a material to repeat localized loading. The actual mechanisms producing shock waves of sufficient energy to cause material damage are a continual point of debate. Table 2 gives some examples of cavitation pressure loadings reported in the literature. Comparing these values is, however, difficult because some are estimates while others are measured using different methods and different ways of producing the cavitation phenomenon. In addition, the extreme pressure produced in the centre of the bubble decreases dramatically over very short distances. Spherical bubble collapse was the focus of initial investigations, but this is now known to be only a part of a more complex phenomenoa, since not all bubbles collapse spherically and their effect cannot be considered in isolation.

Bubbles that interact with a surface (rigid boundary) and with other bubbles will collapse in a non-spherical or asymmetrical manner, which in turn results in a re-entrant jet that is capable of delivering a directional and much higher local impact. Many authors believe that the shock waves produced by single bubble collapse and jet formation cannot account for much of the observed macroscopic damage and they focus on the combined effect of multiple bubble systems (clouds) and the so-called "splashing effect" as a major damage mechanism, [29] to [33].

Table 2. *Examples of cavitation load pressure*

Source	Pressure [GPa]	Bubble collapse	Cavitation source
[34]	10	single bubble	spark induced
[35]	0.2	micro-jet	ultrasound
[36]	4 (200 μm) 4.8 to 8.1 (200 μm)		hydrodynamic, vibratory
[37]	0.1	single bubble	
[37]	0.15	micro-jet	
[38]	2.5		simulated and hydrodynamic
[39]	1.7	single bubble	hydrodynamic
[40]	1		
[41]	1.85 to 2.24 (200 μm) 285 to 336 (10 μm)		hydrodynamic
[42]	4.3 (70 μm) 720 (4 μm)		hydrodynamic, vibratory
[43]	0.55	single bubble	ultrasound
[44]	0.1	multi -bubble	ultrasound
[45]	4 to 16 MPa (10 mm from bubble)		ultrasound
[46]	4 to 6		
[47]	8 (at bubble wall) 1.3 ± 0.3 (68 μm from bubble)	single bubble	ultrasound
[48]	7	single bubble	hydrodynamic
[49]	1.5	hemi-spherical cloud (760 μm)	ultrasound

Developing an understanding of cloud phenomena is difficult because whereas individually collapsing bubbles can be observed experimentally, shock waves arising from a concerted collapse of bubbles in a cloud system involve more complex dynamics [50] and [51]. In a bubble cloud, the entire bubble population dominates the cavitation effect and the collapse of the cloud creates a shock wave that radiates out into the fluid, the magnitude of which is attenuated as it travels

Strojniški vestnik - Journal of Mechanical Engineering 59(2013)4, 203-215

toward a solid surface. Williams et al. [52] suggest that jet formation may be enhanced by bubble-shockwave interaction. Brujan et al. [47] believe that collapsing clouds are potentially the most destructive form of cavitation as they produce short duration pressure pulses of large magnitude (1.5 GPa). Van Terwisga et al. [53] argue that the acoustic power released from a synchronized bubble cloud collapse is greater than that released via a micro jet. These shock waves are of interest in those cases where bubbles collapse at a distance from a boundary so that no jets form [53] and [54]. More recently, Brujan et al. [55] investigated secondary shock waves, which are a consequence of the free collapse of a bubble within the cloud by the ambient pressure in the fluid. In the second case, it is a consequence of the interaction of the cloud-collapse-induced shock wave with micro-bubbles situated close to the collapse site of the cloud. The latter can be very powerful, resulting in a secondary shock wave emission with a maximum amplitude of about 0.5 GPa. Despite this, Brujan [56] finds that, whereas small jet velocities do not have the potential to produce erosion of metals, they can play an important role in the fragmentation of brittle materials, since the yield strength is much lower than for ductile materials. Also of interest is a study by Barrow et al. [57] using atomic force microscopy, where the authors suggest that rapidly growing cavities have the potential to damage adjacent structures by the development of tension rather than by the evolution of a (positive) pressure shock. This type of damage together with micro-streaming could have a significant effect on the removal of the poorly adhering dendritic crystal structure, i.e. aragonite.

3 INFLUENCES OF MATERIAL PROPERTIES ON CAVITATION EROSION

From the published studies it can be seen that cavitation erosion is a function of material properties, including macro-properties, such as: tensile strength, strain energy, resilience, ductility, hardness, fatigue resistance and its microstructure [58]. To date, no overall single or combination of material properties can adequately predict cavitation erosion [59] and [60]. What is certain is that cavitation erosion is a time dependent phenomenon classically represented by an S-shaped erosion curve (Fig. 4) of material loss or rate of material loss against time [61]. The four distinct stages identifiable are the following: an incubation period, an acceleration period, a deceleration period, and finally a period of steady state erosion. The S-curve is a generalisation and the actual shape is specific to a material's properties.

The incubation period represents the accumulation of plastic deformation and internal stresses under the surface that precedes significant material loss [62] and [63]. It is related to the accumulation of fatigue damage but many other factors including, for example, grain size, hardness, and plasticity are also relevant. In ductile materials, cavitation shock waves impacting the surface will cause work hardening. Eventually, micro-cracks appear around grain boundaries and surface heterogeneities and begin to propagate outwards. In metals, these include notches, tears, undercuts, welding defects, inclusions or at heterogeneous areas of the material such as at the directionality of metal flow and decarburized sections [64]. Eventually the material will no longer be able to withstand such shocks and material will break loose [65] and [66]. This represents the transition from the incubation to the acceleration period. Initially the rate of material loss is exponential but becomes linear as the volume loss rate reaches a maximal value.

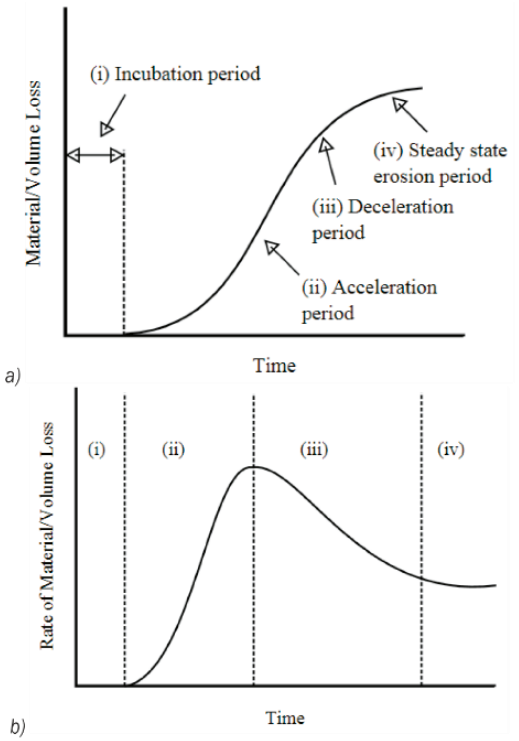


Fig. 4. *General cavitation erosion s-curve of material loss with time (a) showing four distinct stages (b). The rate that material is lost is initially slow but then steadily increases up to a point of maximum damage after which it (the damage rate) decreases until a steady-state condition is achieved. Adapted from [67]*

Strojniški vestnik - Journal of Mechanical Engineering 59(2013)4, 203-215

A lessening in the rate of this damage typifies the deceleration period. The volume loss rate decreases and removal of new material uncovers major areas with no accumulated internal stresses. Eventually, the erosion reaches a steady state with an almost constant volume loss rate since the surface, that is already strongly fractured, behaves as a protective cushion.

In brittle materials, zero or only a limited amount of plastic deformation occurs. Instead, micro-fractures will appear at the onset and cracks will rapidly propagate without increasing the overall applied stress. The erosion curve can still show the four characteristic stages of cavitation erosion since the incubation period reflects the accumulation of micro-cracks up to a point where material will break free. In addition, when erosion begins it becomes much more intensive than in ductile materials. The slope of the acceleration part of the cavitation erosion curve will be much steeper so that, in the end, the cumulated mass loss will be greater than in ductile materials given the same exposure time and cavitation intensity.

Fatjo et al. [68] find that for silicon nitride and zirconia pseudoplastic deformation pits are visible, but, unlike the work hardening seen in metals, there is a softening effect on the surface and the observable pits are linked to crack creation. The authors also describe how in ceramics these erosion pits have micro-cracks extension at the boundaries and cracking is mainly intergranular, although some cracks are visible within large or elongated grains. According to Karunamurthy et al. [69], material is removed as cracking eventually leads to dislodging of partial grains, grains, and eventually whole grain clusters. The transition from the incubation period to the acceleration period will occur when erosion of the entire surface is at a depth approximately equal to the average grain size [70]. Lu et al. [71] state that micro-structures including grain size, phases at grain boundaries, cavities or pores, and defects, such as cracks, inclusions, single agglomerates of large grains, and scratches from machining, promote fracture between grains. These structures are important in controlling the cavitation erosion behaviour of ceramic materials. Grain size is also important; increasing grain size leads to a greater erosion rate and vice versa [63].

Cavitation erosion is a natural process but only a few studies exist that investigate the cavitation of carbonate rocks. Carbonate rocks are made up of calcite crystals and hence provide valuable information about how cavitation can affect hard scale deposits. For instance, Momber, [72] having studied the cavitation erosion of limestone and marble using a flow cavitation chamber, finds that the most important parameters influencing cavitation erosion are exposure time, cavitation intensity, and materials properties. Grabco et al. [73] find that, in addition to mineral composition and mechanical properties like hardness, strength, fracture, and stability, microstructure is an important factor in the erosion resistance of brittle minerals. Calcite is unusual in that the presence of cleavage plane slip bands allows a limited amount of plastic deformation, while aragonite, having a single plane cleavage, does not. Generally, in such material, plastic deformation is relatively small and the formation of micro-cracks is the most important dissipation mechanism of inelastic deformation and brittle failure. This is enhanced by the presence of structural homogeneities like pores and interfaces, and pre-existing flaws are important sites where damage initiates while additional energy is absorbed due to crack surface friction (frictional resistance to sliding), crack bridging, and micro-crack formation [74].

There exist two possible mechanisms of brittle fracture: transcrystalline and intercrystalline cleavage. Lubarda et al. [75] find that, in most cases, it is inelastic deformation that occurs in rocks. As with ceramics, micro-cracks begin and propagate at the surface of pores and grain boundaries, and most evidence is for the damage being intercrystalline rather than transcrystalline fracture. In the case of limestone and marble, Momber [72] observes two erosion zones of high and low intensity in his samples of carbonaceous rocks. In the high intensity zone there is considerable erosion, while in the low intensity zone there are only a few single erosion events, which is a result of the flow conditions in the cavitation chamber. For marble and limestone, the transition or threshold time (critical exposure time) from there being just a few singular erosion events to producing a large cavity (damage) was 30 and 90 s, respectively. Low intensity cavitation of the limestone exposed coarse grain conglomerates 800-1000 μm in diameter. At higher intensity, individual grains 100 μm in diameter (approximately two times cleavage spacing of the calcite crystals) were exposed and removed. For marble, the author observes exposed individual calcite crystals (800 μm) at the surface and transcrystalline cleavage (200 μm cleavage planes) in the calcite minerals, indicating that marble is eroded in a two-step mode. The author proposes that fracture toughness and, secondly, structural homogeneity (pre-existing flaws) are good indicators of cavitation erosion, as erosion mainly occurs in an intergranular or intercrystalline mode and erosion resistance decreases with grain size. Wagterveld et al. [19] investigating cavitation erosion of suspended calcite crystals find that crystal breakage

Strojniški vestnik - Journal of Mechanical Engineering 59(2013)4, 203-215

can only occur if the energy input is higher than the energy required for maximum elastic deformation.

For transcystralline cleavage, the strength of the shock wave pressure pulses would have to be significant given the hardness of calcite (Vickers hardness of 1.2 to 1.5 GPa), with aragonite being slightly harder [76] and [77]. This is feasible given the strength of cavitation pressure pulses (> 1.5 GPa) reported in the literature. There is evidence suggesting that the strength of the crystal bonds may be higher than actually necessary to cause transcrystalline crystal cleavage. However, Wagterveld et al. [19], observing suspended calcite crystals, find that less energy is required to break off small fragments of corners by attrition compared to large fragments as total crystal breakage. The authors also find a discrepancy between theoretical surface fracture energies, defined by material bond strength, and their experimentally observed surface fracture energies, which they relate to so-called "Griffith cracks". These exist as microscopic flaws in the crystal grains. The numbers of these cracks are known to increase with volume, causing large grains to fracture more easily. This may also explain why cavitation erosion resistance increases with decreasing crystal grain size. Fatjo et al. [78] observe in ceramic materials that, while cracking is mainly intergranular, some cracks are also visible within larger or elongated grains. Wagterveld et al. [19] find no evidence of re-entrant jet impacts.

Amongst those studies that look at removing scale using cavitation erosion specifically, most are involved with the precipitation of scale in the bulk fluid rather than how cavitation actually affects surface deposits. In addition, the effects of ultrasound on preventing mineral scale from forming are not fully understood, despite several studies that have looked directly at preventing scale deposits [79] to [82]. In most cases they do not directly discuss the effects of cavitation erosion.

Dalas [79] was one of the first to apply ultrasound to preventing scale and reports that ultrasound retards $CaCO_3$ precipitation (reduction in scale by 62 to 76%) but has no effect on morphology. According to Li et al. [81], during cavitation, scale is "shattered and abscised". The authors find that temperature is an important factor when removing scale with ultrasound, e.g. 40 °C is preferable for preventing scale, whereas 50 °C is better for removing scale. They also conclude that a stronger acoustic intensity is better for removing scale deposits and vice versa a lower acoustic intensity is better for mitigating scale precipitation. Similarly, Feng et al. [83] also find that distance to the transducer is a factor.

Nishida [84], performing a sonochemical study, describes how ultrasonic irradiation and not cavitation increases the precipitation rate of $CaCO_3$ by enhancing nucleation. They also find that physical mixing by macro-streaming, rather than either a chemical effect or micro-streaming, is responsible for the observed increase in the rate of precipitation. Mihai et al. [85] also observed that ultrasound increases the precipitation rate (nucleation) by 40%, but reduces "association" (sic), i.e. crystal growth and agglomeration of the precipitated particles. He et al. [86] make similar observations but suggest that the reduction in average measured particle size is due to rapid nucleation resulting from the supersaturation of Ca^{2+} around the cavitating bubbles. Santos et al. [87] have investigated ultrasound as a means to break up the particle size of a $CaCO_3$ powder as a method for increasing mineral carbonation. The authors found a significant reduction in particle size. More recently, Price et al. [88], investigating the composition of $CaCO_3$ polymorphs precipitated using ultrasound, did not observe the retardation effect reported by Dalas [79] and state that this contradiction is a result of different reaction conditions. Price et al. [88] also find that the yield of $CaCO_3$ increases in the presence of an ultrasonic field until a maximum is reached, which is consistent with Nishida [84].

There is also the potential for cavitation to break up agglomerates. Marković et al. [89] investigated acoustic cavitation and fracture de-agglomeration of barium titanate powder and report that cavitation pressure must be larger than the cohesive strength by which primary particles are bound together. The authors find little evidence of changes in crystal structure, but were able to break up agglomerates and found that damage is maximised at crystal boundaries. Price et al. [88], however, unlike Dalas [79], did find that under specific reaction conditions different polymorphs of calcite are formed during irradiation with ultrasound, but that ultrasound has only a small effect on the polymorphs produced. The most important factor is initial concentration (supersaturation). This was not the case for Kojima et al. [90] who, by applying larger amplitudes, could promote the formation of the less stable vaterite phase and who suggest that morphological control of $CaCO_3$ is possible. Mateescu et al. [91] find that an ultrasonic field accelerates the formation of stable phases (calcite) from metastable ones (aragonite). Santos et al. [92] successfully use ultrasound combined with the addition of Mg^{2+} to promote aragonite synthesis

Strojniški vestnik - Journal of Mechanical Engineering 59(2013)4, 203-215

and suggest it as a potential method for industrial production of pure aragonite powder.

Since, in many cases, scale forms a coherent layer, information about damage from repeated shock impact can be gained from studies investigating surface treatments and coatings as strategies for improving cavitation erosion resistance. Such studies, besides investigating polymers, composites, and fillers, also investigate hard brittle coatings made of ceramics [93]. On their own, these coatings are resilient to cavitation but, despite some initial success, fail over time [94]. Buravova and Gordopolov [95] observe that pressure loading on the outer surface, albeit of insufficient strength to fracture the surface, i.e. below the yield stress, can still cause damage. Failure mechanisms include debonding, delamination, and spallation [96] to [99]. Damage occurs when a reflected shock wave is generated when the incident shock hits the material boundary. The interaction and focusing of the incident and reflected shock waves cause subsurface cracks to form parallel to the interface. Delamination then occurs as these cracks extend along a plane parallel to the film/substrate interface, while spalling occurs when the subsequent propagation travels up through the film to the surface. Spalling is a common damage mechanism seen in hard coatings [100]. Ledrappier et al. [101] observe that such damage mechanisms depend on impact parameters and coating characteristics. Additional factors include residual stresses, substrate properties and substrate coating adherence issues, porosity and interfacial defects, and other imperfections [102]. Such sites (imperfections) can also act as nucleation sites for cavitation, thus further accelerating material removal. Loh et al. [103] find that spalling only occurs at defective regions of a coating, while nondefective regions are apparently immune to spalling.

Acoustic pressure also differs according to material properties that affect the speed of sound waves as they travel through different materials. This in itself can lead to a damaging shearing force [104]. Such a force acting on a scale deposit is therefore another damage mechanism causing material (scale) to become loose and break free.

Cavitation erosion creates free particles in solution, making particulate abrasion a possibility since cavitation is accompanied by acoustic streaming [105]. Krella et al. [97] provide evidence of possible abrasion/erosion that results from collisions of the hard coating micro-particles torn off during cavitation, while Chen et al. [106] report enhanced cavitation erosion in the presence of particles. Zeiger et al. [107], investigating the molecular crystals (aspirin), rule out particle-particle interaction as a viable damage mechanism.

Removal of material could result from cavitation affecting changes in the chemical equilibrium that exist close to a surface deposit. Stephanis et al. [108] find that for gypsum, another common scale forming mineral, dissolution from the solid occurs since solvent is being continuously renewed at the point of jet impact due to asymmetrical bubble collapse. Vinten'ko and Gumnitskii [109], investigating the dissolution of the mineral Langbeinite ($K_2Mg_2(SO_4)_3$), draw a similar conclusion and also suggest that cavitation enhances the dissolution of solids. In the case of $CaCO_3$ this would benefit from further investigation.

Another minor removal mechanism of interest is possibility the direct volatilisation of $CaCO_3$ to CaO and CO_2. Impact simulations of carbonaceous material suggest that approximately 10 GPa is the minimum shock pressure required for partial release of CO_2 from $CaCO_3$, while 60 to 70 GPa is necessary for complete conversion. Recent studies continue to show lower shock pressure required for incipient devolatilization of calcite, e.g. $<24.9 \pm 2.6$ GPa [110] and 18 GPa [111], which is significantly lower than reported in previous experimental studies. Grady [112] referenced in [113] states that at a "Static high pressure, high temperature experiments up to 3.5 GPa on calcite show that below 4 MPa it decomposes into solid CaO and gaseous CO_2 without melting". Pressure pulses from cavitation, especially when bubbles collapse close to a surface, may be sufficient to cause partial devolatilization since pressures of 10 GPa are potentially feasible at liquid-solid interfaces [114]. The presence of a back reaction resulting in the re-precipitation of secondary carbonates may also greatly diminish this effect. Overall, too little is known about the extent of devoltaliszation of $CaCO_3$ under cavitating conditions.

4 CONCLUSIONS

Our objective in writing this paper was to review the major aspects of the possible cavitation erosion mechanisms affecting tenacious $CaCO_3$ mineral scale as part of a larger study examining the influence of cavitation on different mineral scale coated metal surfaces. Our eventual aim is to formulate a phenomenological model of cavitation erosion, which will link parameters of cavitation intensiveness with damage of the mineral scale surface. This literature study shows how scale formation and cavitation erosion are complex phenomena dependent on many factors. The density, hardness, and tenacity of the

Strojniški vestnik - Journal of Mechanical Engineering 59(2013)4, 203-215

scale will depend on its depositional environment. In the case of $CaCO_3$, this will affect the material and surface properties of the resultant scale layer. Of the different mechanism of cavitation, bubble cloud collapse and the splashing effect following jet formation are considered to be the most important. Cavitation erosion suggests that brittle material fracture occurs with only a limited amount of plastic deformation and that the formation of micro-cracks is the most important erosion mechanism, enhanced by the presence of structural homogeneities. A better understanding of the damage mechanism of cavitation will be useful not only for those looking at improving the efficiency of ultrasonic removal of tenacious mineral scale deposits, but will also prove useful in the field of sonochemistry, medicine (shock wave lithotripsy), and those studying the natural cavitation processes of carbonate materials.

5 REFERENCES

[1] DOE (2011). *EnergySavers: Tips on Saving Money & Energy at Home*, US Department of Energy, Office of Energy Efficiency and Renewable Energy, p. 1-44.

[2] Müller-Steinhagen, H., Malayeri, M.R., Watkinson, P. (2005). Fouling of heat exchangers –new approaches to solve old problem. *Heat Transfer Engineering*, vol. 26, no. 1, p. 1-4, DOI:10.1080/01457630590959250.

[3] Malayeri, M.R., Al-Janabi, A., Müller-Steinhagen, H. (2009). Application of nano-modified surfaces for fouling mitigation. *International Journal of Energy Research*, vol. 33, no. 13, p. 1101-1113, DOI:10.1002/er.1599.

[4] MarketsandMarkets. (2012). *Scale Inhibitors Market (2011-2016)*, from http://www.marketsandmarkets.com/, accessed at: 2012-02-01.

[5] Hasson, D., Shemer, H., Sher, A. (2011). State of the art of friendly "green" scale control inhibitors: a review article. *Industrial & Engineering Chemistry Research*, vol. 50, no. 12, p. 7601-7607, DOI:10.1021/ie200370v.

[6] Hansen, J.T., Saxon G.E. (2004). Improving condenser efficiency with innovative scale removal system technology. *ASME 2004 Conference Proceedings*, p. 19-23, DOI:10.1115/POWER2004-52020.

[7] Širok, B., Dular, M., Stoffel, B. (2006). *Cavitation*. i2, Publishing, Ljubljana.

[8] Brennen, C.E. (1995). *Cavitation and Bubble Dynamics*. Oxford University Press, New York, Oxford.

[9] MacAdam, J., Parsons, S.A. (2004). Calcium carbonate scale formation and control. *Reviews in Environmental Science and Biotechnology*, vol. 3, no. 2, p. 159-169, DOI:10.1007/s11157-004-3849-1.

[10] Karabelas, A.J. (2002). Scale formation in tubular heat exchangers - research priorities. *International Journal of Thermal Sciences*, vol. 41, no. 7, p. 682-692, DOI:10.1016/S1290-0729(02)01363-7.

[11] Crabtree, M., Eslinger, D., Fletcher, P., Miller, M., Johnson, A., King, G. (1999). Fighting scale–removal and prevention. *Oilfield Review*, vol. 11, no. 3, p. 30-45.

[12] Duggirala, P.Y. (2005). Formation of calcium carbonate scale and control strategies in continuous digesters. *CD del II Coloquio Internacional sobre Celulosa de Eucalipto, Concepcion*, Chile, p. 1-34.

[13] Elfil, H., Roques, H. (2001). Role of hydrate phases of calcium carbonate on the scaling phenomenon. *Desalination*, vol. 137, no. 1-3, p. 177-186, DOI:10.1016/S0011-9164(01)00216-8.

[14] Andritsos, N., Karabelas, A.J., Koutsoukos, P.G. (1997). Morphology and structure of $CaCO_3$ scale layers formed under isothermal flow conditions. *Langmuir*, vol. 13, p. 2873-2879, DOI:10.1021/la960960s.

[15] Andritsos, N., Karabelas, A.J. (1999). The influence of particulates on CaCO3 scale formation. *Journal of Heat Transfer-Transactions of the ASME*, vol. 121, no. 1, p. 225-227, DOI:10.1115/1.2825951.

[16] Xia, M.Z., Lei, W., Dai, L.H., Chu, Y. T., Wang, F.Y. (2010). Study of the mechanism of phosphonate scale inhibitors against Calcium carbonate scale. *Acta Chimica Sinica*, vol. 68, no. 2, p. 143-148.

[17] Carteret, C., Dandeu, A., Moussaoui, S., Muhr, H., Humbert, B., Plasari, E. (2009). Polymorphism studied by lattice phonon raman spectroscopy and statistical mixture analysis method. Application to calcium carbonate polymorphs during batch crystallization. *Crystal Growth & Design*, vol. 9, no. 2, p. 807-812, DOI:10.1021/cg800368u.

[18] Yang, Q.F., Liu, Y.Q., Gu, A.Z., Ding, J., Shen, Z.Q. (2002). Investigation of induction period and morphology of $CaCO_3$ fouling on heated surface. *Chemical Engineering Science*, vol. 57, no. 6, p. 921-931, DOI:10.1016/S0009-2509(02)00007-6.

[19] Wagterveld, R.M., Boels, L., Mayer, M.J., Witkamp, G.J. (2011). Visualization of acoustic cavitation effects on suspended calcite crystals. *Ultrasonics Sonochemistry*, vol. 18, no. 1, p. 216-225, DOI:10.1016/j.ultsonch.2010.05.006.

[20] Rushdi, A., Pytkowicz, R., Suess, E., Chen, C.T., (1992). The effects of magnesium-to-calcium ratios in artificial seawater, at different ionic products, upon the induction time, and the mineralogy of calcium carbonate: a laboratory study. *Geologische Rundschau*, vol. 81, no. 2, p. 571-578, DOI:10.1007/BF01828616.

[21] Chen, T., Neville, A., Yuan, M. (2006). Influence of Mg^{2+} on $CaCO_3$ formation-bulk precipitation and surface deposition. *Chemical Engineering Science*, vol. 61, no. 16, p. 5318-5327, DOI:10.1016/j.ces.2006.04.007.

[22] Stashans, A., Chamba, G. (2011). A new insight on the role of Mg in calcite. *International Journal of*

Strojniški vestnik - Journal of Mechanical Engineering 59(2013)4, 203-215

Quantum Chemistry, vol. 111, no. 10, p 2436-2443, DOI:10.1002/qua.22538.

[23] Gaines, W.A., Kim, B.R., Drews, A.R., Bailey, C., Loch, T. (2007). Controlling cooling water quality by hydrodynamic cavitation. *Proceedings of the Water Environment Federation Conference*, vol. 7, p. 538-545, DOI:10.2175/193864707787781656.

[24] Leighton, T.G. (1998). Fundamentals of underwater acoustics and ultrasound. Fahy, F.J., Walker, J.G. (eds.). *Noise and Vibration,* E&F Spon, London, p. 373-444.

[25] Mørch, K.A. (2007). Reflections on cavitation nuclei in water. *Physics of Fluids*, vol. 19, no. 7, p. 1-7, DOI:10.1063/1.2747210.

[26] Davydov, M.N., Kedrinskii, V.K. (2003). Mathematical simulation of bubbly cluster and spall formation in a liquid at dynamic loading. *5th International Symposium on Cavitation*, Osaka.

[27] Riesz, P., Kondo, T. (1992). Free radical formation induced by ultrasound and its biological implications. *Free Radical Biolology and Medicine*, vol. 13, no. 3, p. 247-270, DOI:10.1016/0891-5849(92)90021-8.

[28] Benjamin, T.B., Ellis, A.T. (1966). The collapse of cavitation bubbles and the pressures thereby produced against solid boundaries. *Philosophical Transactions of the Royal Society of London. Series A, Mathematical and Physical Sciences*, vol. 260, no. 1110, p. 221-240, DOI:10.1098/rsta.1966.0046.

[29] Tong, R.P., Schiffers, W.P., Shaw, S.J., Blake, J.R., Emmoy, D.C. (1999). The role of 'splashing' in the collapse of a laser-generated cavity near a rigid boundary. *Journal of Fluid Mechanics*, vol. 380, p. 339-361, DOI:10.1017/S0022112098003589.

[30] Dular, M., Bachert, B., Stoffel, B., Širok, B. (2004). Relationship between cavitation structures and cavitation damage. *Wear*. vol. 257, no. 11, p. 1176-1184, DOI:10.1016/j.wear.2004.08.004.

[31] Hansson, I., Mørch, K.A. (1980). The dynamics of cavity clusters in ultrasonic (vibratory) cavitation erosion. *Journal of Applied Physics*, vol. 51, no. 9, p. 4651-4658, DOI: 10.1063/1.328335.

[32] Dular, M., Stoffel, B., Širok, B. (2006). Development of a cavitation erosion model. *Wear*, vol. 26, no. 5-6, p. 642-655, DOI:10.1016/j.wear.2006.01.020.

[33] Dular, M., Osterman, A. (2008). Pit clustering in cavitation erosion. *Wear*, vol. 265, no. 5-6, p. 811-820, DOI:10.1016/j.wear.2008.01.005.

[34] Jones, I.R., Edwards D.H. (1960). An experimental study of the forces generated by the collapse of transient cavities in water. *Journal of Fluid Mechanics,* vol. 7, no. 4, p. 596-609, DOI:10.1017/S0022112060000311.

[35] Crum, L.A. (1979). Tensile strength of water. *Nature*, vol. 278, no. 5700, p. 148-149, DOI:10.1038/278148a0.

[36] Kirejczyk, J. (1979). The energy flux of cavitating flow. *Proceedings of 6th International Conference on Fluid Machinery*. Budapest Scientific Society of Mechanical Engineers, Budapest, p. 555.

[37] Fujikawa, S., Akamatsu, T. (1980). Effects of the non-equilibrium condensation of vapour on the pressure wave produced by the collapse of a bubble in a liquid. *Journal of Fluid Mechanics*, vol. 97, no. 3, p. 481-512, DOI:10.1017/S0022112080002662.

[38] Patella, R.F., Reboud, J.L. (1998). A new approach to evaluate the cavitation erosion power. *Journal of Fluids Engineering*, vol. 120, no. 2, p. 335-344, DOI:10.1115/1.2820653.

[39] De, M.K., Hammitt, F.G. (1982). Instrument system for monitoring cavitation noise. *Journal of Physics E: Scientific Instruments*, vol. 15, no. 7, p. 745, DOI:10.1088/0022-3735/15/7/012.

[40] Takayama, K., Esashi, H., Sanada, N. (1983) Propagation and focusing of spherical shock waves produced by underwater microexplosions. Shock tubes and waves, Archer, R.D., Milton, B.E. (eds.), *Sydney Shock Tube Symposium*, Sydney, p. 553-562.

[41] Momma, T., Lichtarowicz, A. (1995). A study of pressures and erosion produced by collapsing cavitation. *Wear*, vol. 186-187, no. 2, p. 425-436, DOI:10.1016/0043-1648(95)07144-X

[42] Okada, T., Iwai, Y., Hattori, S., Tanimura, N. (1995). Relation between impact load and the damage produced by cavitation bubble collapse. *Wear*, vol. 184, no. 2, p. 231-239 DOI:10.1016/0043-1648(94)06581-0.

[43] Holzfuss, J., Ruggeberg, M., Billo, A. (1998). *Shock Wave Emissions of a Sonoluminescing Bubble*. eprint arXiv:chao-dyn/9811022:11022, DOI:10.1103/PhysRevLett.81.5434.

[44] Suslick, K.S., McNamara III, W.B., Didenko, Y. (1999). Hot spot conditions during multi-bubble cavitation. *Sonochemistry and Sonoluminescence*. Crum, L.A., Mason, T.J., Reisse, J., Suslick, K.S. (eds.) Kluwer Publishers, Dordrecht, p. 191-204.

[45] Cleveland, R.O., Sapozhnikov, O.A., Bailey, M.R., Crum, L.A. (2000). A dual passive cavitation detector for localized detection of lithotripsy-induced cavitation in vitro. *The Journal of the Acoustical Society of America*, vol. 107, no. 3, p. 1758, DOI:10.1121/1.428572.

[46] Pecha, R., Gompf, B. (2000). Microimplosions: Cavitation collapse and shock wave emission on a nanosecond time scale. *Physical Review Letters*, vol. 84, no. 6, p. 1328-1330, DOI:10.1103/PhysRevLett.84.1328.

[47] Brujan, E.A., Ikeda, T., Matsumoto, Y. (2008). On the pressure of cavitation bubbles. *Experimental Thermal and Fluid Science*, vol. 32, no. 5, p. 1188-1191, DOI:10.1016/j.expthermflusci.2008.01.006.

[48] Yang, S.H., Jaw, S.Y., Yeh, K.C., (2012). *Experimental Study on Generation of Single Cavitation Bubble Collapse Behaviour by a High Speed Camera Record*. Gokcek, D.M., (ed.), Mechanical Engineering, InTech, p. 463-482.

[49] Brujan, E.A., Ikeda, T., Matsumoto, Y. (2012). Shock wave emission from a cloud of bubbles. *Soft Materials*, vol. 8, p. 5777-5783, DOI:10.1039/C2SM25379H.

[50] Hansson, I., Kedrinskii, V., Mørch, K.A. (1982). On the dynamics of cavity clusters. *Journal of Physics D: Applied Physics*, vol. 15, no. 9, p. 1725, DOI:10.1088/0022-3727/15/9/017.

[51] Kumar, S., Brennen, C.E. (1991). Nonlinear effects in the dynamics of clouds of bubbles. *The Journal of the Acoustical Society of America*, vol. 89, no. 2, p. 707-714, DOI:10.1121/1.1894630.

[52] Williams, P.R., Williams, P.M., Brown, S.W.J. (1997). A technique for studying liquid jets formed by cavitation bubble collapse under shockwaves, near a free surface. *Journal of Non-Newtonian Fluid Mechanics*, vol. 72, no. 1, p. 101-110, DOI:10.1016/S0377-0257(97)00020-7.

[53] Van Terwisga, T.J.C., Fitzsimmons, P.A., Ziru, L., Jan Foeth, E. (2009). Cavitation Erosion – A review of physical mechanisms and erosion risk models. *7th International Symposium on Cavitation*, p. 1-13.

[54] Shaw, S.J., Spelt, P.D.M. (2010). Shock emission from collapsing gas bubbles. *Journal of Fluid Mechanics*, vol. 646, p. 363, DOI:10.1017/S0022112009993338.

[55] Brujan, E.A., Ikeda, T., Yoshinaka, K., Matsumoto, Y. (2011). The final stage of the collapse of a cloud of bubbles close to a rigid boundary. *Ultrasonics Sonochemistry*, vol. 18, no. 1, p. 59-64, DOI:10.1016/j.ultsonch.2010.07.004.

[56] Brujan, E.A. (2004). The role of cavitation microjets in the therapeutic applications of ultrasound. *Ultrasound in Medicine & Biology*, vol. 30, no. 3, p. 381-387, DOI:10.1016/j.ultasmedbio.2003.10.019.

[57] Barrow, M.S., Bowen, W.R., Hilal, N., Al-Hussany, A., Williams, P.R., Williams, R.L., Wright, C.J. (2003). A study of the tensile properties of liquids in confined spaces using an atomic force microscope. *Proceedings of the Royal Society of London. Series A: Mathematical, Physical and Engineering Sciences*, vol. 459, no. 2039, p. 2885-2908, DOI:10.1098/rspa.2003.1128.

[58] Fortes-Patella, R., Challier, G., Reboud, J.L., Archer, A. (2001). Cavitation erosion mechanism: numerical simulations of the interaction between pressure waves and solid boundaries. *4th International Symposium on Cavitation*, DOI:CAV2001:sessionA3.006.

[59] Williams, P.R., Williams, P.M., Brown, S.W.J. (1998). A study of liquid jets formed by bubble collapse under shock waves in elastic and Newtonian liquids. *Journal of Non-Newtonian Fluid Mechanics*, vol. 76, no. 1-3, p. 307-325, DOI:10.1016/S0377-0257(97)00124-9.

[60] Pogodaev, L., Tret'yakov, D. (2009). The reference model of the impact of cavitation erosion on materials. *Journal of Machinery Manufacture and Reliability*, vol. 38, no. 1, p 51-57, DOI:10.3103/S1052618809010105.

[61] Thiruvengadam, A. (1963). A Unified Theory of Cavitation Damage. *Journal of Basic Engineering*, vol. 85, no. 3, p. 365-373, DOI:10.1115/1.3656610.

[62] *Standard Test Method for Cavitation Erosion Using Vibratory Apparatus*, ASTM Standard G32-98, vol. 03.02 (1998), American Society for Testing and Materials, West Conshohocken, p. 115

[63] García-Atance Fatjó, G., Hadfield, M., Vieillard, C., Sekulic, J. (2009). Early stage cavitation erosion within ceramics—An experimental investigation. *Ceramics International*, vol. 35, no. 8, p. 3301-3312. DOI:10.1016/j.ceramint.2009.05.020.

[64] Osterman, A., Bachert, B., Širok, B., Dular, M. (2009). Time dependant measurements of cavitation damage. *Wear*, vol. 266, no. 9-10, p. 945-951, DOI:10.1016/j.wear.2008.12.002.

[65] Franc, J.-P. (2009). Incubation time and cavitation erosion rate of work-hardening materials. *Journal of Fluids Engineering*, vol. 131, no. 2, 021303, DOI:10.1115/1.3063646.

[66] Franc, J.-P., Michel, J.M. (2010). *Fundamentals of Cavitation*, Springer, New York, Boston, Doordrecht, London, Moscow.

[67] Zhou, Y.-K., Hammitt, F.G. (1983). Cavitation erosion incubation period. *Wear*, vol. 86, no. 2, p. 299-313, DOI:10.1016/0043-1648(83)90168-0.

[68] Fatjo, G.G.A., Hadfield, M., Tabeshfar, K. (2011). Pseudoplastic deformation pits on polished ceramics due to cavitation erosion. *Ceramics International*, vol. 37, p. 6, p. 1919-1927, DOI:10.1016/j.ceramint.2011.03.043.

[69] Karunamurthy, B., Hadfield, M., Vieillard, C., Morales, G. (2010). Cavitation erosion in silicon nitride: Experimental investigations on the mechanism of material degradation. *Tribology International*, vol. 43, no. 12, p. 2251-2257, DOI:10.1016/j.triboint.2010.06.012.

[70] Tomlinson, W.J., Kalitsounakis, N., Vekinis, G. (1999). Cavitation erosion of aluminas. *Ceramics International*, vol. 25, no. 4. p. 331-338, DOI:10.1016/S0272-8842(98)00043-1.

[71] Lu, J., Zum Gahr, K.-H., Schneider, J. (2008). Microstructural effects on the resistance to cavitation erosion of ZrO_2 ceramics in water. *Wear*, vol. 265, no. 11-12, p. 1680-1686, DOI:10.1016/j.wear.2008.04.028

[72] Momber, A.W. (2003). Cavitation damage to geomaterials in a flowing system. *Journal of Materials Science*, vol. 38, no. 4, p. 747-757, DOI:10.1023/A:1021800812885.

[73] Grabco, D., Palistrant, N., Shikimaka, O., Zhitaru, R., Rahvalov, V., Zugravescu, D. (2002). Hardness and brittleness of rocks studied by microindentation in combination with the acoustic emission method. *8th European Conference on Nondestructive Testing*, p. 17-21.

[74] Momber, A.W. (2004). Wear of rocks by water flow. *International Journal of Rock Mechanics and Mining*

Sciences, vol. 41, no. 1, p. 51-68, DOI:10.1016/S1365-1609(03)00075-3.

[75] Lubarda, V.A., Mastilovic, S. Knap, J. (1996). Brittle-ductile transition in porous rocks by cap model. *Journal of Engineering Mechanics-ASCE*, vol. 122, no. 7, p. 633-642, DOI:10.1061/(ASCE)0733-9399(1996)122:7.

[76] Wang, L.F., Sondi, I., Matijevic, E. (1999). Preparation of uniform needle-like aragonite particles by homogeneous precipitation. *Journal of Colloid Interface Science*, vol. 218, p. 545-553, DOI:10.1006/jcis.1999.6463.

[77] Merriman, R.J., Peacor, D.R. (1999). Very low grade metapelites; mineralogy, microfabrics and measuring reaction progress. Frey, M., Robinson, D. (eds.), *Low-grade Metamorphism*. Blackwell, Oxford, p. 10-60.

[78] Fatjo, G., Hadfield, M., Vieillard, C., Sekulic, J. (2009). Early stage cavitation erosion within ceramics: an experimental investigation. *Ceramics International*, vol. 35, no. 8, p. 3301-3312, DOI:10.1016/j.ceramint.2009.05.020.

[79] Dalas, E. (2001). The effect of ultrasonic field on calcium carbonate scale formation. *Journal of Crystal Growth*, vol. 222, no. 1-2, p. 287-292, DOI:10.1016/S0022-0248(00)00895-2.

[80] Benzinger, W., Schygulla, U., Jager, M., Schubert, K., (2005). Anti fouling investigations with ultrasound in a micro-structured heat exchanger. *6th International Heat Exchanger Fouling and Cleaning - Challenges and Opportunities Conference*, p. 197-201.

[81] Li, H.X., Huai, X.I., Cai, J., Liang, Q. (2009). Experimental research on antiscale and scale removal by ultrasonic cavitation. *Journal of Thermal Science*, vol. 18, no. 1, p. 65-73, DOI:10.1007/s11630-009-0065-x.

[82] Kazi, N., Duffy, G.G., Chen, X.D. (2012). Fouling and fouling mitigation on heated metal surfaces. *Desalination*, vol. 288, no. 0, p. 126-134, DOI:10.1016/j.desal.2011.12.022.

[83] Feng, D., van Deventer, J.S.J., Aldrich, C. (2006). Ultrasonic defouling of reverse osmosis membranes used to treat wastewater effluents. *Separation and Purification Technology*, vol. 50, no. 3, p. 318-323, DOI:10.1016/j.seppur.2005.12.005.

[84] Nishida, I. (2004). Precipitation of calcium carbonate by ultrasonic irradiation. *Ultrasonics Sonochemistry*, vol. 11, no. 6, p. 423-428, DOI:10.1016/j.ultsonch.2003.09.003.

[85] Mihai, M., D. Turtoi, Mateescu, C., Chilibon, I., (2009). Calcium carbonate synthesis in ultrasonic field. *Revista De Chimie*, vol. 60, no. 6, p. 626-631.

[86] He, M.Z., Forssberg, E., Yanmin, W. MHan, Y,. (2005). Ultrasonication-assisted synthesis of calcium carbonate nanoparticles. *Chemical Engineering Communications*, vol. 192, no. 10-12, p. 1468-1481, DOI:10.1080/009864490896025.

[87] Santos, R.M., François, D., Mertens, G., Elsen, J., Van Gerven, T. (2012). *Ultrasound-intensified mineral Carbonation. Applied Thermal Engineering*. In Press. DOI:10.1016/j.applthermaleng.2012.03.035.

[88] Price, J., Mahon, M.F., Shannon, J., Cooper, C. (2010). Composition of calcium carbonate polymorphs precipitated using ultrasound. *Crystal Growth & Design*, vol. 11, no. 1, p. 39-44, DOI:10.1021/cg901240n.

[89] Marković, S., Mitrić, M., Starčecić, G., Uskoković, D. (2008). Ultrasonic de-agglomeration of barium titanate powder. *Ultrasonics Sonochemistry*, vol. 15, no. 1, p. 16-20, DOI:10.1016/j.ultsonch.2007.07.008.

[90] Kojima, Y., Yamaguchi, K., Nishimiya, N. (2010). Effect of amplitude and frequency of ultrasonic irradiation on morphological characteristics control of calcium carbonate. *Ultrasonics Sonochemistry*, vol. 17, no. 3, p. 617-620, DOI:10.1016/j.ultsonch.2009.10.020.

[91] Mateescu, C.D., Sarbu, C., Isopescu, R., Dumitrescu, O., Ghica, D. (2011). Sonocrystallization of calcium carbonate metastable polymorphs in alcoholic solutions as reaction media. *18th International Symposium on Industrial Crystallization*, p. 4.

[92] Santos, R., Ceulemans, P., François, D., Van Gerven, T. (2011). Ultrasound-enhanced mineral carbonation. *The 3rd European Process Intensification Conference*, p. 108-116.

[93] Sollars, R., Beitelman, A. (2011). *Cavitation-resistant coatings for hydropower turbines*. US Army Corps of Engineers, Engineer Research and Development Center, Construction Engineering Research Laboratory, Portland, p. 1-67.

[94] Schramm, B., Dwars, A., Kühl, A. (2005). Do coatings protect against corrosion and wear? *World Pumps*, vol. 470, p. 32-38, DOI:10.1016/S0262-1762(05)70818-X.

[95] Buravova, S., Gordopolov, Y. (2010). Bubble-induced cavitation effect upon solid surfaces. *Technical Physics Letters*, vol. 36, no. 8, p. 717-719, DOI:10.1134/S1063785010080110.

[96] Chernega, S. (1998). On the mechanism of deterioration of composite eutectic coatings by cavitation. *Powder Metallurgy and Metal Ceramics*, vol. 37, no. 7, p. 373-378, DOI:10.1007/BF02676018.

[97] Krella, A., Czyzniewski A. (2007). Influence of the substrate hardness on the cavitation erosion resistance of TiN coating. *Wear*, vol. 263, no 1-6, p. 395-401, DOI:10.1016/j.wear.2007.02.003.

[98] Krella, A. (2011). An experimental parameter of cavitation erosion resistance for TiN coatings. *Wear*, vol. 270, no. 3-4, p. 252-257, DOI:10.1016/j.wear.2010.10.065.

[99] Paik, B.-G., Kim, K.-S., Kim, K.-Y., Ahn, J.-W., Kim, T.-G., Kim, K.-R., Jang, Y.-H., Lee, S.-U. (2011). Test method of cavitation erosion for marine coatings with low hardness. *Ocean Engineering*, vol. 38, no. 13, p. 1495-1502, DOI:10.1016/j.oceaneng.2011.07.008.

[100] Tan, H. (2008). *Spalling and fragmentation Part 1*, p. 1-5, from http://imechanica.org, accessed on 2012-02-01.

[101] Ledrappier, F., Langlade, C., Gachon, Y., Vannes, B. (2008). Blistering and spalling of thin hard coatings submitted to repeated impacts. *Surface and Coatings Technology*, vol. 202, no. 9, p. 1789-1796, DOI:10.1016/j.surfcoat.2007.07.107.

[102] Mishnaevsky, L.L., Gross, D. (2004). Micromechanisms and mechanics of damage and fracture in thin film/substrate systems. *International Applied Mechanics*, vol. 40, no. 2, p. 140-155, DOI:10.1023/B:INAM.0000028592.55112.b9.

[103] Loh, R.L., Rossington, C., Evans, A.G. (1986). Laser Technique for Evaluating Spall Resistance of Brittle Coatings. *Journal of the American Ceramic Society*, vol. 69, no. 2, p. 139-142, DOI:10.1111/j.1151-2916.1986.tb04718.x.

[104] Zhou, A.-D., Yang, H.-X., Zhang, Z.-B. (2005). Application of Ultrasonic in Anti-scaling. *Applied Chemical Industry*, vol. 34, p. 659-661.

[105] Ichida, Y., Sato, R., Morimoto, Y., Kobayashi, K., (2005). Material removal mechanisms in non-contact ultrasonic abrasive machining. *Wear*, vol. 258, no. 1-4, p. 107-114, DOI:10.1016/j.wear.2004.05.016.

[106] Chen, H., Wang, J., Chen, D. (2009). Cavitation damages on solid surfaces in suspensions containing spherical and irregular microparticles. *Wear*, vol. 266, no. 1-2, p. 345-348, DOI:10.1016/j.wear.2008.05.010.

[107] Zeiger, B.W., Suslick, K.S. (2011). Sonofragmentation of molecular crystals. *Journal of the American Chemical Society*, vol. 133, no. 37, p. 14530-14533, DOI:10.1021/ja205867f.

[108] Stephanis, C.G., Hatiris, J.G., Mourmouras, D.E. (1997). The process (mechanism) of erosion of soluble brittle materials caused by cavitation. *Ultrasonics Sonochemistry*, vol. 4, no. 3, p. 269-271, DOI:10.1016/S1350-4177(96)00040-5.

[109] Viten'ko, T., Gumnitskii, Y. (2006). Mass transfer during dissolution of solids using hydrodynamic cavitation devices. *Theoretical Foundations of Chemical Engineering*, vol. 40, no. 6, p. 598-603, DOI:10.1134/S0040579506060078.

[110] Ohno, S., Kadono, T., Ishibashi, K., Kawaragi, K., Sugita, S., Nakamura, E., Matsui, T. (2008). Direct measurements of impact devolatilization of calcite using a laser gun. *Geophysical Research Letters*, vol. 35, no. 13, p. L13202, DOI:10.1029/2008GL033796.

[111] Boslough, M.B., Ahrens, T.J., Vizgirda, J., Becker, R.H., Epstein, S. (1982). Shock-induced devolatilization of calcite. *Earth and Planetary Science Letters*, vol. 61, no. 1, p. 166-170, DOI:10.1016/0012-821X(82)90049-8.

[112] Grady, D.E. (1976). *Processes Occurring in Shock Wave Compression of Rocks And Minerals*, Sandia Laboratories. Albuquerque, p. 1-83.

[113] Gupta, S.C., Love, S.G., Ahrens, T.J. (2002). Shock temperature in calcite (CaCO3) at 95-160 GPa. *Earth and Planetary Science Letters*, vol. 201, no. 1, p. 1-12, DOI:10.1016/S0012-821X(02)00685-4.

[114] Spray, J.G. (1999). Shocking rocks by cavitation and bubble implosion. *Geology*, vol. 27, no. 8, p. 695-698, DOI:10.1130/0091-7613(1999)027<0695:SRBCAB>2.3.CO;2.

3 Non-Contact Method for Analysis of Cavitating Flows

In this chapter, the manuscript entitled "Non-contact Method for Analysis of Cavitating Flows" by Ignacijo Biluš, Luka Lešnik, Benjamin Bizjan, Brane Širok, Matevž Dular, Boštjan Pečnik (under review in Ultrasonics) is presented.

The work presents a novel computer-aided method for investigation of velocity fields and pressure fluctuations in cavitating flows. The results presented in the manuscript are important for this thesis, as the discussed method has been tested in a setup with acoustic cavitation generated by an ultrasonic probe above the scaled specimens. The method provides a new means of analyzing the dynamics of cavitation structure growth and collapse visible from high speed images.

The method has been successfully evaluated by comparison to simultaneous hydrophone measurements of fluid pressure fluctuations. The main advantage of presented method is the ability to measure instantaneous two-dimensional pressure fields, which is achieved without any intrusions to the flow of interest. This is particularly important to study the relation between fluid pressure fluctuations and related scale erosion intensity. The algorithm for the flow pressure calculation is incorporated into our own open-source software *ADMflow*, which also allows for simultaneous calculation of flow velocity fields.

The graphical abstract of the paper is shown in Figure 4.

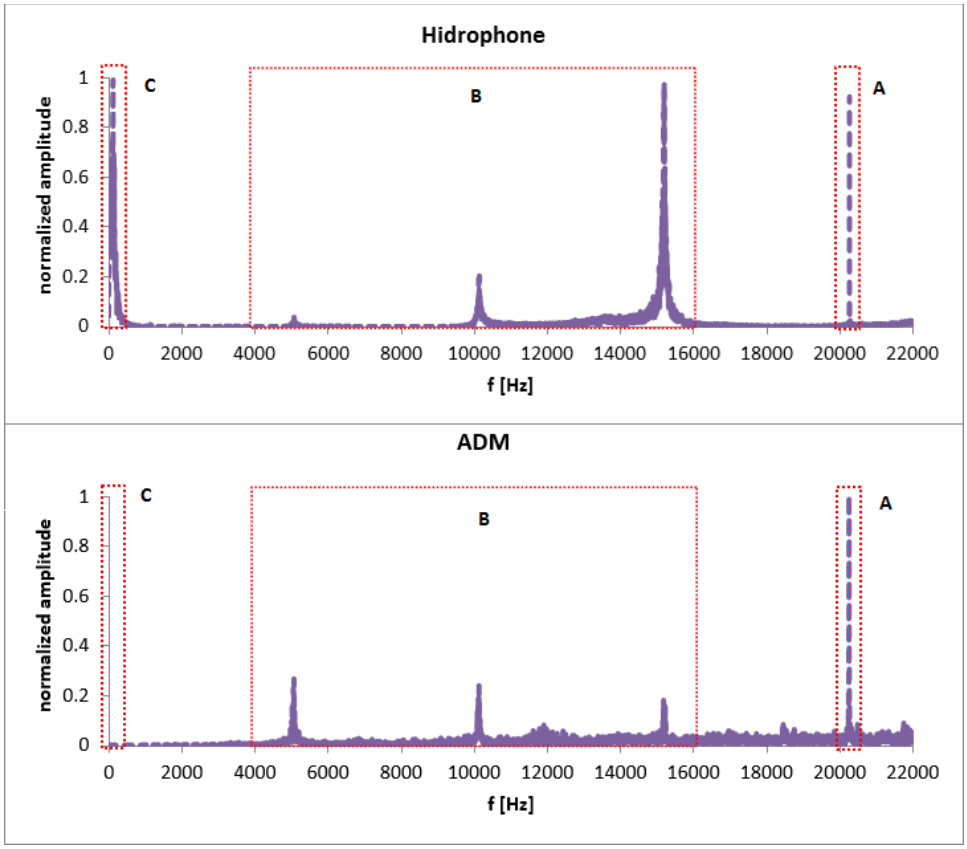


Figure 4**:** Pressure fluctuations spectra for 40% sonicator power level.

Elsevier Editorial System(tm) for Ultrasonics

Manuscript Draft

Manuscript Number:

Title: Non-contact Method for Analysis of Cavitating Flows

Article Type: Research paper

Section/Category: Process monitoring (F. Balle)

Keywords: Acoustic cavitation; sonicator; pressure measurement; hydrophone; computer-aided visualization; image velocimetry

Corresponding Author: Mr. Benjamin Bizjan,

Corresponding Author's Institution: University of Ljubljana, Faculty of Mechanical Engineering

First Author: Ignacijo Biluš

Order of Authors: Ignacijo Biluš; Luka Lešnik; Benjamin Bizjan; Brane Širok; Matevž Dular; Boštjan Pečnik

Abstract: This paper presents a novel non-contact method for simultaneous analysis of pressure and velocity conditions in cavitating flows. The method (implemented in our software ADMflow) is based on high-speed camera flow visualization and was evaluated in an experiment with ultrasonically induced acoustic cavitation of different intensities. Attached cavitation with clearly visible cavitation structures occurred on the tip of an ultrasonic probe immersed in distilled water. Using the high-speed imaging data, pressure fluctuations were calculated by a computer-aided algorithm based on the Brennen's theory of cavitation cloud kinematics and a modified version of the Rayleigh-Plesset equation. Reference measurements of the pressure pulsations were conducted by a hydrophone installed at the bottom of the liquid container. The analysis of cavitation structure dynamics was complemented by calculation of velocity fields from the imaging data, the algorithm for which is based on the advection-diffusion equation. Calculated pressure fluctuations were analyzed in the spatial, temporal and spectral domain. Presented results indicate a strong correlation between the fields of velocity and pressure fluctuations during the growth and collapse of cavitation structures. A comparison of time series and power spectra demonstrates that our cavitation analysis method is in a good agreement with results of the reference measurement methods and can therefore be used for non-contact analysis of pressure and velocity conditions in cavitating flows.

Manuscript
Click here to view linked References

Non-contact Method for Analysis of Cavitating Flows

Ignacijo Biluš[a], Luka Lešnik[a], Benjamin Bizjan*[b], Brane Širok[b], Matevž Dular[b], Boštjan Pečnik[c]

[a] University of Maribor, Faculty of Mechanical engineering, Smetanova ulica 17, 2000 Maribor, Slovenia

[b] University of Ljubljana, Faculty of Mechanical engineering, Aškerčeva 6, 1000 Ljubljana, Slovenia

[c] Gorenje d.d., Partizanska 12, 3503 Velenje, Slovenia

*Corresponding author. Email address: benjamin.bizjan@fs.uni.lj.si; Phone: +386 14771423

Abstract

This paper presents a novel non-contact method for simultaneous analysis of pressure and velocity conditions in cavitating flows. The method (implemented in our software *ADMflow*) is based on high-speed camera flow visualization and was evaluated in an experiment with ultrasonically induced acoustic cavitation of different intensities. Attached cavitation with clearly visible cavitation structures occurred on the tip of an ultrasonic probe immersed in distilled water. Using the high-speed imaging data, pressure fluctuations were calculated by a computer-aided algorithm based on the Brennen's theory of cavitation cloud kinematics and a modified version of the Rayleigh-Plesset equation. Reference measurements of the pressure pulsations were conducted by a hydrophone installed at the bottom of the liquid container. The analysis of cavitation structure dynamics was complemented by calculation of velocity fields from the imaging data, the algorithm for which is based on the advection-diffusion equation. Calculated pressure fluctuations were analyzed in the spatial, temporal and spectral domain. Presented results indicate a strong correlation between the fields of velocity and pressure fluctuations during the growth and collapse of cavitation structures. A comparison of time series and power spectra demonstrates that our cavitation analysis method is in a good agreement with results of the reference measurement methods and can therefore be used for non-contact analysis of pressure and velocity conditions in cavitating flows.

Keywords: Acoustic cavitation, sonicator, pressure measurement, hydrophone, computer-aided visualization, image velocimetry

1 Introduction

Cavitation is a highly complex hydrodynamic phenomenon in which vapor phase in form of bubbles or clouds is formed within the liquid as the pressure is locally decreased below the vaporization pressure [1]. Upon collapse of unstable cavitation structures, very high pressures and velocities occur locally, causing the erosion of exposed solid surfaces [1]. Cavitation can be induced hydrodynamically (i.e. due to the flow velocity) or ultrasonically (e.g. on an oscillating ultrasonic probe). Despite the rapid development of numerical modeling methods in the recent years, experimental methods remain important in research of complex cavitation phenomena. The methods most commonly used for this purpose are local measurements of pressure and temperature, as well as flow visualization (Verhaagen, Rivas [2]).

The main advantage of flow visualization techniques is the ability to obtain a large amount of flow dynamics data with a single measurement. Numerous flow visualization experiments were performed on cavitating hydrofoils (Wade and Acosta [3], Kubota et al. [4], Reisman and Brennen [5], Franc et al. [6], Kato et al. [7]). Apart from visualization, Reisman and Brennen [5] also performed spectral analysis of hydrophone-measured pressure fluctuations, and classified them to a local and global scale. Reisman et al. [8] applied high-speed flow visualization to study the highly complex mechanism of shock wave formation in cavitation clouds, and related mechanisms of noise formation and erosion. Osterman et al. [9] conducted simultaneous pressure measurements and visualization of incipient cavitation in a valve, demonstrating the visualization method to be more sensitive to cavitation and its signal independent of the operating pressure. An experiment with similar measurement techniques has recently been performed by Tzanakis et al. [10] to study ultrasonically induced acoustic cavitation in different liquids. A different approach was taken by Kato et al. [7], who combined the visualization of a cavitating flow with PIV velocity field measurements. Apart from pressure and velocity, another important property of cavitating flows is the volume fraction of the vapor phase. For typical high-speed imaging setups lit from the side opposite to the camera, light attenuation methods are used most commonly (Leppinen and Dalziel [11]).

For the most accurate characterization of cavitating phenomena, it is desired to combine measurements of different flow properties in the same experiment. However, using a different measurement method and device for each flow property (e.g. hydrophones for pressure, PIV for velocity and high-speed cameras for visualization) adds to the complexity and price of the measurement set-up, and is often impractical. The rapid development of high-speed imaging devices and flow analysis algorithms in the recent years has created the opportunity to measure several cavitating flow properties from a single image sequence, and possibly replace some of the more conventional measurement techniques. Speaking of the flow velocity measurement, it is known that the PIV and similar correlation-based methods require a quite complex measurement setup and may not always perform well when used with normal imaging sequences. The flow velocimetry methods based on the optical flow theory present a more robust alternative (i.e. less sensitive to the quality of imaging setup). An extensive overview of the optical flow methods is presented in works of Barron et al. [12] and Zimmer et al. [13]. Recently, a flow velocimetry method based on the optical flow and the advection-diffusion equation was developed by our research group at the University of Ljubljana (Bajcar et al. [14], Bizjan et al. [15][16]), and validated on several laboratory and industrial flow phenomena. This method will also be presented and applied in this manuscript.

Unlike velocity measurements, little research has been dedicated to the calculation of fluid pressure from flow visualization images in cavitating flows. Nevertheless, the mathematical modeling of bubble and cloud cavitation is extensively covered in the literature. The basic mathematical formulation for dynamics of cavitating spherical bubbles is the Rayleigh-Plesset equation (Plesset and Prosperetti [17]). The equation was later applied to the models for cloud cavitation (Brennen [1], d'Agostino and Brennen [18], Wang and Brennen [19], Shimada and Kobayashi [20]), which is much more common in practical technical applications than the simpler single bubble cavitation. The purpose of our manuscript is to apply the known theoretical cloud cavitation models to the analysis high-speed imaging data, and develop a non-contact method for measurement of fluid pressure fluctuations as a result.

2 Theoretical background

2.1 Pressure fluctuations in cavitating flow

As one of the most important physical quantities in cavitation phenomena, pressure is an inherent part of the Rayleigh-Plesset equation - Eq. (1) [20] [21]. Although the Rayleigh-Plesset equation was originally derived for a single spherical bubble, it is also valid for spherically shaped bubble clouds, provided that a correct form of mass and momentum conservation is used (Wang and Brennen [19]).

$$R\left(1-\frac{\dot{R}}{c}\right)\ddot{R}+\frac{3}{2}\left(1-\frac{\dot{R}}{3c}\right)\dot{R}^2=\frac{1}{\rho_L}\left(1+\frac{\dot{R}}{c}+\frac{R}{c}\frac{d}{dt}\right)\left(p-p_\infty-4\frac{\mu_L}{R}\dot{R}\right) \quad (1)$$

In Eq. (1), *R* represents the equivalent diameter of cavitation cloud, *c* speed of sound in fluid, *p* pressure inside the cavitation cloud observed, μ_L fluid kinematic viscosity, ρ_L fluid density, and p_∞ fluid ambient pressure. The effect of surface tension is neglected. According to d'Agostino and Brennen [18], the bubble cloud interfacial velocity $\dot{R}$ is largely subsonic in fluids whose oscillatory dynamics is analyzed in the neighborhood of an equilibrium configuration and at excitation frequencies not much larger that the natural frequencies of individual bubbles. When c >> $\dot{R}$, a simplified formulation can be derived from Eq. (1) for calculation of pressure fluctuation in cavitation cloud observed:

$$R\ddot{R}+\frac{3}{2}\dot{R}^2=\frac{1}{\rho_L}\left(p-p_\infty-4\frac{\mu_L}{R}\dot{R}\right) \quad (2)$$

Taking grayscale image sequence as input data, the equivalent diameter of cavitation cloud *R* can be assumed to be proportional to the mean image gray level *A* in the monitoring window, $R \propto A$ [11], with proportionality constant *K* = *R*/*A* (unit: m). The value of *A* at particular time t can be calculated using Eq. (3).

$$A(t)=\sum_{i=1}^{i=N}\sum_{j=1}^{M}E(i,j,t); \quad E(i,j,t)\epsilon\{0 \div 1\} \quad (3)$$

The equivalent cloud diameter (i.e. the intensity of gray level fluctuations) was monitored in a rectangular monitoring window of height *M* and width *N* (in pixels), where *E* was the gray level value of a particular pixel at position (*i*, *j*, *t*). The first and second temporal derivatives of *A* ($\dot{A}$ and $\ddot{A}$, respectively) are calculated using standard numerical derivation schemes. Finally, the instantaneous flow pressure *p*(*t*) can be expressed as:

$$p(t)=p_\infty+K^2\rho_L\left(A\ddot{A}+\frac{3}{2}\dot{A}^2\right)+4\frac{\mu_L}{A}\dot{A} \quad (4)$$

Resulting time series can be, depending on selection of calculation parameters and software implementation, 1D (integral values of instantaneous pressure within selected window) or 2D (instantaneous pressure fields within selected window).

2.2 Cavitation structure velocity

The image sequence previously used for pressure calculation can also be used to compute velocity fields of cavitation structures during the growth and collapse phase. Velocity field calculations in this manuscript will be performed according to the algorithm developed by Bajcar et al. [14] and Bizjan et al. [15][16]. This velocity calculation algorithm is based on a simplified advection-diffusion equation for incompressible fluid, formulated as:

$$\frac{\partial N}{\partial t} + \frac{\partial (N v_x)}{\partial x} + \frac{\partial \left(N v_y\right)}{\partial y} = D\left(\frac{\partial^2 N}{\partial x^2} + \frac{\partial^2 N}{\partial y^2}\right) \tag{5}$$

where the concentration of cavitation phase N is assumed to be proportional to the intensity of gray level A in the monitoring window [15][16]. D represents the diffusion coefficient of the liquid phase, while v_x and v_y are unknown components of velocity vector **v** = (v_x, v_y) obtained on location (i, j) for each image. In order to close the equation system the temporal and spatial smoothing models were used combined with the image downsampling. The final solution of the equation system is obtained using the least squares method. Details about the velocity calculation algorithm can be found in references [15] and [16].

Both velocity and pressure calculation algorithms presented in this paper are now implemented in our flow visualization software *ADMflow* (available at https://amdflow.net), which was also used for calculations in this paper.

3 Experimental set-up

Experimental measurements of ultrasonically introduced cavitation below the sonicator probe were conducted in a transparent PMMA (poly methyl methacrylate) glass chamber with dimensions of 100x100x100 mm (experimental setup shown in Fig. 1). The chamber was filled with 600 mL of distilled water at the ambient temperature (20°C). Cavitation was generated with an ultrasonic probe of the sonicator (Cole Parmer 4710 series ultrasound homogenizer, model CO300), which had a 3mm diameter on its bottom. The ultrasonic probe resonated at a frequency of 20 kHz and was operated at different dimensionless power levels *P*. *P* was defined as the ratio between the current and maximum allowable sonotrode tip oscillation amplitude, and was varied between 20% and 40%. The tip of the probe was placed in the center of the chamber, 5 mm above the measuring bore, perpendicular to the chamber bottom and submerged in distillated water, as shown in Fig. 1. The exact placement was achieved using a positioning table which allowed accurate adjustments of sonicator height.

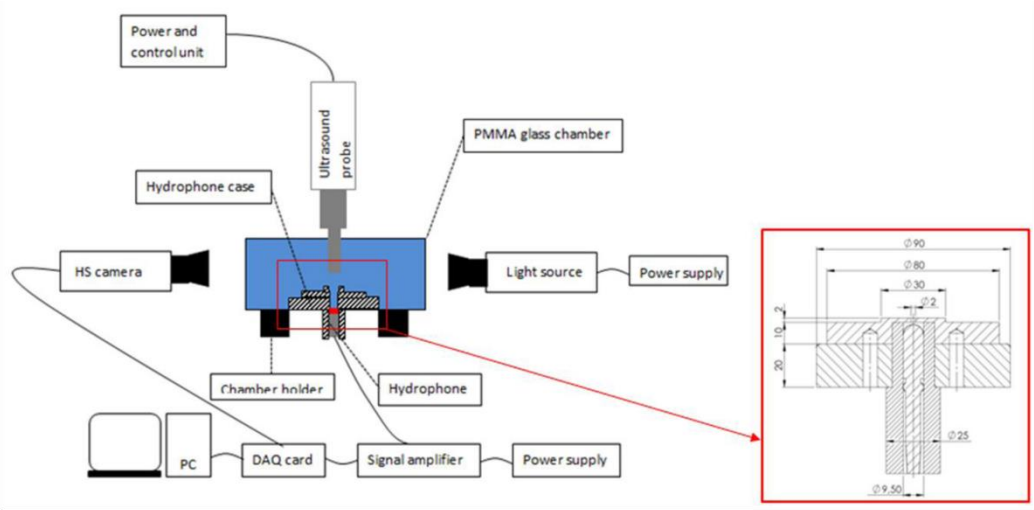


Fig. 1. Experimental set-up

Cavitation induced pressure fluctuations were measured by a hydrophone (Teledyne-Reson TC4013), which worked on a piezoelectric principle and had a sensitivity of -211dB ±3db with an output of 1V/µPa. Hydrophone output signal was sampled with 200 kHz and acquired to a computer. The hydrophone was mounted in a specially designed casing at the bottom of the glass chamber (detailed view in Fig. 1), so that its tip was located in a bore 2mm below the casing bottom.

Simultaneously with the hydrophone measurements, cavitation structures were also visualized by a high-speed camera (Fastec Imaging Hispec 4 Mono) with 85 mm Samyang AE macro lens placed 420 mm away from the chamber wall. A light source for illumination of the viewing area was placed on the side of the chamber opposite to the camera so that the ultrasonic probe was placed in the center between them. High-speed imaging data was acquired with 64031 frames per second and 2 µs exposure time. Image resolution was 128x80 pixels, with 0.03 mm pixel size.

After acquisition, high-speed images of cavitation structures were imported in the *ADMflow* software, where velocity and pressure fields were calculated following the methodology presented in the "Theoretical background" section.

4 Results and discussions

4.1 Hydrophone measurements

Pressure fluctuations measured by the hydrophone were acquired in form of discrete time series $p(t)$. A sample time series for 30% sonicator power level is shown in Fig. 2.

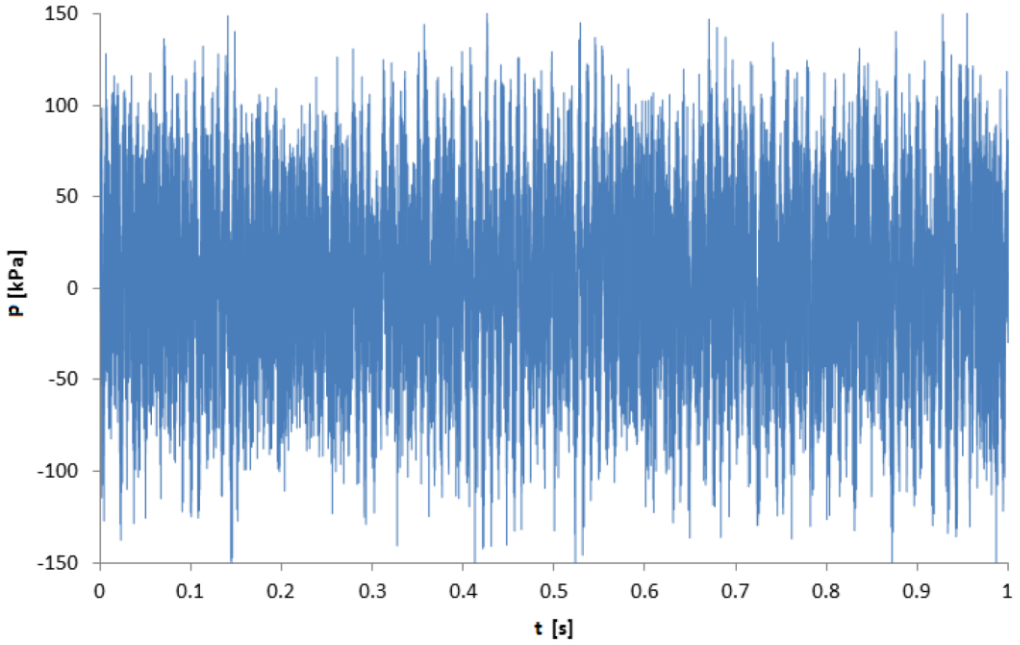


Fig. 2. Time series of pressure fluctuations measured by the hydrophone

To characterize the magnitude of pressure fluctuations (and consequently, acoustic cavitation), root-mean-square (RMS) values of the time series were calculated. In Fig. 3, pressure RMS values (p_{RMS}) are shown with respect to the sonicator power level *P*. It can be seen that higher sonicator powers lead to an almost linear increase in pressure RMS values, which indicates a more intense cavitation.

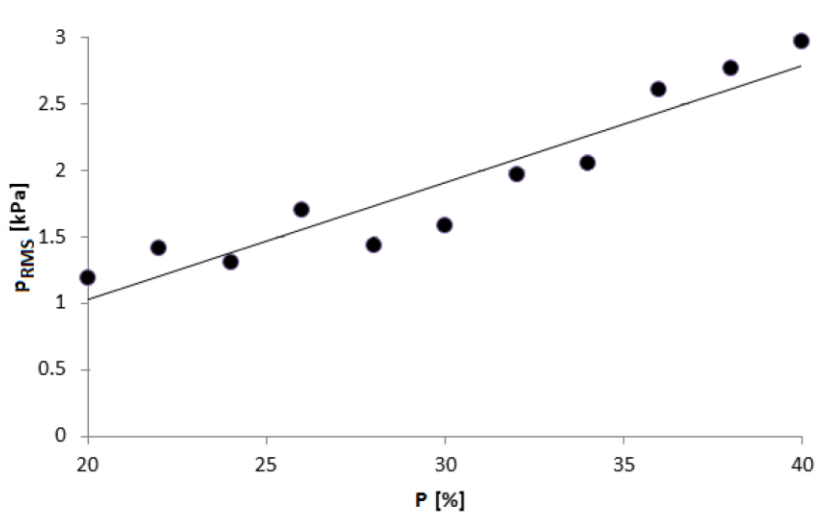


Fig. 1. Influence of sonicator power level on cavitation pressure fluctuation intensity

4.2 Image analysis results

The region in which the cavitating flow was visualized is presented in Fig. 4, where three consecutive flow images are shown along with the windows which were used for pressure and velocity calculations in *ADMflow*. In the upper central part of the images, the tip of the ultrasonic probe can be seen.

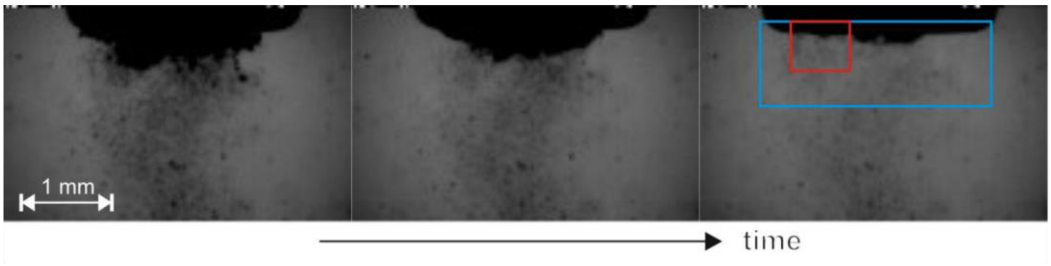


Fig. 2. Consecutive images of cavitation structure (frame separation 15.6 µs) with pressure/velocity field calculation area (blue rectangle) and pressure time series calculation area (red rectangle)

In Figs. 5, 6 and 7, results of cavitation structure image analysis are presented for different sonicator power levels (20%, 30% and 40%, respectively) and compared to the hydrophone data. In these figures, a) panels show calculated normalized pressure fields, b) panels velocity vector fields on visualization image background, and c) panels comparisons between normalized pressure fluctuations (Δp_{norm}) calculated in *ADMflow* (ADM) and those measured by the hydrophone (HF). Pressure and velocity fields in panels a) and b) were calculated for three consecutive frames 15.6 µs apart. Calculations were performed according to the presented pressure calculation model (Eqs. 2 and 3) and the velocity field calculation model (Eq. 5).

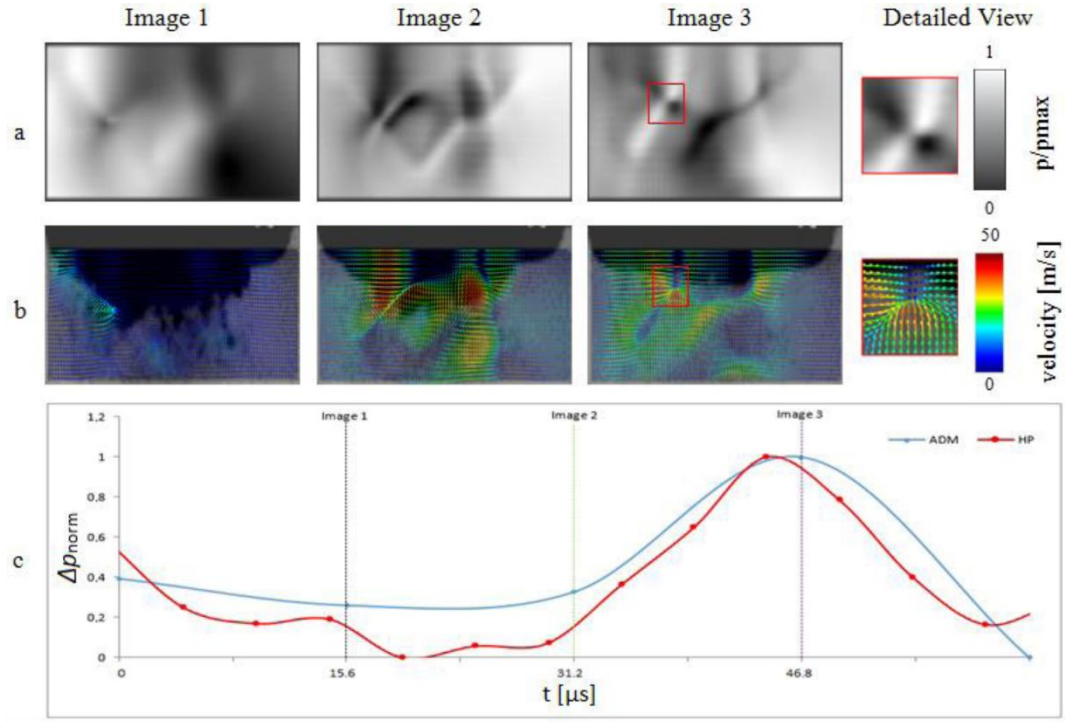


Fig. 3. Pressure and velocity fields at 20% sonicator power level

In Fig. 5, cavitation phenomena were investigated at the lowest sonicator power level used (20%). Consecutive images in Fig. 5b show the cavitation cloud collapse, which is marked by a decrease of the vapor volume fraction drops in the region of attached cavitation on sonicator probe. The calculated sequence of pressure distributions is shown in Fig. 5a, where lighter shades of grey present the region with higher pressures. Evident are intense spatial fluctuations of pressure field topology which take linear or spherical shape. A detailed view of the pressure field topology is shown in the red window on the right side of Figs. 5a.

Velocity fields (Fig. 5b) characterize the kinematics of vapor phase in the cavitation cloud and its neighborhood. It is evident that the velocity magnitude increases when the cavitation cloud shrinks (image 2), especially at its edges. Similarly to the pressure distribution images in Fig. 5a, the regions with intensified kinematics exist in velocity fields. The velocity vector field shown in Fig. 5b (image 3) can be connected to the local linear or spherical shape of vapor phase sink (images at Fig. 5a) as shown in the detailed view (red window on the right side of Fig. 5b).

The comparison of flow fields in analyzed windows indicates causality between velocity and pressure fields. The inhomogeneity of pressure distribution is connected to velocity field distributions around it. It can be seen that velocity vectors are oriented in the direction of maximum pressure gradients. Also, the locations of maximum pressure gradients coincide with areas of the maximum velocity magnitude.

Besides the two dimensional flow field analysis, the time series (Fig. 5c) of mean pressures within the window of interest (red window in Fig. 5a right) were also analyzed and compared to the hydrophone signal. The window of interest was selected according to most intense pressure change expected from the pressure distribution images in Fig. 5a. The blue curve in

the diagram in Fig. 5c shows calculated pressure values in the window of interest while the red curve shows pressures simultaneously measured by a hydrophone. In the pressure time series diagrams, a significant pressure increase can be observed between image 2 and image 3, which is a consequence of the local cavitation structure collapse. The collapse begins as the pressure curve rises, which is seen in as the formation of a distinct anomaly in the pressure field and velocity field gradients perpendicular to the pressure extreme. The process is followed by a pressure increase in the region of collapse which has linear or spherical shape. Considering the pressure time series, pressure field distribution and velocity field in the window of interest it can be concluded that the analyzed phenomenon belongs to the local collapse of the cavitation cloud.

Several cavitation structures in selected time intervals were analyzed in present study. The examples presented in Figs. 6 and 7 were selected with consideration to the intensity of the linear structure in pressure and velocity fields. Resulting pressure and velocity fields (similar to Fig. 5) are presented in the following part of the paper. It is evident that the onset of the pressure anomalies and the increase in velocity magnitude correspond to a reduction of the vapor phase volume fraction on an integral level, and consequently of the attached cavitation on the sonicator. Regional reduction of the attached cavitation (Figs. 6 and 7) is followed by pressure and velocity field inhomogeneity. The increase of pressure gradients is evident in both analyzed cases at successive images 2 and 3. Distinct local minima with velocity vectors oriented in the maximum gradient direction are evident in the first phase of the collapse shown in image 2 for both analyzed cases. This indicates the movement of the continuum in the direction of local pressure minimum and corresponds to the second point on blue curves of the pressure time series presented in Figs. 6c and 7c. This phase is followed by a rapid increase of pressure whereby local extreme is achieved in image 3 and confirmed by the extremes of the blue curve (point 3) in the diagram. Similarly to analysis results presented in Fig. 5, also in Figs. 6 and 7 there is a good agreement between hydrophone-measured and *ADMflow*-calculated pressure time series. Clearly, the hydrophone-measured pressure follows the changes in the magnitude of the pressure field, as well as the magnitude and direction of velocity vectors in the region of local collapses in cavitation clouds. The causal link between local pressure anomalies and excited speed oscillations in their close proximity can also be concluded from the analyzed cases.

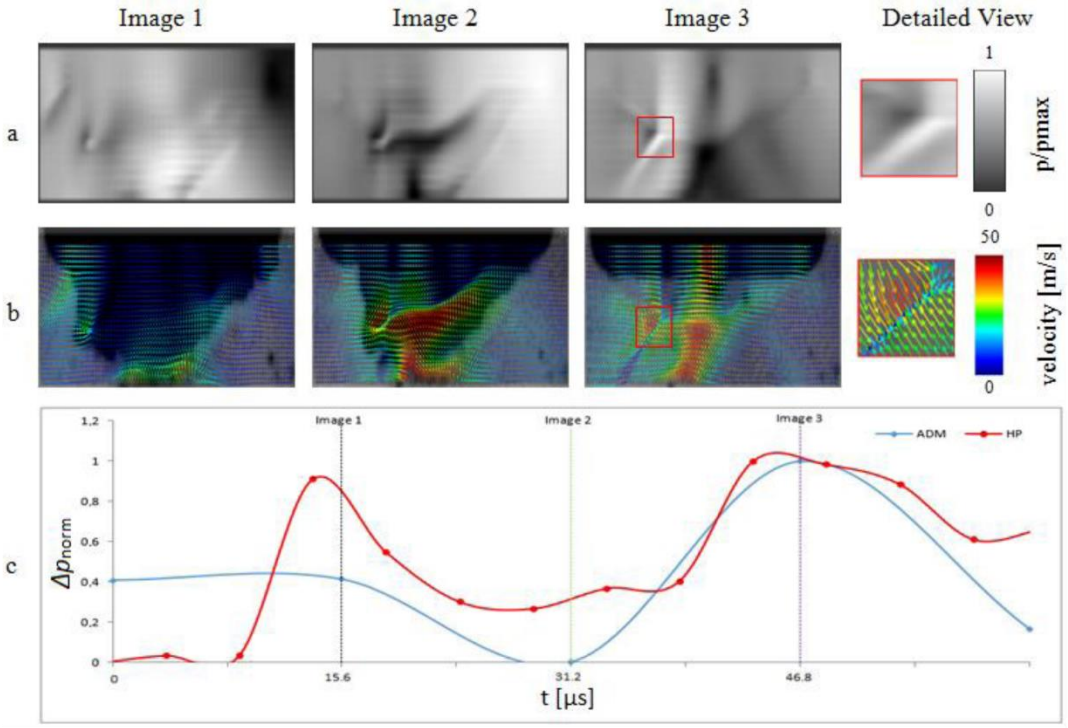


Fig. 4. Pressure and velocity fields at 30% sonicator power level

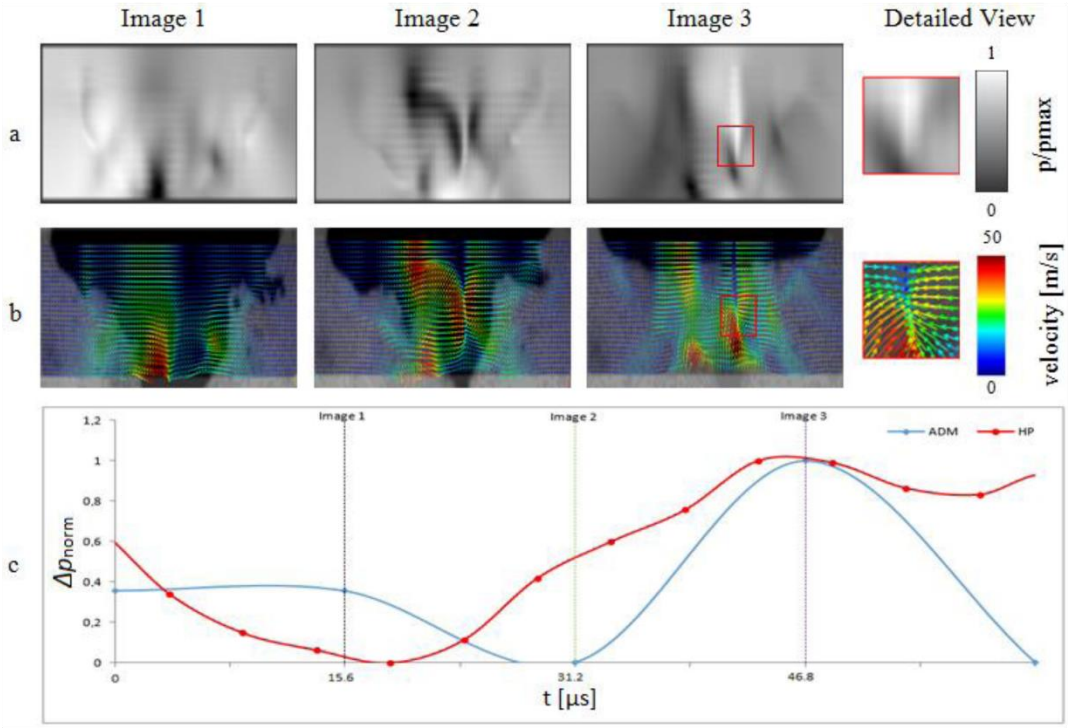


Fig. 5. Pressure and velocity fields at 40% sonicator power level

4.3 Spectral analysis of pressure time series

The diagrams in Fig. 8 shows the power spectra of pressure time series obtained by hydrophone measurements (upper panel) and those calculated by our algorithm in *ADMflow* (lower panel) using flow visualization images as input. The power spectra comparison will serve for a physical interpretation of flow phenomena in individual ranges of frequency (*f*), and to assess the suitability of our pressure calculation algorithm as a cavitation diagnostic method.

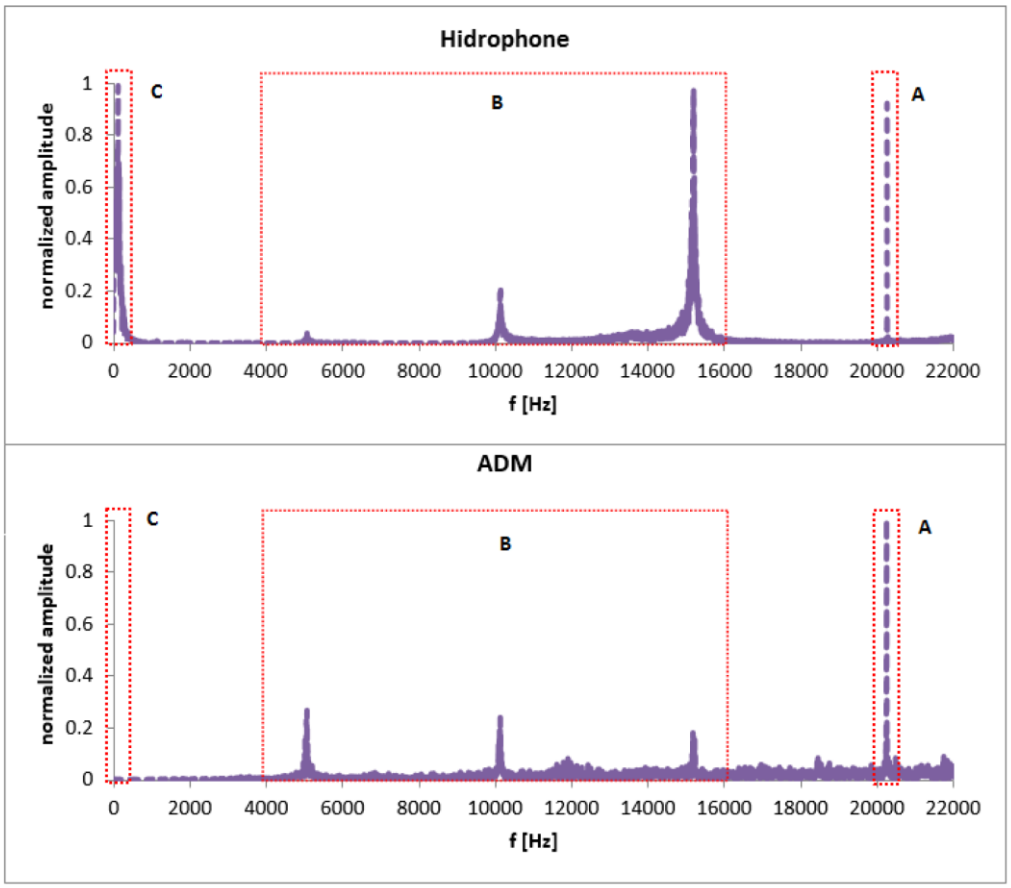


Fig. 8. Pressure fluctuations spectra for 40% sonicator power level

Power spectra in Fig. 8 can be divided to a low-frequency range (A), medium frequency range (B) and high frequency range (C). In the frequency range (A), it is possible to observe that both methods respond similarly to the excitation frequency of the sonicator (20 kHz). It can be concluded that periodical oscillation of attached cavitation on the sonicator reflects in the form of a pressure disturbance in the cavitation cloud and results in pulsations at hydrophone as well.

The frequency range (B) (4-16 kHz) is likely to be connected to oscillations due to the cloud cavitation under the region of attached cavitation. Distinct pressure pulsations can be seen in this area, which are connected to collapses in the cavitation cloud (Figs. 5, 6 and 7). This is

the main mechanism of cavitation shocks associated with erosion effects [8]. Resulting pressure pulsations occur in a broad band of frequencies, which depend on sonicator excitation power. When comparing both diagrams, it can be concluded that the positions of frequency peaks in the frequency range 4 d 16 kHz is in good agreement for both methods used.

At the lowest frequency range (C), only the hydrophone was able to detect pulsations in the frequency range below 500Hz (with most significant peaks occurring between 0 and 30 Hz), while the calculated pressure yields zero amplitude in this part of the power spectrum. Considering the fact that the oscillations after the Brennen´s model [18] [19] directly reflect the oscillations of the vapor phase, the hydrophone signal pulsations most likely result from the fluid-solid interaction between water and reservoir walls, which is not visible in flow images. Since such low frequency pulsations are not significant for characterization of cavitation phenomena, it can be concluded that our pressure calculation algorithm is able to detect all cavitation-related fluctuations otherwise detectible by the hydrophone, provided that the imaging frame rate is sufficiently high.

To compare power spectra of calculated and hydrophone-measured pressure signals at other sonicator power levels, three-dimensional spectra are shown in Fig. 9. Such representation allows for assessment of sonicator power level effect on cavitation dynamics.

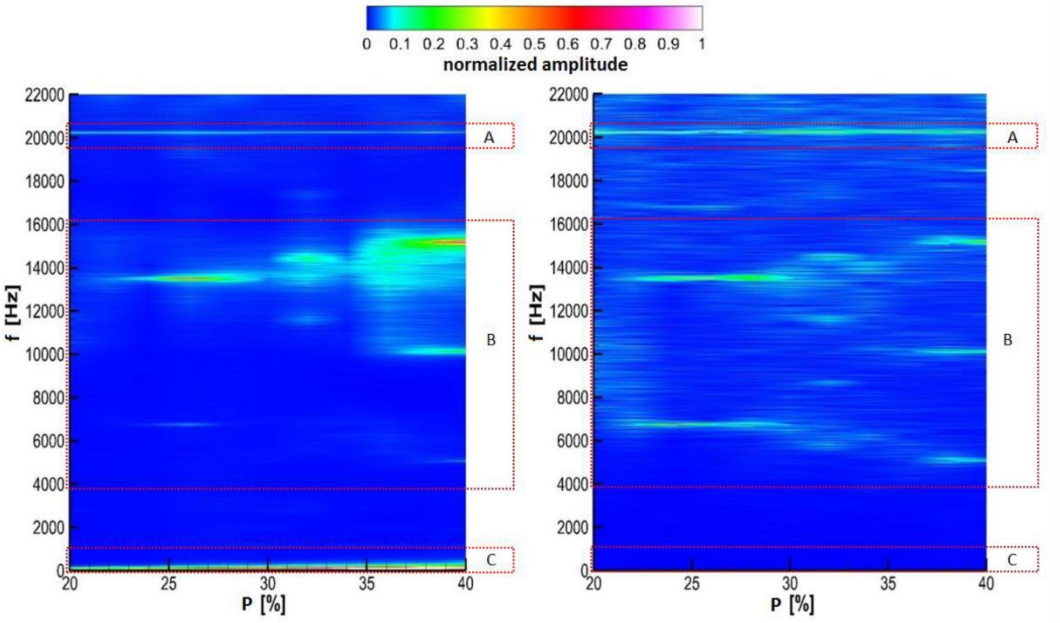


Fig. 9. Frequency specters at different sonicator power levels (left – hydrophone, right – *ADMflow*)

As in Fig. 8, the frequency range can be divided into three frequency subranges (A, B and C). The excitation frequency of 20 kHz (subrange A) is expressed in the entire range of sonicator power levels for modeled and measured pressure signal. Also in the medium frequency subrange (B) of 4-16 kHz, the spectral amplitude dependence is similar for both measured

and calculated pressures. The phenomenon is broad banded and its frequency band expands at higher sonicator power levels as the cavitation collapses become more intense. Similarly to Fig. 8, some frequency peaks are more pronounced than the others. Also, once again, the pressure pulsations occurring at the lowest frequencies are only detectible in the hydrophone pressure signal. As expected, their amplitude and bandwidth increases with the sonicator power level.

5 Conclusions

The paper presents a novel non-contact method for the measurement of pressure and velocity fields of cavitating flows, which uses high-speed imaging data as its input and is implemented in the *ADMflow* software. The method was tested on the case of attached cavitation below the ultrasonic probe and validated with hydrophone pressure measurements. Experimental results confirm causality between velocity and pressure fields in the phase of cavitation structures collapse, as velocity maxima occur near the maximum pressure gradients. Also, the boundaries of the high velocity areas seem to coincide with the linear or spherical shape of observed cavitation phenomena. Regardless of the sonicator power level and related probe oscillation amplitude, the cavitation cloud collapse causes the pressure and velocity field to become highly inhomogeneous. The progress of local pressure and velocity disturbance is also reflected in local averaged pressure values in the selected regions of interest and has been shown to fit well to the values measured by a hydrophone.

Results of the spectral analysis of pressure signals indicate that the cloud cavitation phenomenon is broad banded and dependent on sonicator excitation power. As in the case of the time series, there is a good agreement in the power spectra for the calculated and hydrophone-measured signal. This confirms the suitability of presented visualization method for the diagnosis and prediction of cavitation strokes mechanism, which can be further linked to the effects of cavitation erosion. The presented flow visualization and analysis system can be adapted to different fluid flow examples in a variety of engineering applications.

References

[1] C.E. Brennen, *Cavitation and Bubble Dynamics*, Oxford University Press, 1995.

[2] B. Verhaagen, D.F. Rivas, *Measuring cavitation and its cleaning effect*. Ultrasonics sonochemistry, 29, 619-628, 2016.

[3] R.B. Wade, A.J. Acosta, *Experimental observation on the flow past a plano-convex hydrofoil*, Transaction of ASME, Journal of Basic Engineering, 87, 273–283, 1966.

[4] A. Kubota, H. Kato, H. Yamaguchi, M. Maeda, *Unsteady structure measurement of cloud cavitation on a foil section using conditional sampling technique*, Journal of Fluids Engineering, 111(2), 204–210, 1989.

[5] G.E. Reisman, C.E. Brennen, *Pressure pulses generated by cloud cavitation*, ASME Fluids Engineering Division Conference, 1996.

[6] J.P. Franc, E. Janson, P. Morel, C. Rebattet, M. Riondet, *Visualizations of leading edge cavitation in an inducer at different temperatures*. Proceedings of the 4 International Symposium on Cavitation CAV2001, California Institute of Technology, Pasadena, CA USA, 2001.

[7] K. Kato, H. Dan, Y. Matsudaira, *Lock-in Phenomenon of Pitching Hydrofoil with Cavitation Breakdown (Unsteady Fluid Force Characteristics and Visualization of Flow Structures)*, Department od Systems Engineering Science, Tokyo Metropolitan Institute of Technology, 6-6 Asahigaoka, Hino-shi, Tokyo 191-0065, Japan, 2006.

[8] G.E. Reisman, Y.C. Wang, C.E. Brennen, *Observations of shock waves in cloud cavitation*, Journal of Fluid Mechanics, 355, 255-283, 1998.

[9] A. Osterman, M. Hočevar, B. Širok, M. Dular, *Characterization of incipient cavitation in axial valve by hydrophone and visualization*. Experimental Thermal and Fluid Science, 33, 620-629, 2009.

[10] I. Tzanakis, G.S.B. Lebon, D.G. Eskin, K.A. Pericleous, *Characterizing the cavitation development and acoustic spectrum in various liquids*, Ultrasonics Sonochemistry (2016), doi: http://dx.doi.org/10.1016/j.ultsonch.2016.06.034

[11] D. M. Leppinen, S.B. Dalziel, *A light attenuation technique for void fraction measurement of microbubbles*, Experiments in Fluids, vol.30, no. 2, 214-220, 2001.

[12] J.L. Barron, D.J. Fleet, S. Beauchemis, *Performance of optical flow techniques*. Int J Comput Vis, 12, 43–77, 1994.

[13] H. Zimmer, A. Bruhn, W. Joachim, *Optic flow in harmony*. Int J Comput Vis, 93, 368–88, 2011.

[14] T. Bajcar, B. Širok, M. Eberlinc, *Quantification of flow kinematics using computer-aided visualization*. Strojniški vestnik – Journal of Mechanical Engineering, 55(4), 215-223, 2009.

[15] B. Bizjan, A. Orbanić, B. Širok, T. Bajcar, L. Novak, B. Kovač *Flow Image Velocimetry Method Based on Advection-Diffusion Equation*, Strojniški vestnik – Journal of Mechanical Engineering, 60(7-8), 483-494, 2014.

[16] B Bizjan, A Orbanić, B Širok, B Kovač, T Bajcar, I Kavkler. *A computer-aided visualization method for flow analysis.* Flow Measurement and Instrumentation, 38, 1-8, 2014.

[17] M.S. Plesset, A. Prosperetti, *Bubble Dynamics and Cavitation*. Annual Review of Fluid Mechanics, 9, 145–185, 1977.

[18] L. d'Agostino, C. E. Brennen, *Linearized dynamics of spherical bubble clouds*. J. Fluid Mech. 199, 155-176, 1989.

[19] Y.C. Wang, C.E. Brennen, *Numerical Computation of Shock Waves in a Spherical Cloud of Cavitation Bubbles*. Journal of Fluids Engineering, 121 (4), 872-880, 1999.

[20] M. Shimada, T. Kobayashi, *Dynamics of Cloud cavitation and Cavitation erosion*, Proceedings of the 1999 ASME Fluids Engineering Summer meeting 1999, San Francisco, 1-6, 1999.

[21] A. Prosperetti, Bubble phenomena in sound Fields: Part one. Ultrasonics, March, 69-78, 1984.

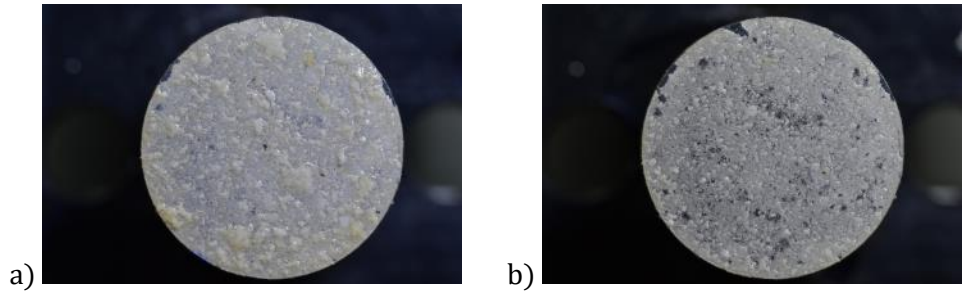
4 Cavitation Erosion of the Calcium Carbonate Deposits

In this chapter, the paper entitled "Cavitation erosion of the calcium carbonate deposits" by Boštjan Pečnik, Roman Sturm, Marko Hočevar, Matevž Dular and Brane Širok (Pečnik et al., 2015) is presented.

The work aimed to research erosion effects caused by acoustic cavitation on metallic and enamelled specimens coated with calcium carbonate (limescale). Simultaneously with the monitoring of cavitation above the specimens, the destruction of scale on the surface of specimens was analysed.

The results of experiments indicate a characteristic effect of cavitation intensity on the destruction (i.e. removal) of scale on the surface of specimens. The intensity of cavitation erosion is proportional to the voltage on the sonotrode and consequently, the intensity of pressure fluctuations. It is also affected by the roughness of the surface of specimens, on which the scales were deposited, with erosion effect generally decreasing on rougher surfaces. However, the spallation and delamination mechanisms of scale removal were found to also depend on factors other than the specimen surface roughness.

The graphical abstract of the paper is shown in Figures 5 and 6.



a) b)

Figure 5: Specimen 7 with deposited scale (a) before cavitation and (b) after cavitation (π=0,547(-), ε=0,238(-)).

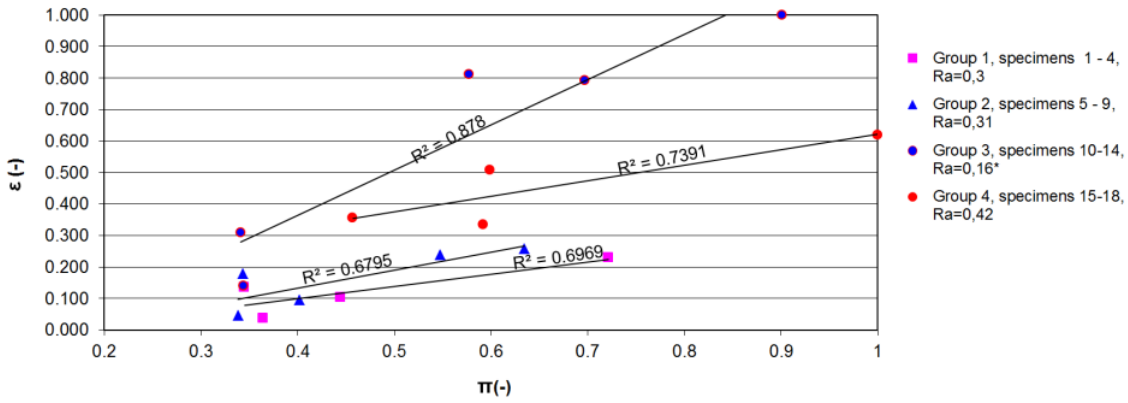


Figure 6: Model of cavitation cloud dynamics and different basic material (Ra for metal and Ra* for enamel).

Int. J. Microstructure and Materials Properties, Vol. 10, Nos. 5/6, 2015 445

Cavitation erosion of the calcium carbonate deposits

Boštjan Pečnik*

Jožef Stefan International Postgraduate School,
Jamova cesta 39,
1000 Ljubljana, Slovenia and Gorenje d.d.,
Partizanska 12, 3503 Velenje, Slovenia
Email: bostjan.pecnik@gorenje.com
*Corresponding author

Roman Šturm, Marko Hočevar, Matevž Dular and Brane Širok

Faculty of Mechanical Engineering,
University of Ljubljana,
Aškerčeva 6, 1000 Ljubljana, Slovenia
Email: roman.sturm@fs.uni-lj.si
Email: marko.hocevar@fs.uni-lj.si
Email: matevz.dular@fs.uni-lj.si
Email: brane.sirok@fs.uni-lj.si

Abstract: The paper presents the research of erosion effects caused by acoustic cavitation on metallic and enamelled specimens coated with calcium carbonate – scale. The deposition of calcium carbonate was performed under controlled laboratory conditions. The deposition took place at the same integral conditions to the specimens of different surface roughness. Cavitation as a cause of erosion was generated in a vessel with ultrasonic excitation. Simultaneously with the monitoring of cavitation above the specimens, the destruction of scale on the surface of specimens was analysed. The results of experiments indicate a characteristic effect of cavitation intensity on the destruction of scale surface layer. The intensity of cavitation erosion is proportional to the voltage on the sonotrode or the intensity of pressure fluctuations, and depends on the roughness of the surface of specimens, on which the scales were deposited.

Keywords: cavitation erosion model; scale; cavitation; material properties.

Reference to this paper should be made as follows: Pečnik, B., Šturm, R., Hočevar, M., Dular, M. and Širok, B. (2015) 'Cavitation erosion of the calcium carbonate deposits', *Int. J. Microstructure and Materials Properties*, Vol. 10, Nos. 5/6, pp.445–462.

Biographical notes: Boštjan Pečnik received his Bachelor of Science degree at the University of Ljubljana, Faculty of Mechanical Engineering in 1995. He has close to 20 years experiences in household appliances business in the field of R&D, product management and production. He was Head of Cooking Appliances R&D in Gorenje Group from 1997 to 2002. From 2002 to 2003, he was Head of R&D for small motorised appliances in Bosch und Siemens Haushaltsgeräte Department in Nazarje, Slovenia. Since 2006, he is an Executive Director for R&D of the Gorenje Group.

Copyright © 2015 Inderscience Enterprises Ltd.

Roman Šturm is an Associate Professor at the Faculty of Mechanical Engineering, University of Ljubljana, Slovenia. His main field of interest is laser surface heat treatment, and materials characterisation. Till now, he had published more than 40 scientific articles and had presentations at more than 60 international conferences. In the past he worked in industry. After that he was four years the Head of Laboratory for Creep Testing at the Institute of Metals and Technology, Slovenia. Now, he is the Head of Laboratory for heat treatment, and vice dean of the Faculty of Mechanical Engineering.

Marko Hočevar has received a BSc in Physics in 1996. Later, he worked in Turboinstitut, Institute for Turbine Machinery until 2000. Later, he worked at the Faculty of Mechanical Engineering, University of Ljubljana as Assistant and 2011 as an Associate Professor. He is involved in experimental work in a broad field of energy engineering. Until now, he has published more than scientific journal 60 papers with review.

Matevž Dular finished his undergraduate studies in 2002 at the University of Ljubljana. He then worked as a PhD student at the TU Darmstadt. Later, he was for two years and was a project manager of high temperature pump development at the Hidria Corporation. He was appointed as an Assistant Professor in 2007 and as an Associate Professor in 2012. His main fields of interest include general fluid mechanics, turbine machinery, cavitation, erosion, computational fluid dynamics and visualisation. He authored 42 reviewed journal papers. He advised six PhD and 20 BSc or MSc students.

Brane Širok has received a BSc from Faculty of Mechanical Engineering, University of Ljubljana in 1980. Later, he was Head of Applied Aerodynamics Department at Turboinstitut, Institute of Turbine Machinery. In 1996, he moved to a position of Professor Faculty of Mechanical Engineering, where he is a dean since 2013. His research interests are flow and process visualisation, experiment-based modelling and turbine machinery. He authored more than 150 reviewed journal papers.

1 Introduction

The accumulation of $CaCO_3$ (scale) is one of significant disturbances that affects a series of industrial processes, such as the membrane filtration (desalination) and heat transfer. The heat exchangers include two effects: the first one, where the heat transfer from the water to the heat exchanger wall is reduced already in case of thin scale layers, and the second one, where the scale acts as a thermal insulator causing the overheating of heating bodies that result in their malfunctions. The scale deposits may also cause a characteristic decrease of pipe flow. In the households in a hard water environment, the function and energy efficiency of machines is decreased in case of household appliances, such as boilers and washing machines. This causes additional operational costs as a result of servicing, parts replacement and higher electricity bills up to 25% (DOE, 2011). Currently, the use of chemicals is the most efficient method for preventing scale deposits. However, chemicals are expensive and prone to environmental concerns. We therefore search for cheaper and environment-friendly procedures, where, as stated in recent review (Hasson et al., 2011), the most promising green scale inhibitors are based on polyaspartic acid. Among them are the methods with surface treatment lime layer

(MacAdam and Parsons, 2004). The purpose of this paper is to present ultrasonic cavitation as a promising hydrodynamic procedure for the scale removal. The paper will present an evaluation of the impact of ultrasonic cavitation on the removal of calcium carbonate deposited on a metallic and enamelled surface with different roughness. It will include the research of the parameters of roughness and intensity of ultrasonic cavitation on the removal of calcium carbonate, which will be assessed using a visualisation comparison method on a macro-scale.

The formation of $CaCO_3$ (scale) is a complex process that depends on numerous factors, such as the level of oversaturation, the composition of fluid, the temperature, the hydrodynamic – flow conditions and the properties of surfaces on which it accumulates, such as the surface energy and roughness (MacAdam and Parsons, 2004; Karabelas, 2002). The dissolved CO_2 in water forms a weak carbon acid that dissociates into hydrogen carbonate, hydrogen and carbonate ions. Calcium ions react with bicarbonate which then exists in balance with calcium carbonate and carbon dioxide. The entire reaction may be written as

$$Ca^{2+} + 2HCO_3^- \rightarrow CaCO_{3(s)} + CO_{2(g)} + H_2O$$

The physical process of the formation of solid structure of $CaCO_{3(s)}$ includes the formation of ions, clustering, nucleation and growth of crystals in agglomerated clusters on solid surfaces. Calcium carbonate is formed in different polymorphic crystal forms, which, in spite of the fact that they are chemically identical, have different crystal structures, which is why they differ in the macro- and micro-structural properties. Calcium carbonate may appear in the form of three crystal structures: vaterite, aragonite and calcite (Elfil and Roques, 2001). Calcite and aragonite are the most common polymorphic structures.

Factors that affect the level of deposition, the extent and type of polymorphic structure on solid walls, include the following: pH factor, temperature T, flow conditions in a liquid at solid walls, surface properties, presence of impurities, presence of other ions and time t.

The paper will present the aragonite structure of calcium carbonate deposited under controlled conditions on the steel and enamelled surfaces with different roughnesses. The specimens, prepared in this manner, were exposed to ultrasonic-generated cavitation in a vessel with sonotrode excitation.

The ultrasonic cavitation is formed by periodic oscillation of sonotrade in the liquid, causing pressure fluctuations. When the longitudinal pressure waves pass through a liquid, they form compressions (areas of pressure load/high pressure) and rarefactions (areas of tensile load/low pressure). If the oscillation amplitude is sufficiently high, the pressure in the rarefaction may decrease to the vaporisation pressure. This forms the vapour phase. Real liquid also includes dissolved gases, various solid and gas inclusions in the form of bubbles in small cracks and pockets on the surface of solid particles (Mørch, 2007; Davydov and Kedrinskii, 2003). Cavitation is a process of vapour bubble growth and collapse. During the process extremely high pressure and temperature fluctuations occur which may cause the destruction of solid walls. Two high pressure peaks may be found during one cavitation cycle. One relates to the cavitation collapse and the other one corresponds to the cavitation shed off, both contributing to a distinctive stepwise erosion damage growth pattern (Dular et al., 2013; Petkovšek and Dular, 2013). Latest cavitation research provides new insights in the mechanism of cavitation erosion

which may be interesting for scale removal. It was determined (Dular et al., 2013) that larger single pits result from several impacts of shock waves on the same area, which means that they are merely special cases of pit clusters (pit clusters where pits overlap perfectly). The indicated effects generate enough energy that may cause a local mechanical destruction of solid substance in the vicinity of the collapse of cavitation cloud. Although research (Petkovšek and Dular, 2013) was performed on thin aluminium foil, analysis of the results revealed that damage only occurs at cavitation cloud collapse that the size of the cloud and it distance from the surface at collapse do not influence the extent of the damage and that an irregular or 'broken' type of cavitation cloud causes the most damage to the foil. These data confirm that intensity cavitation erosion is difficult to evaluate from images alone, while also strong pressure pulsations alone, although below the yield stress, may still cause limited damage to the surface.

The purpose of the paper is the following. We will present a model of cavitation cloud dynamics, which we will link with the cavitation erosion. For this, we will introduce a simple estimator of relative change in the texture of specimen ε, which will be obtained from images of test samples. We want to show that scale removal is dependent on intensity of cavitation and on the surface material properties.

2 Preparation of samples: deposition of scale on the specimens

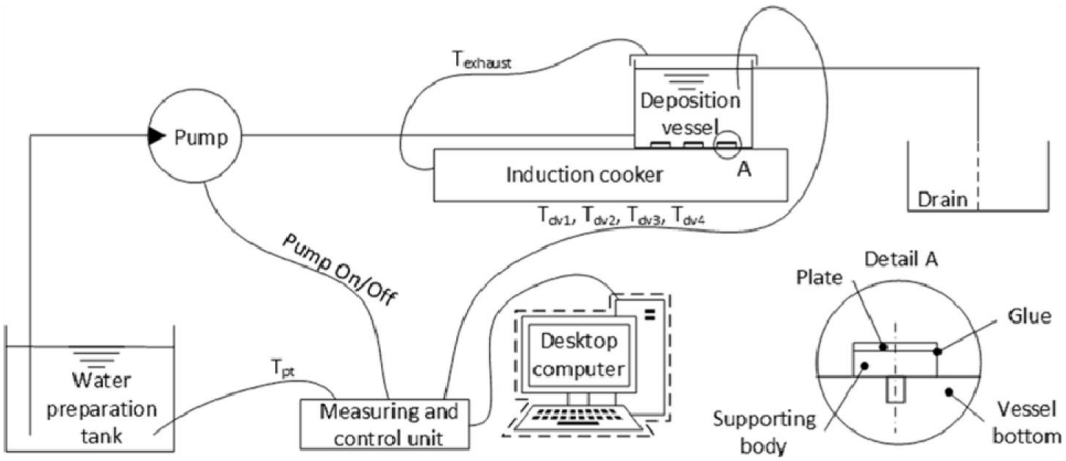
We tested four different groups of surfaces. Eighteen specimens were prepared. The specimens were assembled from substrate and sheet metal plate. The substrate was same for all specimens, while sheet metal plates with scale deposits were different for all 18 specimens. The specimen substrate was made of stainless steel. Substrate stem with M10x1 thread served for fastening to the bottom of the vessel. From the upper side, the specimen had a flat surface with a diameter of 16 mm, to which a sheet metal plate of the same diameter was fixed. Fixing of the sheet metal plate to the substrate was performed using a thin layer of the two-component water-resistant glue (Araldite 2052, Huntsman Advanced Materials). The plates were made of four different materials. Three stainless sheet metal types of different composition and roughness was used (13 specimens), while one enamelled sheet metal was used (5 specimens). The material and the roughness of surface are shown in Table 1. The roughness of surface, to which the deposition of calcium carbonate was performed, was measured using a surface roughness tester Mitutoyo SJ – 301. After the deposition of scale, the roughness was not measured.

Table 1 Data on the specimens, to which the scale was deposited

Group	*Specimen*	*Material*	*Description*	*Roughness Ra* (μm)
1	1–4	2.4858	Nickel alloy with high chemical and temperature resistance	0.30
2	5–9	1.4845	Austenitic stainless steel with excellent high-temperature resistance	0.31
3	10–14	Colorobbia AMSP 1211M	Powder enameled (Colorobbia, type AMSP 1211M) metal sheet ED4	0.16
4	15–18	1.4016	Brushed ferritic stainless steel with good corrosion resistance	0.42

The deposition of scale on the metallic and enamelled surface of specimens was carried out using an in-house designed scale deposition station shown in Figure 1. The scale deposition station consisted of a water preparation tank, a pump, deposition vessel with specimen, induction cooker, drain, measuring and control unit and personal computer. The specimens were placed into the vessel for the deposition of scale (Figure 1, detail A). Using a bolted joint, they were fastened to the bottom of the vessel that consisted of two plates. The upper 10 mm thick plate was made of stainless austenitic sheet metal and served for attachment of specimens. The lower 10 mm thick plate was made of ferromagnetic sheet metal and welded to the upper plate in the middle and along the circumference. Thus, we ensured that the bottom of the vessel was heated as equally as possible under the influence of high-frequency magnetic field generated by the induction cooker.

Figure 1 Measuring station for deposition of scale with an enlarged detail of specimen (Detail A). Specimen after the scale deposition was transferred to cavitation erosion test rig (Figure 2)

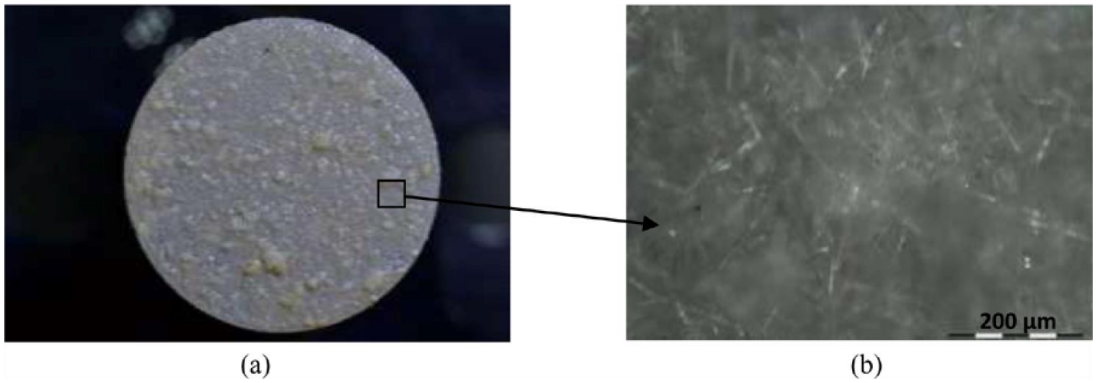


The station for the deposition of scale was composed of two subsystems. The first one regulated the operation of the flow pump, which pumped the water from the water preparation tank, in order to provide the exchange of water in the deposition vessel and capture the data on water temperature in the deposition vessel. The temperatures of water in the deposition vessel T_{dv1}, T_{dv2}, T_{dv3}, T_{dv4} were measured at four locations (three times at the height of the surface of deposition of scale to the specimens, and once just below the surface of water level in the deposition vessel). PT-100 sensors were used, located at equidistant radii from the centre of the vessel. The flow of water from the preparation vessel into the vessel for deposition of scale during the exchange was provided by the pump with a nominal water flow of 0.6 l/min, controlled by a software application in the LabView software environment.

The other system provided the appropriate temperature of water in the deposition vessel. It was based on the induction cooker Gorenje IQcook (Gorenje and Velenje, 2014), where the temperature on the exhaust T_{exhaust} of the deposition vessel was measured. For the needs of the test, we adjusted the regulation so that the temperature of water in the vessel was around 78 ± 2°C.

The water, which we used in the experiment, included high mineral content. Its hardness amounted to 19.4°dH, while its pH was practically neutral and amounted to 7.02. We manually filled the water preparation tank with water and activated both subsystems. The flow pump pumped the water into the deposition vessel above the induction cooker. During the water change, the temperature of water in the deposition vessel decreased to 30°C, but never reached the temperature of water in the water preparation tank T_{pt}, because the system started reheating the inflowing water immediately after the start of the change. In order to change all the water in the deposition vessel, the inlet of water into the vessel was placed in the wall close to the bottom of the vessel. The temperature of water in the deposition vessel reached the nominal water temperature of 78°C in the period of 25 min since the moment when the water in the deposition vessel was exchanged. In the entire period of depositing scale to the specimens, the water change mode was the same. The deposition of scale was carried out for 42 days at an increased temperature, and then the specimens waited 5 days more at an ambient temperature of ~24°C before the cavitation erosion experiment was performed. Figure 2(a) presents a typical specimen of the deposition of scale to the surface of specimen sheet metal. Figure 2(b) presents the structure of calcium carbonate at the selected segment of specimen surface.

Figure 2 Specimen 1(a) with the belonging structure (b) of scale (see online version for colours)



The scale surface on the specimen in Figure 2(a) contains randomly distributed deposition anomalies, which are the results of the growth of crystal structure of calcium carbonate and the local anomalies on the deposition surface, which are, as a rule, related to the roughness – the geometric properties of the surface, to which the scale has been depositing. Figure 2(b) presents a micro-structure of scale surface, which, according to the shape, belongs to the aragonite structure of scale. In the structure, there is a visible basic stick structure of aragonite as the basic building block of the deposition of calcium carbonate to the metallic surface of the specimen. The average length of aragonite sticks was 80 µm.

The preparation of specimens, which is described in this chapter, was concluded with a transfer of individual specimen into the cavitation vessel, where the specimen attached itself, and we have exposed it to the ultrasonic cavitation in the subsequent phase. Before and after the cavitation, the surface of specimen was photographed as shown in Figure 2(a). The photographing conditions were identical for all the specimens in the experiment. For the photographing, we used the camera Nikon D3100 with spacers for macro photography and the lens SAMYANG AE 85 mm. The illumination was

implemented with two LED-sources, each having seven LEDs CREE XM-L U2 on an oval PCB. The illumination was located at a 10 cm distance from specimen. All LED diodes were operating at constant current of 3 A per LED diode. In comparison with complex topography measurements, this simple macro photography of specimen surface estimation provides much less data, but has proved suitable for analysis of cavitation erosion using equations (7)–(9).

3 Scale removal

The cavitation of scale specimens was performed in the ultrasonic homogeniser model CP300, series 4710, manufactured by Cole Parmer. The sonotrode was used as a source of acoustic cavitation. The experimental configuration is shown in Figure 3. The sonotrode was excited with a frequency 20 kHz and was installed coaxially to the specimen. The clearance of the sonotrode from the specimen was identical for all specimens, amounting to 7.5 mm. The diameter d of the sonotrode stem was 4.75 mm. The specimen was fastened to the bottom of a cylindrical vessel using a threaded joint. The diameter of the vessel was 150 mm. The cylindrically shaped vessel contained a constant amount of distilled water (600 ml). The temperature of water was measured before the start of each experiment and was within the range of 22 ± 1ºC. The duration of cavitation for each experiment was 4 min.

As a parameter of cavitation intensity, the electrical supply voltage for sonotrode excitation was used. We estimate that electrical supply voltage is proportional to the cavitation intensity.

For illumination, eight LEDs CREE XM-L T6 with supply current 2 A were used. The LED lights were arranged at a distance of 10 cm from the centre of specimen. In addition the illumination was provided from the background with the LED light and a lens. The lens was attached to the LED light such that the LED light was positioned in focus of the lens. In such configuration the illumination beams were almost parallel to the upper sample surface and perpendicular to the Seoul P7 LED light with a 25 mm mount lens were used. The LED light supply current was 1.6 A. The distance from the centre of specimen to the LED light was 20 cm. The detection of cavitation was performed using the visualisation of time-variable topological structures of cavitation clouds in the area between the peak of the sonotrode and the specimen, as presented in Figure 4.

Figure 3 Schematic diagram of the cavitation erosion experiment. The specimen after scale deposition from Figure 1 was mounted here in the place labelled as the specimen

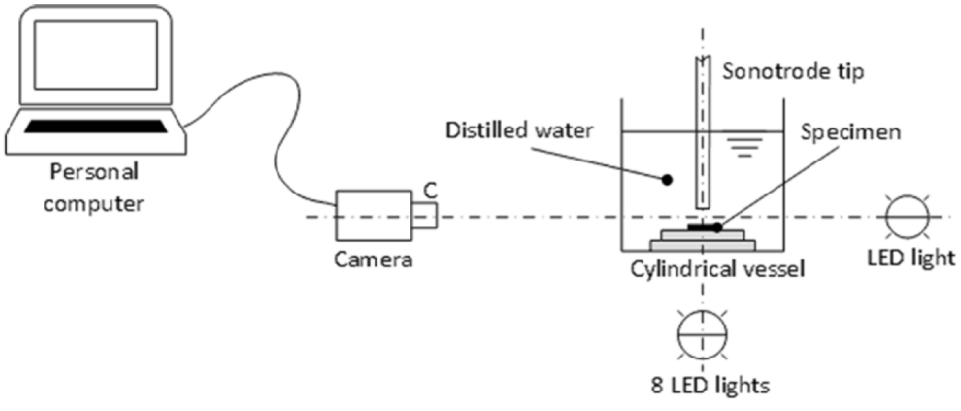
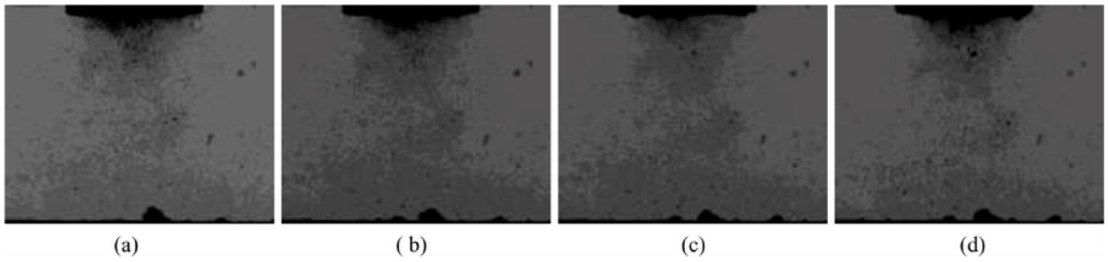


Figure 4 Time sequence of cavitation structures between the sonotrode in the upper part and the specimen in the lower part of the image dt = 0.5 ms

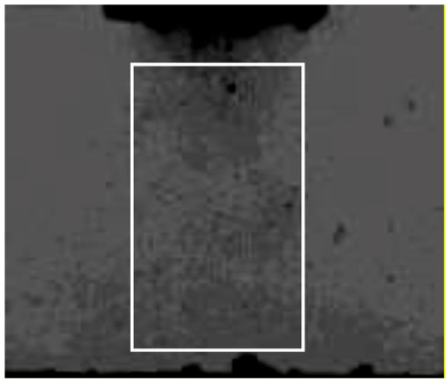


For images acquisition, the camera Hispec 4, manufactured by Fastec Imaging, was used. The camera was equipped with the lens Nikkor 50 mm 1 : 1.2. The distance of the camera sensor to the sonotrode was 33 cm. The focal point of camera lens was set to indefinite. The frequency of image capturing was 2 kHz. The number of consecutively taken images was 1000 images per each sample. The image resolution was 608 by 514 pixel. Pixel size was 15.3 μm. The size of the image was selected such that image covered entire region between the specimen and the sonotrode tip.

Quantitative analysis of surface details from Figure 4 is not possible. These figures were not intended for surface analysis, they were intended for the use with the cavitation cloud dynamics model. The surface details, as seen in Figures 4 and 5 are cavitation clouds, attached to the specimen surface. These cavitation clouds change slowly as can be seen from consecutive high speed images shown in Figure 4.

Results in Figure 4 show cavitation clouds induced by periodic oscillation of the sonotrode in the vertical direction. Cavitation appear in the form of cavitation clouds and individual cavitation bubbles between the sonotrode tip in the upper part of the image and the specimen surface in the lower part of the image. A large cavitation cloud is present at the sonotrode surface, which is shaped by an attached cavitation and the cavitation cloud which follows the kinematics of the sonotrode and decreases with distance from the sonotrode. The lower part of images in Figure 4 includes visible parts of already eroded scale as well as cavitation bubbles. For the eroded parts of scale, it is characteristic that they are can be traced in many subsequent images, which indicates that their velocity is relatively low.

Figure 5 Observation window between the tip of sonotrode and the specimen. A is estimated according to equation (3), while $\dot{A}$ in $\ddot{A}$ are time derivatives and thus calculated from $\overline{E}$ time series. For the image shown here the values are $A = 9.51 \times 10^{-4}$, $\dot{A} = 1.19$ [m], $\ddot{A} = -1.07 \times 10^{3}\,\mathrm{m}^2/\mathrm{s}$ and $\overline{E} = 74.53$ [-]



In order to connect the intensity of ultrasonic cavitation with erosion effects on the surface of specimens with the deposition of scale, the following section presents the phenomenological model of cavitation cloud dynamics. The model is able to predict the pressure waves – the pressure pulsations as a result of the dynamics of emerging cavitation clouds.

4 Model of cavitation cloud dynamics

One of the issues of cavitation erosion is the measurement of pressure fluctuations, when the specimen surface is subject to cavitation erosion. The dynamics of the spherical cavitation cloud of bubbles was already described by Brennen (1995). His model was based on the work that he had performed together with d'Agostino and Brennen (1989) and was supplemented by Shimada and Kobayashi (1990). However, measurements to confirm this cannot be performed during scale removal due to the scale debris. We have therefore used instead of pressure measurement the method of estimating pressure from the cavitation high speed imaging using the Brennen (1995) model:

$$A\left(1-\frac{\dot{A}}{c}\right)\ddot{A}+\frac{3}{2}\left(1-\frac{\dot{A}}{3c}\right)\dot{A}^2=\frac{1}{\rho_L}\left(1+\frac{\dot{A}}{c}+\frac{A}{c}\frac{\mathrm{d}}{\mathrm{d}t}\right)\left(p-p_\infty-4\frac{\mu_L}{A}\dot{A}\right) \tag{1}$$

where A [m] represents equivalent diameter of cavitation cloud of bubbles, c [m/s] speed of sound in fluid, p [N/m^2] pressure inside the cavitation cloud of bubbles, μ_L [m^2/s] fluid kinematic viscosity, ρ_L [kg/m^3] fluid density, and p_∞ [N/m^2] fluid ambient pressure. According to d'Agostino and Brennen (1989) the interface velocity $\dot{A}$ is largely subsonic with reference to the speed of sound in fluid in cloud of bubbles in water whose oscillatory dynamics is analysed in the neighbourhood of an equilibrium configuration at excitation frequencies not much larger that the natural frequency of the each individual bubble. With assumption that $c \gg \dot{A}$ the following algorithm can be used for calculation of pressure fluctuation in cavitation cloud observed:

$$A\ddot{A}+\frac{3}{2}\dot{A}^2=\frac{1}{\rho_L}\left(p-p_\infty-4\frac{\mu_L}{A}\dot{A}\right) \tag{2}$$

For the equivalent diameter of cavitation cloud A we assume proportionality to the intensity of grayscale level $\overline{E}$ [-] in observation window in Figure 5: $A \propto \overline{E}$. Similar assumptions were already reported in Bizjan et al. (2014). Under such assumption changes of cavitation cloud equivalent diameter in time t can be calculated using equation (3).

$$\overline{E}(t)=\sum_{i=1}^{i=N}\sum_{j=1}^{M}E(i,j,t);\ \ E(i,j,t)\epsilon\{1\div256\}. \tag{3}$$

In relation to equation (3), pressure fluctuations were monitored in rectangular observation window which has a size of $N \times M = 240 \times 410$ pixels. Window location is shown in Figure 5. The results of pressure fluctuation are written in time series. The pressure fluctuations are calculated from cavitation structures changes observed in selected window.

If boundary conditions and material properties of the liquid are known, then the instantaneous value of pressure $p(t)$ may be calculated from equation (2). We have used the statistical estimator π (equation (4)) as a parameter of cavitation intensity for the analysis of pressure fluctuations caused by sonotrode ultrasonic excitation.

$$\pi = \frac{\sigma_j}{\sigma_{\max,j}}, \tag{4}$$

where σ_j is the standard deviation of the selected pressure time series $p(t)$ for the specimen j, which belongs to the individual experiment on the selected specimen. $\sigma_{\max,j}$ is the maximum standard deviation among all the conducted experiments. Equation (4) sets the intensity level of pressure fluctuations $p(t)$, which is used as an integral parameter of cavitation in the assessment of erosion damage on the specimens of scale.

With the above procedure we have provided an estimation of integral pressure fluctuations above the specimen surface. In the following, we will show how parameter π is related to the cavitation erosion.

5 Evaluation of erosion effects

The intensity of cavitation erosion on the specimens, which were exposed to ultrasonic cavitation, was assessed on the basis of the change in the specimen surface. In this case, the visualisation method was used. Figure 6 presents a sample specimen of deposited scale before and after the exposure to ultrasonic cavitation (specimen 5, as shown in Table 1).

Figure 6 Specimen 5 with deposited scale: (a) before cavitation and (b) after cavitation (see online version for colours)



(a) (b)

Figure 6(a) presents a sample specimen after the finished deposition of scale and immediately before the performance of ultrasonic cavitation. Figure 6(b) presents the specimen scale surface after the performed cavitation. All images were recorded under identical photographing conditions as described in subsection (Scale removal). From the qualitative comparison between the textures on the photographs, we may conclude that the specimen after ultrasonic cavitation shows visible areas, where intensive erosion removed the scale up to the specimen surface. It also shows visible differences in the areas where the cavitation erosion was the cause for partial removal of scale. Partial scale

removal is expressed as the change of the scale surface. The quantitative erosion evaluation was conducted by comparing the images of specimens before and after the cavitation test. First, the specimens RGB colour images were converted into an 8-bit grey image with the pixel value of 0 for black colour and 255 for white colour. The mean value μ of grey image level intensity was assessed in the circle with radius $D/2$ in the centre of specimen. The observation area was the same in all cases. The difference of mean values before and after cavitation gives an indication of the change of specimens surface:

$$\Delta\mu = \mu_{\text{before}} - \mu_{\text{after}}. \tag{7}$$

In order to perform the comparisons between all specimens in the experiment, a relative assessment of the change of surface is submitted:

$$ER = \frac{\mu_{\text{before}} - \mu_{\text{after}}}{\mu_{\text{before}}} \tag{8}$$

which is standardised to the maximum value in the entire set of measurement.

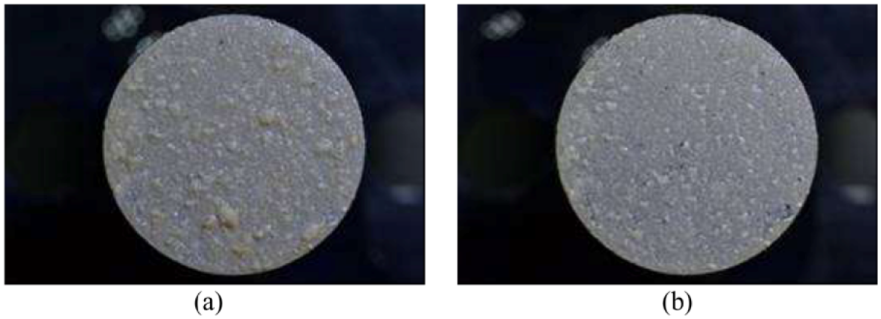
$$\varepsilon = \frac{ER_j}{ER_{j,\max}}, \tag{9}$$

where ER_j is the calculated relative assessment of the change of surface of specimen j, while $ER_{j,\max}$ is the maximum relative change between all the specimens discussed. Relative change in the surface of specimen ε will hereinafter be used for the comparison with the standardised estimator of the standard deviations of statistical estimator π (equation (4)).

6 Results of measurement

The results of measurements of cavitation erosion are presented as the change of specimen surface before and after the cavitation. Figures 7–10 show the cavitation erosion effects on the specimens surfaces in case of the same basic specimen material (Group 1, specimens 1–4, as shown in Table 1). The specimens before cavitation are presented in figures designated with (a). Figures designated with (b) represent the specimens after the performed cavitation test. The specimens in Figures 7–10 were exposed to increasing cavitation intensities for 240 s.

Figure 7a Specimen 1 with deposited scale: (a) before cavitation and (b) after cavitation (π = 0.364(–), ε = 0.038(–))(see online version for colours)



(a) (b)

Figure 7b Specimen 2 with deposited scale: (a) before cavitation and (b) after cavitation (π = 0.444(–), ε = 0.103(–)) (see online version for colours)

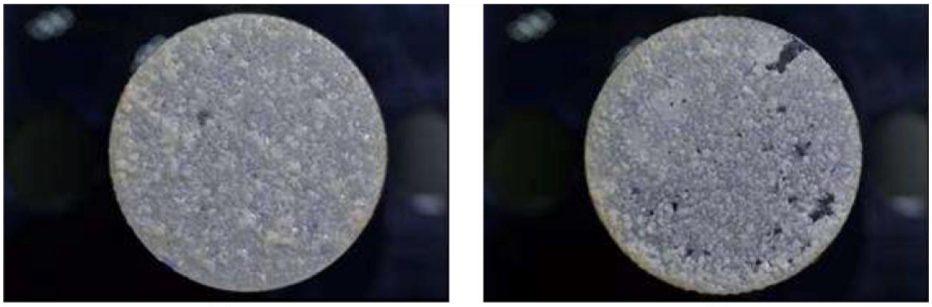


Figure 7c Specimen 3 with deposited scale: (a) before cavitation and (b) after cavitation, (π = 0.345(–), ε = 0.141(–)) (see online version for colours)

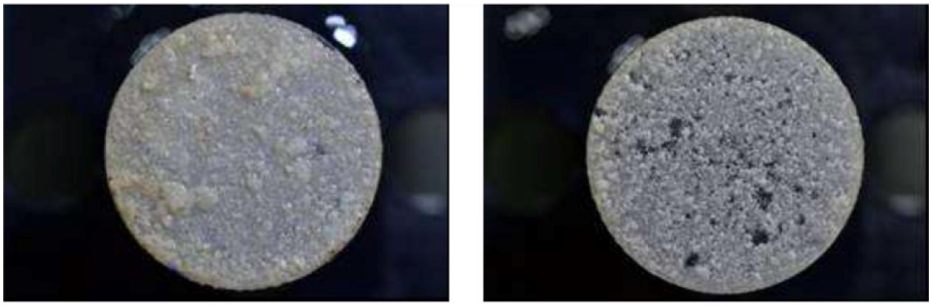


Figure 7d Specimen 4 with deposited scale (a) before cavitation and (b) after cavitation (π = 0.721(–), ε = 0.230(–)) (see online version for colours)



Figure 8a Specimen 5 with deposited scale: (a) before cavitation and (b) after cavitation (π = 0.3385(–), ε = 0.046(–))

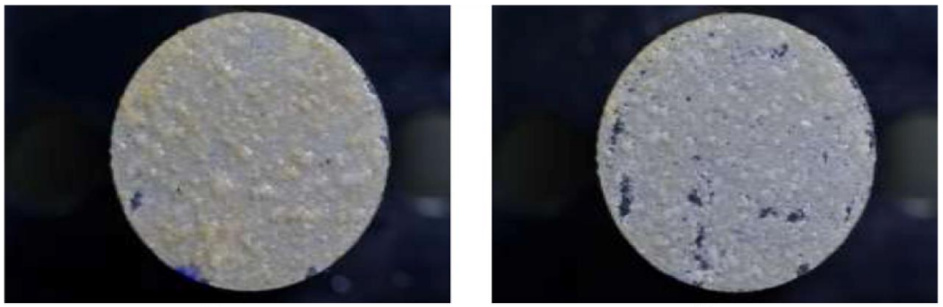
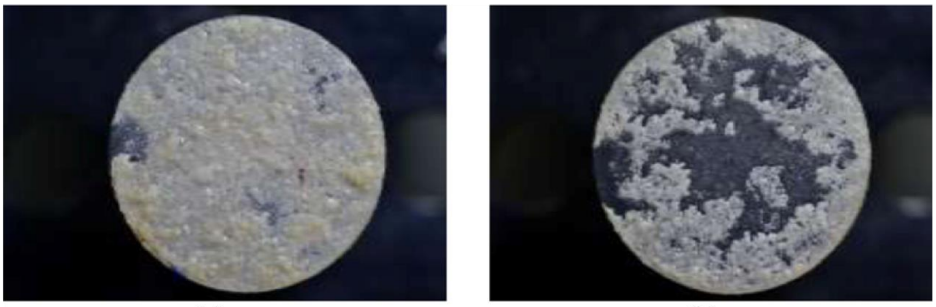
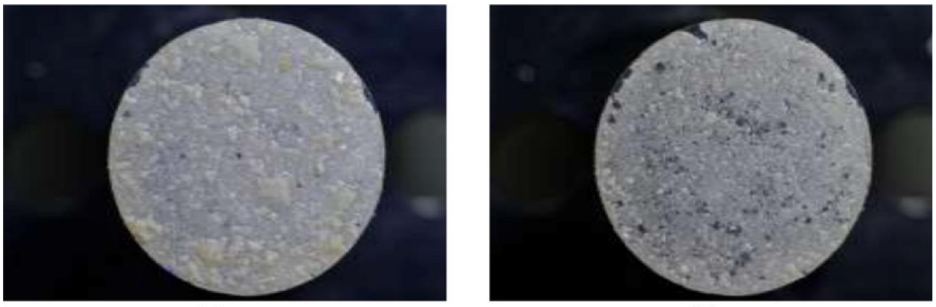


Figure 8b Specimen 6 with deposited scale (a) before cavitation and (b) after cavitation (π = 0.6345(–), ε = 0.259(–)) (see online version for colours)



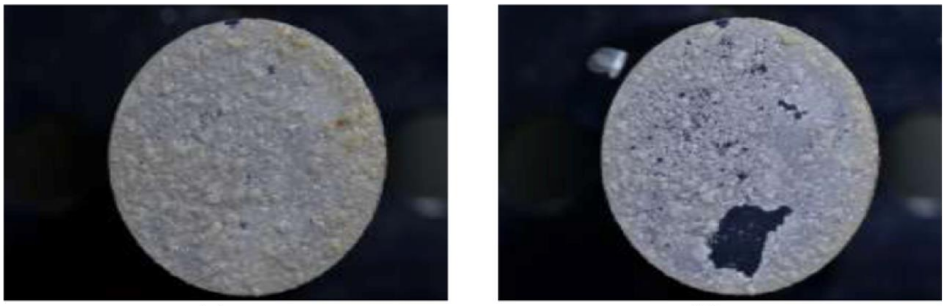
(a) (b)

Figure 8c Specimen 7 with deposited scale: (a) before cavitation and (b) after cavitation, (π = 0.547(–), ε = 0.238(–)) (see online version for colours)



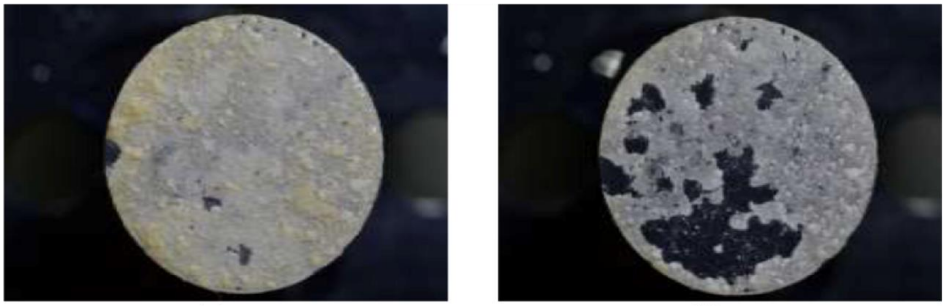
(a) (b)

Figure 8d Specimen 8 with deposited scale: (a) before cavitation and (b) after cavitation (π = 0.402(–), ε = 0.095(–)) (see online version for colours)



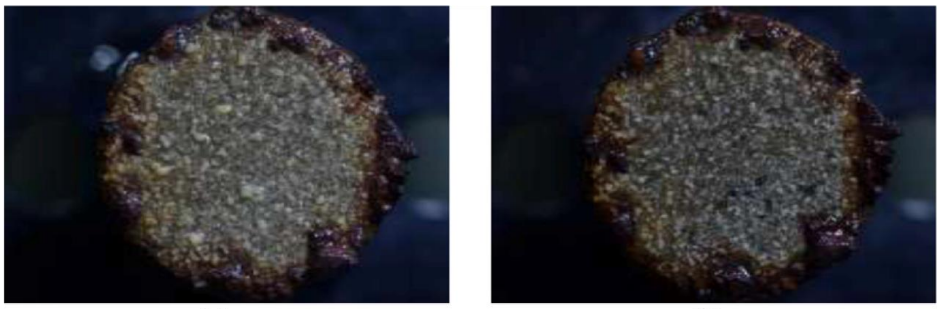
(a) (b)

Figure 8e Specimen 9 with deposited scale: (a) before cavitation and (b) after cavitation (π = 0.343(–), ε = 0.178(–)) (see online version for colours)



(a) (b)

Figure 9a Specimen 10 with deposited scale: (a) before cavitation and (b) after cavitation (π = 0.341(–), ε = 0.308(–)) (see online version for colours)



(a) (b)

Figure 9b Specimen 11 with deposited scale: (a) before cavitation and (b) after cavitation (π = 0.901(–), ε = 1.00(–)) (see online version for colours)



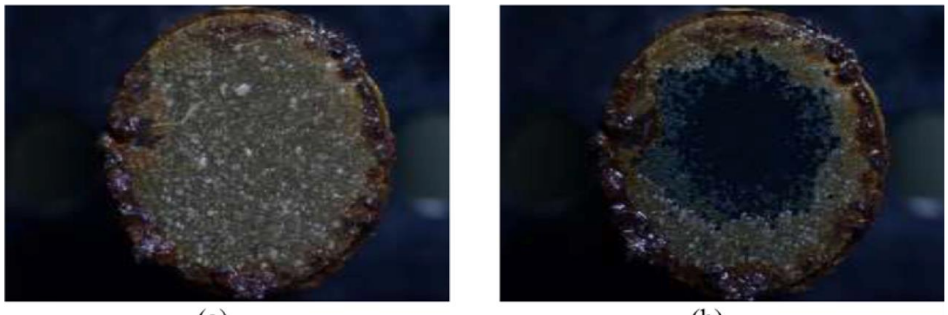
(a) (b)

Figure 9c Specimen 12 with deposited scale: (a) before cavitation and (b) after cavitation (π = 0.577(–), ε = 0.812(–)) (see online version for colours)



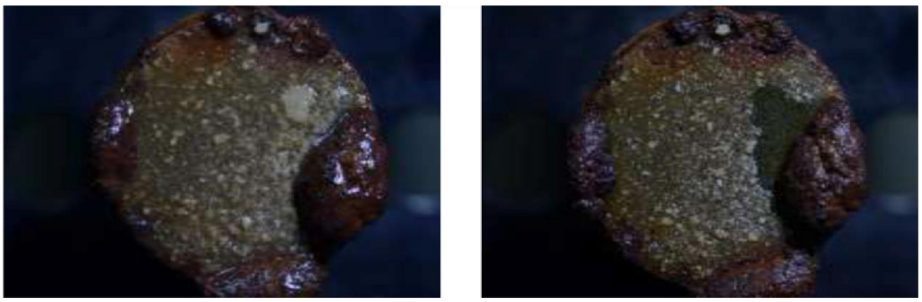
(a) (b)

Figure 9d Specimen 13 with deposited scale: (a) before cavitation and (b) after cavitation (π = 0.697(–), ε = 0.793(–)) (see online version for colours)



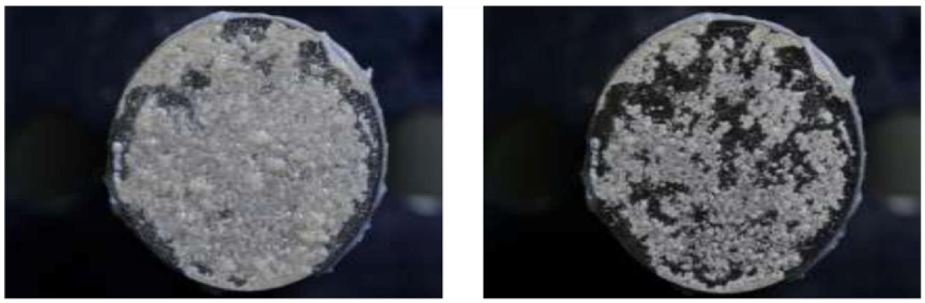
(a) (b)

Figure 9e Specimen 14 with deposited scale: (a) before cavitation and (b) after cavitation (π = 0.344(–), ε = 0.141(–)) (see online version for colours)



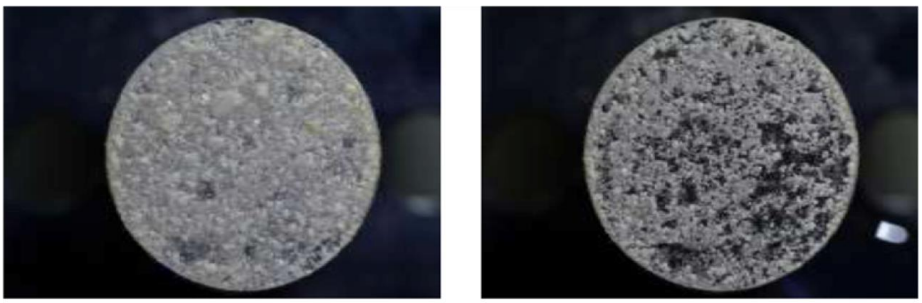
(a) (b)

Figure 10a Specimen 1 with deposited scale: (a) before cavitation and (b) after cavitation (π = 0.507(–), ε = 0.599(–)) (see online version for colours)



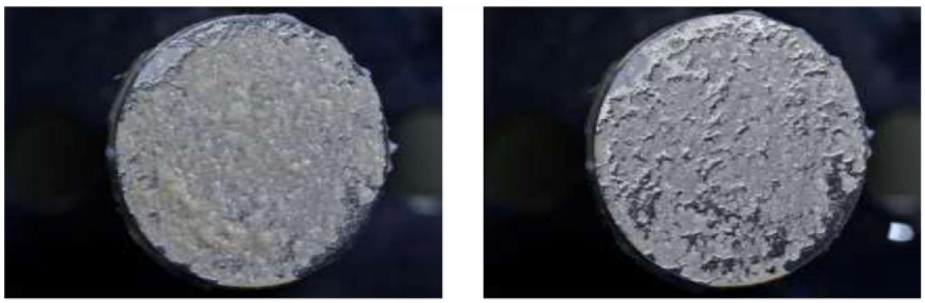
(a) (b)

Figure 10b Specimen 2 with deposited scale: (a) before cavitation and (b) after cavitation (π = 0.620(–), ε = 0.998(–)) (see online version for colours)



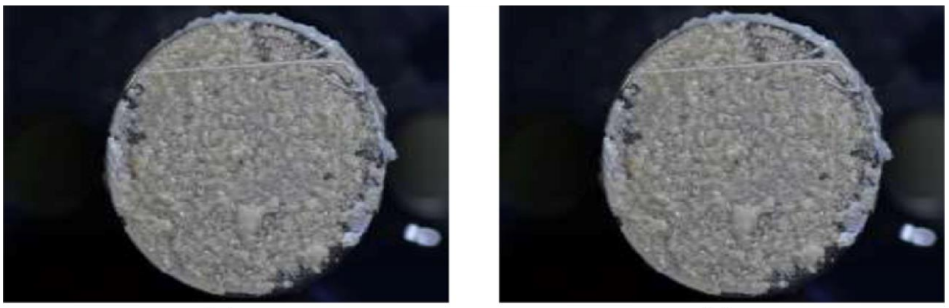
(a) (b)

Figure 10c Specimen 3 with deposited scale: (a) before cavitation and (b) after cavitation, (π = 0.335(–), ε = 0.592(–)) (see online version for colours)



(a) (b)

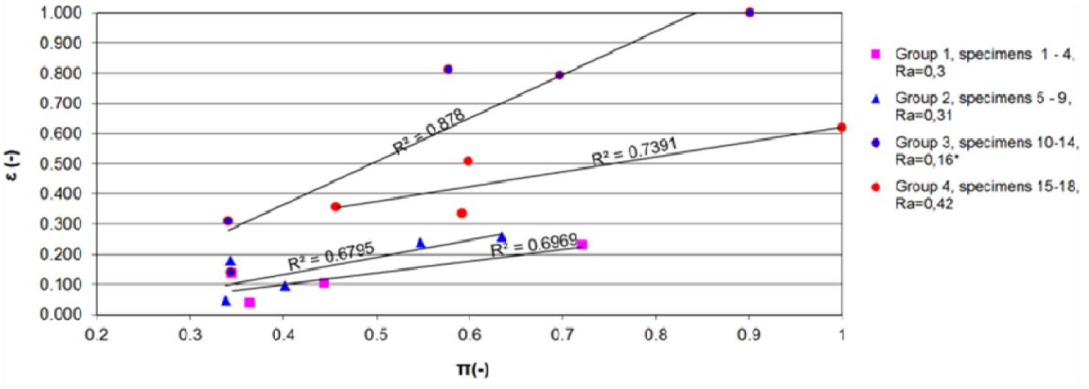
Figure 10d Specimen 4 with deposited scale: (a) before cavitation and (b) after cavitation (π = 0.355(–), ε = 0.457(–)) (see online version for colours)



The cavitation test was performed for all samples from Table 1. Results of cavitation tests are further evaluated below. In several cases, the result of cavitation test was the complete removal of scale from the specimen surface. In the case when the intensity of cavitation was low, we can notice only the changes in the scale surface, while the scale remained attached to the entire surface of the specimen (Figure 7(a)). This is mainly reflected as the modest changes of limited area and corresponding small changes in specimen surface grey level intensity. For these specimens, we did not notice the areas with complete removal of scale. The increasing intensity of cavitation increases the area of complete scale removal. In case of Figure 7(d), such an area is already very pronounced. Figure 8 shows samples from group 2, Figure 9 shows samples from group 3 and Figure 10 shows samples from Figure 10.

A quantitative analysis of erosion effects is presented in Figure 11. It is based on the implemented estimators of relative change in the surface of specimen ε (equation (9)) from the standard deviation of pressure statistical estimator π (equation (4)).

Figure 11 Model of cavitation cloud dynamics and different basic material (Ra for metal and Ra* for enamel) (see online version for colours)



From the diagram in Figure 11, we may conclude that the intensity of pressure fluctuations affects the cavitation erosion of scale on specimens. Beside pressure fluctuations, the growth of cavitation damage mainly depends on the structure of surface and material properties of the surface, to which the scale was deposited. The most expressed damage is present on the group of specimens 3, for which a relatively small roughness of basic enamelled surface is characteristic (Ra = 0.16 μm). With regard to the

other specimens, we may notice that the difference is in both the increased erosion and the inclination angle of the regression line. In case of enamelled surface, the erosion of scale on the surface is increasing faster than in case of specimens made of steel alloys. In the group of specimens, which were made of steel alloys, we may see that the inclination angles of regression lines are approximately the same. The lowest cavitation erosion is present on the specimens of group 1 and 2, which belong to the nickel alloy with high chemical and temperature resistance and austenitic stainless steel with excellent high-temperature resistance. For both cases, we may establish that the intensity of cavitation erosion is the lowest, or that the bond between the scale and the basic surface of specimens is the strongest. The influence of material structure for the indicated groups of specimens 1 and 2 is not characteristic. Contrary to this, the intensity of cavitation erosion in the group of specimens 4 is exceeding the erosion effects on the group of specimens 1 and 2 in spite of increased level of roughness.

In brittle materials, micro-fractures appear at the onset and cracks rapidly propagate without increasing the overall applied stress. The erosion curve can still show the four characteristic stages (Thiruvengadam, 1963) of cavitation erosion since the incubation period reflects the accumulation of microcracks up to a point where material will break free. Due to the experimental procedure used here, we unfortunately cannot confirm this. Also, there are no to us known reports of cavitation erosion of scale, deposited on a substrate, with regards to the substrate surface properties.

In samples in group 2 (Ra = 0.31) in Figure 8, we see a strong tendency for spallation. We make this claim on the fact that cavitation damage in Figure 8 exhibits the sharp edges. We must compare present results with studies on surface treatments and coatings as strategies for improving cavitation erosion resistance, among them are studies investigating hard brittle coatings made of ceramics. Among them, reports (Krella, 2011) indicate failure mechanisms which include debonding, delamination and spallation. Samples in group 3 show strong tendency for delamination. Results of cavitation erosion from group 1 (Figure 7) with Ra = 0.3 or group 3 (Figure 9) does not show such properties, although group 3 exhibits the strongest dependency of cavitation erosion on pressure fluctuations as seen from Figure 11.

Additional factors contributing to scale removal include residual stresses, substrate properties and substrate coating adherence issues, porosity and interfacial defects and other imperfections (Mishnaevsky and Gross, 2004). From this, we conclude that roughness of specimen surfaces alone is unable to determine the tendency of scale layer to spallation or delamination on these specimen surfaces.

7 Conclusions

The paper presents the research of erosion effects caused by ultrasonic cavitation on metallic specimens covered by calcium carbonate – scale. The methodology of scale deposition was the same for all specimens. The ultrasonic cavitation with intensity control was selected as the generator of cavitation scale erosion. The results of experiment indicate a characteristic effect of cavitation intensity on the destruction of scale on the surface of specimens. It was established that the increasing of pressure pulsations also increases the intensity of cavitation erosion of scale on the surface of specimens as well as erosion is dependent upon the roughness of specimen surfaces,

on which the scale was deposited. The most expressed scale erosion was found on surface with smallest roughness of Ra = 0.16 μm. We have found that spallation mechanism or delamination mechanism of scale removal are not dependent solely on the roughness of specimen surfaces.

References

Bizjan, B., Orbanić, A., Širok, B., Kovač, B., Bajcar, T. and Kavkler, I. (2014) 'A computer-aided visualization method for flow analysis', *Flow Measurement and Instrumentation*, Vol. 38, August, pp.1–8.

Brennen, C.E. (1995) *Cavitation and Bubble Dynamics*, Oxford University Press, Oxford, New York.

d'Agostino, L. and Brennen, C.E. (1989) 'Linearized dynamics of spherical bubble clouds', *J. Fluid Mech.*, Vol. 199, pp.155–176.

Davydov, M.N. and Kedrinskii, V.K. (2003) 'Mathematical simulation of bubbly cluster and spall formation in a liquid at dynamic loading', *5th International Symposium on Cavitation*, Osaka, Paper No. CAV-03-GS-4-003.

DOE (2011) *Energy Savers: Tips on Saving Money and Energy at Home*, US Department of Energy, Office of Energy Efficiency and Renewable Energy, pp.1–44.

Dular, M., Coutier-Delgosha, O. and Petkovšek, M. (2013) 'Observations of cavitation erosion pit formation', *Ultrasonics Sonochemistry*, Vol. 20, No. 4, pp.1113–1120.

Elfil, H. and Roques, H. (2001) 'Role of hydrate phases of calcium carbonate on the scaling phenomenon', *Desalination*, Vol. 137, Nos. 1–3, pp.177–186.

Gorenje, D.D. and Velenje, S. (2014) *IQcook*, www.gorenje.com/iqcook/ww/ (Accessed 19 October, 2014).

Hasson, D., Shemer, H. and Sher, A. (2011) 'State of the art of friendly 'green' scale control inhibitors: a review article', *Industrial and Engineering Chemistry Research*, Vol. 50, No. 12, pp.7601–7607.

Karabelas, A.J. (2002) 'Scale formation in tubular heat exchangers – research priorities', *International Journal of Thermal Sciences*, Vol. 41, No. 7, pp.682–692.

Krella, A. (2011) 'An experimental parameter of cavitation erosion resistance for TiN coatings', *Wear*, Vol. 270, Nos. 3–4, pp.252–257.

MacAdam, J. and Parsons, S.A. (2004) 'Calcium carbonate scale formation and control', *Reviews in Environmental Science and Biotechnology*, Vol. 3, No. 2, pp.159–169.

Mishnaevsky, L.L. and Gross, D. (2004) 'Micromechanisms and mechanics of damage and fracture in thin film/substrate systems', *International Applied Mechanics*, Vol. 40, No. 2, pp.140–155.

Mørch, K.A. (2007) 'Reflections on cavitation nuclei in water', *Physics of Fluids*, Vol. 19, No. 7, pp.1–7.

Petkovšek, M. and Dular, M. (2013) 'Simultaneous observation of cavitation structures and cavitation erosion', *Wear*, Vol. 300, Nos. 1–2, pp.55–64.

Shimada, M. and Kobayashi, T. (1990) 'Dynamics of cloud cavitation and cavitation erosion', *Proceedings of the 1999 ASME Fluids Engineering Summer Meeting 1999*, San Francisco, pp.1–6.

Thiruvengadam, A. (1963) 'A unified theory of cavitation damage', *Journal of Basic Engineering*, Vol. 85, No. 3, pp.365–373.

5 Scale Deposit Removal by Means of Ultrasonic Cavitation

In this chapter, the paper entitled "Scale deposit removal by means of ultrasonic cavitation" by Boštjan Pečnik, Marko Hočevar, Brane Širok and Benjamin Bizjan (Pečnik et al., 2016) is presented.

The purpose of this paper was to present a study of the mechanism of acoustic cavitation-generated erosion on metallic specimens coated with calcium carbonate (scale). In fact, the analysis was performed on the results of the same experimental setup as in the previous paper by Pečnik et al. (Cavitation erosion of the calcium carbonate deposits, Chapter 4), but introduces several new qualitative and quantitative measures for the cavitation erosion process.

The rate of scale removal was determined to be proportional to the pressure amplitude generated by the sonotrode, and inversely proportional to the substrate surface roughness. The duration of specimen's exposure to cavitation is also important, as on some specimens, the scale surface seemingly hardened after a certain time, inhibiting further erosion. However, several specimens with visible local inhomogeneities on the scale surface experienced continued erosion until their surface was clear of scale. This indicates a significant dependence of the scale destruction mechanism to the microstructure of the scale deposit, as local inhomogenities may intensify the erosion rate.

Scale deposits can, depending on the hardness of their surface and substrate surface finish, as well as their microstructure, either be eroded layer by layer, or by breakage of larger areas from the substrate. To quantify the geometric properties of descaling areas and the distribution of erosive forces, the edge-to-length ratio of descaled surfaces was introduced as new parameter. Regardless of the exact descaling mechanism, the edge length-to-area ratio decreases with time, leading to a gradual reduction of descaling efficiency.

The graphical abstract of the paper is shown in Figures 7 and 8.

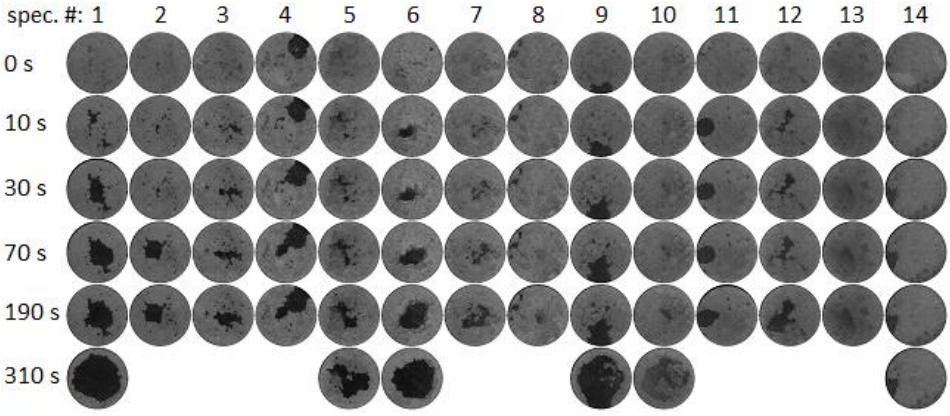


Figure 7: Specimen macro photos. Horizontal axis: specimens No. 1-14, vertical axis: time from the start of cavitation.

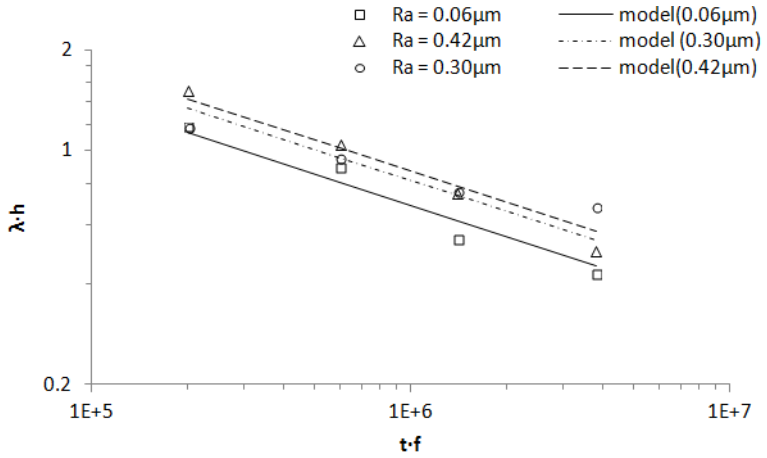


Figure 8: Multiple regression model for λ..

Wear 356-357 (2016) 45–52

Contents lists available at ScienceDirect

Wear

journal homepage: www.elsevier.com/locate/wear

Scale deposit removal by means of ultrasonic cavitation

Boštjan Pečnik [a,b], Marko Hočevar [c], Brane Širok [c], Benjamin Bizjan [c,*]

[a] Jožef Stefan International Postgraduate School, Jamova 39, 1000 Ljubljana, Slovenia
[b] Gorenje d.d., Partizanska 12, 3503 Velenje, Slovenia
[c] Faculty of Mechanical Engineering, University of Ljubljana, Aškerčeva 6, 1000 Ljubljana, Slovenia

ARTICLE INFO

Article history:
Received 25 January 2016
Received in revised form
9 March 2016
Accepted 11 March 2016
Available online 19 March 2016

Keywords:
Calcium carbonate
Scale
Ultrasonic cavitation
Cavitation erosion
Stainless steel
Aragonite

ABSTRACT

This paper presents a study of the mechanism of acoustic cavitation-generated erosion on metallic specimens coated with calcium carbonate (scale). Specimens were produced by scale deposition on steel substrates with different surface roughness, and then exposed to sonotrode-generated acoustic cavitation. The rate of scale removal was determined to be proportional to the pressure amplitude generated by the sonotrode. Descaling can also be intensified by reducing the substrate surface roughness. However, the scale destruction mechanism is largely dependent on the microstructure of the scale deposit, as local inhomogenities may intensify the erosion rate. Scale deposits can, depending on the hardness of its surface and substrate surface finish, either be eroded layer by layer, or by breakage of larger areas. Regardless of the exact descaling mechanism, the edge length-to-area ratio of descaled surfaces decreases with time, leading to a gradual reduction of descaling efficiency.

© 2016 Elsevier B.V. All rights reserved.

1. Introduction

The build-up of $CaCO_3$ (lime) scale is a major operational problem in several industrial processes including membrane filtration (desalination), drilling and especially those involving heat transfer. In heat exchangers, scale coating acts as a thermal insulator, significantly reducing the heat transfer efficiency while causing heating elements to overheat, leading to premature component failure. Scale can also drastically reduce the flow rate in pipes. Apart from industrial applications, household appliances such as boilers, washing machines, solar collectors and others that heat hard water from the municipal water supply, are also affected by scale deposits. In these applications, scale formation can significantly reduce product performance and life time. Additional consequences are increased service charges, frequent equipment replacement and higher energy consumption, up to 25% [1]. The costs incurred in preventing and remedying scale deposits both industrially and domestically are considerable. Scale inhibitors are the third largest product segment of the water treatment chemicals market (corrosion inhibitor market being the largest) and by 2016 will be worth $ 3.6 billion [2].

Currently, the most efficient way to prevent scaling is by using chemical inhibitors or descalers. However, chemical treatment is costly and can produce a negative environmental impact. Consequently, cheaper and environmentally more acceptable alternatives have been investigated [3,4], including natural chemical agents and surface treatments by coatings, magnetic and electronic conditioning, all of which show varying degrees of efficacy (Table 1). Once formed, the removal of a tenacious scale involves either chemical treatment (e.g. by acids) to dissolve the scale or some form of mechanical removal [5]. The main benefit of using a mechanical method is that it avoids the use of chemicals, but can be time consuming if performed manually. A possible alternative approach is by using ultrasound. Ultrasonic cleaning is a well established and efficient technology for dislodging solid residues and removal of biological fouling. It is also the best known application of acoustic cavitation. Cavitation is the phenomenon of rapid formation and implosion of low-pressure bubbles in liquids by means of mechanical forces [6,7].

The purpose of this paper is to present ultrasonic cavitation as a promising procedure for hydrodynamic scale removal. An extensive literature and technology overview of calcium carbonate scale removal by the cavitation method was provided by Heath et al. [8]. According to [8], most of the cavitation erosion research has so far been focused on the hydrodynamic mechanism of this phenomenon, and on undesired erosion mechanism of metallic surfaces and coatings. While the theory for cavitation erosion of brittle coatings can be partly applied to the scale deposits, the effect of

* Corresponding author. Tel.: +386 14771423.
E-mail addresses: bostjan.pecnik@gorenje.com (B. Pečnik), marko.hocevar@fs.uni-lj.si (M. Hočevar), brane.sirok@fs.uni-lj.si (B. Širok), benjamin.bizjan@fs.uni-lj.si (B. Bizjan).

http://dx.doi.org/10.1016/j.wear.2016.03.012
0043-1648/© 2016 Elsevier B.V. All rights reserved.

Table 1
The effectiveness of different scale treatments. Adapted from [7].

Scale treatment	Effectiveness (% reduction)
Ion exchange	100
Acid dosing	100
Chemical inhibitors	100
Metal ions	80
Magnetic conditioners	80
Electronic conditioners	80
Electrolytic	40
Ultrasound	30
Surface modification	90

irregular calcium carbonate microstructure is not well understood. Momber [9] and Grabco el at. [10] studied cavitation erosion of limestone and marble minerals and determined the following parameters to be the most decisive for the extent of the surface damega: exposure time, cavitation intensity and materials properties (hardness, strength and microstructure).

However, the microstructure of calcite and aragonite deposits are very different from the microstructure of limestone, and existing studies dealing with scale mitigation and removal (Dalas [11], Benzinger et al. [12], Li et al. [13], Kazi et al. [14]) do not directly discuss the effects of cavitation erosion. For this reason, our study will analyze the actual mechanism of calcium carbonate deposit removal by ultrasononic cavitation. Depositing and removal process will be investigated for metallic surfaces with different roughness will be evaluated. The effect of operating parameters such as the surface roughness and ultrasonic cavitation intensity on scale removal will be assessed using a macroscale visualization comparison method.

Formation of calcium carbonate ($CaCO_3$) deposits is a complex process that depends on numerous variables, such as the level of oversaturation, the chemical composition of the fluid, the temperature, the hydrodynamic (flow) conditions and the properties of surfaces on which it accumulates, such as the surface energy and roughness [7,15]. Carbon dioxide (CO_2) dissolved in water forms a weak carbon acid which dissociates into hydrogen carbonate, hydrogen and carbonate ions. Calcium ions react with bicarbonate which then exists in equilibrium with calcium carbonate and carbon dioxide. The corresponding chemical reaction can be written as:

$$Ca^{2+} + 2HCO_3^- \rightarrow CaCO_{3(s)} + CO_{2(g)} + H_2O \quad (1)$$

The physical process of the solid structure formation of CaCO3 (s) includes the formation of ions, clustering, nucleation and growth of crystals in agglomerated clusters on solid surfaces. Calcium carbonate is formed in different polymorphic crystal forms, which, in spite of the fact that they are chemically identical, have different crystal structures, which is why they differ in the macro- and micro-structural properties. Calcium carbonate may appear in the form of three crystal structures: vaterite, aragonite and calcite [16]. Calcite and aragonite are the most common polymorphic structures.

Variables that affect the level of deposition, the extent and type of scale polymorphic structure on solid walls, include the following: pH value, temperature, liquid flow properties, particularly near solid walls, surface properties, presence of impurities, presence of other ions and time. Upon these variables depend not only the scale deposit properties, but also the efficiency of scale removal (descaling) from exposed surfaces, which in our case will be achieved by the means of ultrasonic cavitation.

The ultrasonic cavitation is formed by periodic oscillations of sonotrode in the liquid, causing pressure fluctuations. When the longitudinal pressure waves pass through the liquid, compressions (high pressure areas) and rarefactions (low pressure areas) are formed. If the oscillation amplitude is sufficiently high, the pressure in the rarefaction may decrease below the vapor pressure of liquid. Consequently, the vapor phase may be formed in form of bubbles or similar flow structures, which then grow and rapidly collapse in a process known as cavitation. The onset and intensity of cavitation is affected by presence of dissolved gases, various solid and bubble-shaped gas inclusions in the liquid, as well as micro-scale cracks and pockets on the surface of solid particles [17,18]. During the bubble collapse process, extremely high pressure and temperature fluctuations occur and may damage the solid surfaces immersed in liquid. Two high pressure peaks may be found during one cavitation cycle. One relates to the cavitation collapse and the other one corresponds to the cavitation shed-off, both contributing to a distinctive stepwise erosion damage growth pattern [19,20]. These effects may become sufficiently strong to cause local mechanical destruction of exposed solid materials.

The article will present the deposition of calcium carbonate structure under controlled conditions on the steel and enameled surfaces with different roughness. The specimens, prepared in this manner, were later exposed to ultrasonic-generated cavitation in a vessel with sonotrode excitation.

2. Experimental set-up

2.1. Preparation of samples: deposition of scale on the specimens

14 specimens with three different groups of surface properties were prepared. The specimens were assembled from a substrate and a sheet metal plate. Identical substrates were used for all specimens, while sheet metal plates to which the scale was deposited varied in material composition and surface roughness. The specimen substrates were made of stainless steel and fastened to the bottom of the vessel. The upper substrate surface was flat and of circular shape with a 16 mm diameter. A thin sheet metal plate of the same diameter was attached to the top of the substrate using a thin layer of the two-component water-resistant glue (Araldite 2052, Huntsman Advanced Materials). Three different kinds of stainless steel plates were used for the specimens (Table 2). The surface roughness of specimens was measured prior to the calcium carbonate deposition, using a surface roughness tester Mitutoyo SJ – 301.

Scale deposition on the specimen surface was carried out using a custom-made scale deposition station shown in Fig. 1. The scale deposition set-up consisted of a water preparation tank, a pump, a deposition vessel with specimen, an induction cooker, a drain, a measuring and control unit and a personal computer. The specimens were placed into the vessel (Fig. 1, detail A) and fastened to its bottom using a bolted joint. The bottom of the vessel consisted

Table 2
Data on the specimens, to which the scale was deposited.

Group	*Specimen number*	*Specimen material*	*Description*	*Roughness Ra (μm)*
1	1–5	1.4541	Austenitic stainless steel with high inter-granular corrosion resistance	0.06
2	6–8	2.4858	Nickel alloy with high chemical and temperature resistance	0.30
3	9–14	1.4016	Brushed ferritic stainless steel with good corrosion resistance	0.42

of two plates. The upper 10 mm thick plate was made of stainless austenitic sheet metal and served for attachment of specimens. The lower 10 mm thick plate was made of ferromagnetic sheet metal and welded to the upper plate in the middle and along the circumference. This way, uniform heating of the vessel bottom by the induction cooker was attained.

The scale deposition station was composed of two subsystems. The first subsystem regulated the operation of the flow pump, which pumped the water from the water preparation tank, in order to provide the exchange of water in the deposition vessel and measure water temperature. The water temperatures in the deposition vessel T_{dv1}, T_{dv2}, T_{dv3}, T_{dv4} were measured at four locations (three times at the height of the surface of deposition of scale to the specimens, and once just below the surface of water level in the deposition vessel). PT-100 sensors were used, located at equidistant radii from the center of the vessel. The flow of water from the preparation vessel into the vessel for deposition of scale during the exchange was provided by the pump with a nominal water flow of 0.6 l/min, controlled by a software application in the National Instruments LabView software environment.

The second subsystem controlled the water temperature in the deposition vessel. It was based on the induction cooker Gorenje IQcook [21], where the temperature on the exhaust $T_{exhaust}$ of the deposition vessel was measured.

The water used in the experiment was characterized by high mineral content. Its hardness amounted to 19.4 °dH, while its pH was neutral at 7.02. After the water preparation tank had been filled with water, both subsystems shown in Fig. 1 were activated. The flow pump pumped the water into the deposition vessel above the induction cooker, where the water was then heated to 78 °C, with its temperature maintained within the ± 2 °C interval. To allow for prolonged scale deposition, water within the vessel was regularly replaced by the fresh water from the preparation tank. During the water change, the temperature of water in the deposition vessel decreased to 30 °C, but was reheated back to its nominal temperature (78 °C) in approximately 25 min. Scale deposition was carried out for 79 days at an elevated temperature (78 °C), and then the specimens were left in the vessel for additional 345 days at the ambient temperature of approximately 24 °C before performing the cavitation erosion experiment. For all specimens, final deposit thickness of approximately $h=0.17$ mm was measured using a scanning electron microscope (SEM) Jeol JSM 5610. Fig. 2a presents a macro photo of the sample specimen with a scale deposit on its surface. In Fig. 2b, a microscope (SEM) image of the deposit microstructure is shown for a small segment of the specimen surface. The SEM image in Fig. 2b reveals a typical aragonite microstructure [22] of the calcium carbonate deposit.

The scale surface on the specimen in Fig. 2a contains randomly distributed deposition anomalies. These result from the growth of calcium carbonate crystal structure and local anomalies on the deposit surface. Scale structure properties, including the strength of adhesion and the aforementioned anomalies, are related to the roughness of the underlying surface, to which depositing occurs [23,24]. SEM images of the scale deposit surface (Fig. 2b) reveal an aragonite mineral structure, which is characterized by stick-shaped $CaCO_3$ crystals [22].

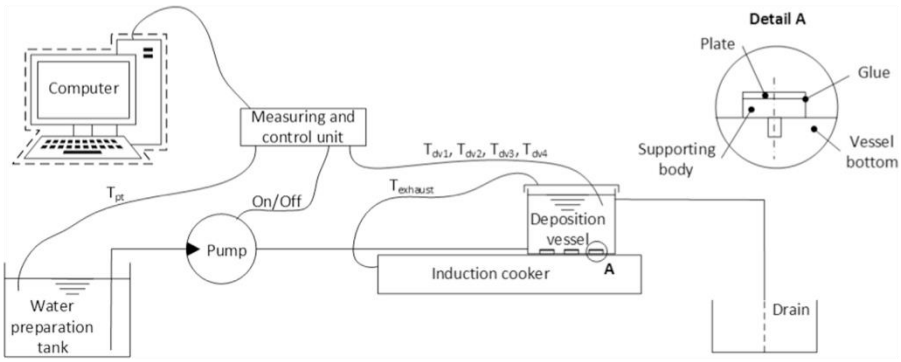


Fig. 1. Measuring station for deposition of scale with an enlarged detail of specimen (Detail A). After the scale deposition, the specimen was transferred to cavitation erosion test rig (Fig. 2).

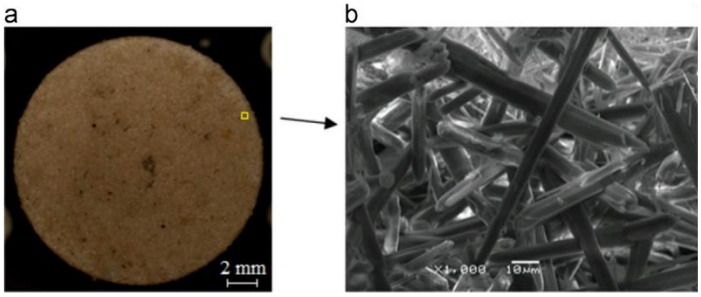


Fig. 2. Specimen 2 macro photography (a) and the SEM image of the scale microstructure (b). SEM image was taken in the region of interest marked by yellow square (gray in printed manuscript). The average length of aragonite sticks was 80 μm.

2.2. Scale removal by ultrasonic cavitation

In the final phase of our experiments, the specimens were transferred into a cavitation vessel (Fig. 3) of the ultrasonic homogenizer "VCX-750 Ultrasonic processor".

Each individual specimen was attached to the vessel bottom and immersed in distilled water at the ambient temperature (22 °C), then exposed to ultrasonic cavitation which was generated by a sonotrode (sonotrode tip 422-17 with diameter 3mm). The sonotrode was excited with a frequency of 20 kHz and was installed coaxially to the specimens, with a 7.5 mm axial clearance. The purpose of the sonotrode was to cause cavitation damage to the scale layer, thus removing it.

The development of cavitation damage is typically measured by weighing the specimen or counting cavitation pits [25]. However, these methods require drying of specimens, which was not acceptable in our case as the scale microstructure could be affected. A more appropriate method for cavitation erosion monitoring is by visualization of immersed scale specimens. Recently, Pečnik et al. [26] used high-speed camera imaging to investigate the cavitation erosion mechanism of scale specimens, but the specimen surface itself was not visible. The study in this paper, however, is focused on the scale microstructure, thus the macro photography of specimens was employed. Photos were taken before and after cavitation (sample image shown in Fig. 2a), as well as during the cavitation experiment at times specified in Table 3. SEM images were only taken after the end of the experiments.

In the range $t=0\ldots190$ s, sonotrode voltage was set to 20% of its nominal value, which resulted in root-mean-square (RMS) pressure of $p_{RMS}=1200$ Pa. After $t=190$ s, the sonotrode voltage was increased to 40% of the nominal value ($p_{RMS}=2900$ Pa) for additional 120 s. The p_{RMS} values were determined by computing the RMS value of instantaneous pressure measurements that were acquired by the hydrophone (Teledyne-Reson TC4103).

The imaging setup was identical for all the specimens in the experiment. It consisted of a camera Nikon D3100 with 36 mm spacers for macro photography and the lens Nikkor 50 mm F1:1.2. The focal distance was set at 1 m, shutter time at 0.004 s and aperture at f/16. The specimens were illuminated by the "Vega" collimated light source with macro adapter.

3. Results and discussions

3.1. Qualitative analysis

The process of calcium carbonate layer removal was investigated on 14 different specimens (Tables 2 and 3). In Fig. 4, temporal development of cavitation erosion damage to the scale layer is presented for all specimens in form of macro photos. Scale deposits can be seen as brighter areas of the specimen surfaces, while the dark areas mark the regions without scale, i.e. bare metallic surface.

It can be observed that the descaling process rate and spatial direction varies significantly between individual specimens. The largest effect of cavitation on scale removal can be seen for specimens No. 1, 6 and 9 where the surface was nearly free of scale after $t=310$ s. In the case of these specimens, the descaled area rose steadily until 190 s, when the amplitude of sonotrode-generated pressure pulsations was increased from 1200 Pa to 2900 Pa RMS value. As a result, the rate of scale erosion significantly increased – note a much larger increase in descaled area in the time interval $190\text{ s} < t < 310\text{ s}$ compared to the preceding and equally long interval $70\text{ s} < t < 190\text{ s}$. In fact, the increase in pressure amplitude intensified the cavitation erosion process on all specimens except for the specimen No. 14. This is likely due to the fact that the surface of the specimen No. 14 was relatively rough ($R_a=0.42$ μm) and contained less initial anomalies than other specimens. Descaling efficiency was also poor for specimens No. 2, 4 and 11, where the scale was only removed in areas weakened by the faults and voids which formed in the scale application process. On the other hand, the boundaries of the thicker, more uniform scale layer remained almost unaffected by the cavitation.

Regarding the cavitation erosion process, two different mechanisms were observed. In the case of specimens No. 5,7,8,10 and 13, scale was removed gradually by erosion of one deposit layer after another, until the metallic specimen surface was exposed. In some areas, instead of complete scale removal, only the upper layers were eroded while the harder underlying layers were only polished by the ultrasonic cavitation (Fig. 5).

Another important scale erosion mechanism (predominant for specimens No. 1–4, 6, 9, 11, 12 and 14) was formation of cracks followed by breaking free of larger scale regions, which, according to Heath et al [8], is the most likely cavitation erosion mechanism for brittle coatings. Under the action of liquid pressure pulsations, erosion leads to dislodging of partial grains, grains, and eventually whole grain clusters. Pressure pulsations along the exposed edges can be expected to result in shear and bending forces within the scale layers, causing larger grain clusters of scale to break away. The fact that in many cases, the scale surface suffered little erosion before eventually breaking up, suggests that the breakage mechanism is predominant for deposits with greater surface hardness. While the surface of such scale deposits is more resistant to thinning by cavitation erosion, the deposit structure is likely to be more brittle, especially if it is locally weakened by inhomogeneities in thickness or chemical composition.

Table 3
Temporal dependence of operating conditions.

Specimen photo no.	0	1	2	3	4	5
t (s)	0	10	30	70	190	310
p_{RMS} (Pa)	1200	1200	1200	1200	1200	2900
Spec. No.	1–14 (All)	1–14 (All)	1–14 (All)	1–14 (All)	1–14 (All)	1,5,6,9,10,14

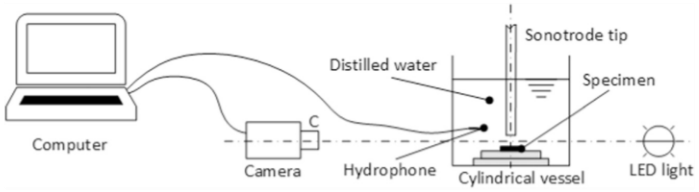


Fig. 3. Experimental setup for ultrasonic cavitation of specimens.

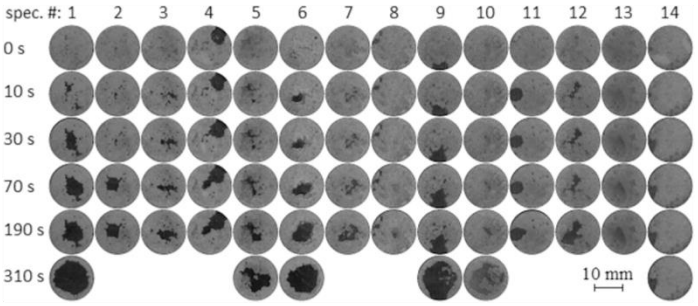


Fig. 4. Specimen macro photos. Horizontal axis: specimens No. 1–14, vertical axis: time from the start of cavitation.

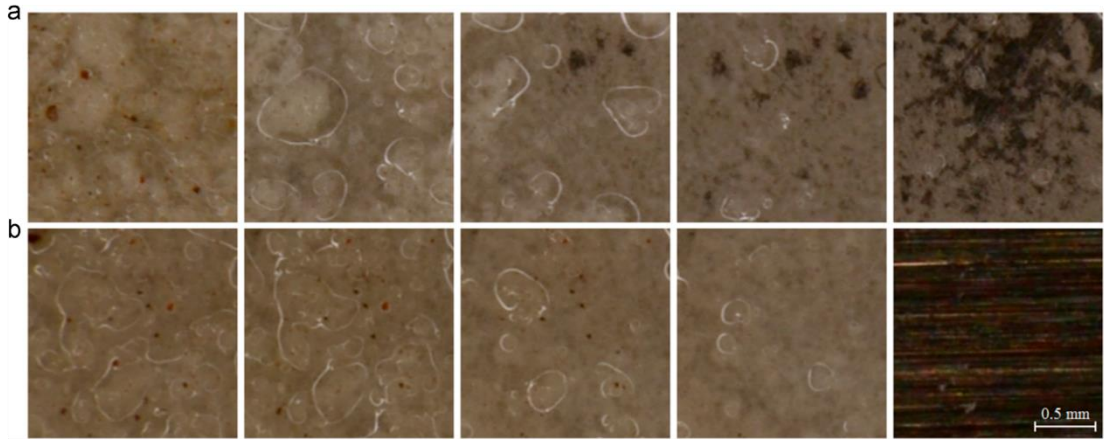


Fig. 5. Two different descaling mechanisms (shown are the 1.75 mm × 1.75 mm specimen segments); (a) layer-by-layer erosion (specimen No. 8); (b) erosion by layer breakage (specimen No. 9).

3.2. Scale removal efficiency

To assess the efficiency of scale (calcium carbonate) removal from the specimen surface, the area fraction of descaled surface E will be introduced as:

$$E = \frac{A_d}{\pi R^2} \tag{1}$$

In Eq. (1), A_d is the total descaled area of the specimen surface and R is the specimen radius. A_d was obtained by gray level thresholding combined with the low pass image filtering. Image regions with the normalized gray level $G < 0.25$ were classified as descaled surfaces (i.e. bare substrate surface), while the brighter regions ($0.25 \leq G \leq 1$) were assumed to represent the scale. This threshold was estimated as the arithmetic value of the mean gray levels of scaled ($G \approx 0.4$) and descaled ($G \approx 0.1$) areas, and was also verified by visual inspection of input grayscale images – consider Fig. 6 for sample image of descaled area. Due to the large contrast and relatively sharp borders between brighter scale regions and darker descaled regions, the A_d value calculated by Eq. (1) was not very sensitive to the G threshold.

Time dependence of E is shown in Figs. 7–9. Clearly, the descaled specimen area increases with time for all specimens, but the maximum E values vary significantly even for specimens with the same surface roughness R_a. After t = 190 s, the scale removal was most efficient for specimens No. 1 (R_a = 0.06 μm), No. 6 (R_a = 0.30 μm) and No. 9 (R_a = 0.42 μm), respectively. For all of these specimens, the micro fractures have developed early in the cavitation erosion process, and the predominant descaling mechanism was by breakage of the scale layer. On the other hand, scale removal on samples with predominant layer-by-layer erosion (i.e. samples No. 5, 7, 8, 10 and 13) was at least 50% slower, indicating a lower descaling efficiency of this mechanism. Also worth noting is a relatively high E value for specimens No. 4 and 9, which can be explained by the fact that the scale surface was already cracked and eroded at the beginning of the experiment (E (t = 0) = 12.5% and 6.8%, respectively). Therefore, these samples were more prone to cavitation damage.

In the case of specimens No. 1, 5, 6, 9, 10 and 14, acoustic cavitation was extended past t = 190 s, and the RMS value of pressure pulsations was increased from 1200 Pa to 2900 Pa. As a result, specimen surface was descaled much more rapidly, with an exception of specimen No. 14, which only experienced measurable erosion until t = 30 s.

The rate of substrate surface descaling, e, can be computed as the temporal derivative of E between selected times t_a and t_b:

$$e = \frac{E(t_b) - E(t_a)}{t_b - t_a} \tag{2}$$

Results presented in Fig. 10 suggest that the descaling rate increases with the RMS value of sonotrode pressure pulsations. In the time period between 190 s and 310 s, the descaling rate was approximately 3 times larger as for the first 190 s of the

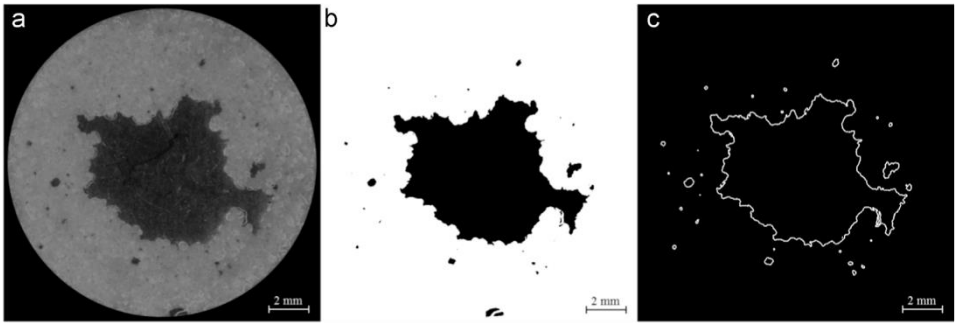


Fig. 6. Sample grayscale image (a) of specimen 1 at $t=190$ s; (b) binary image of descaled specimen area (black color); (c) edges of descaled area.

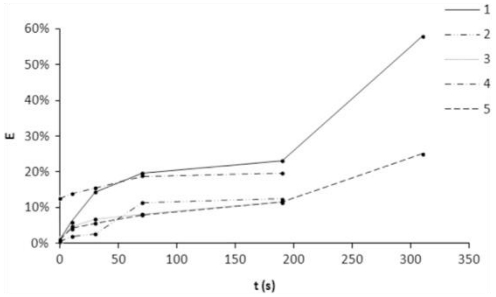


Fig. 7. Descaled surface fraction for specimens with R_a=.06 μm (specimens No. 1–5).

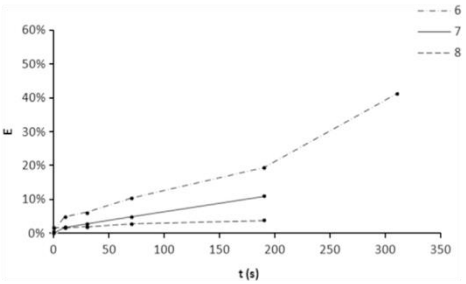


Fig. 8. Descaled surface fraction for specimens with R_a=0.30 μm (specimens No. 6–8).

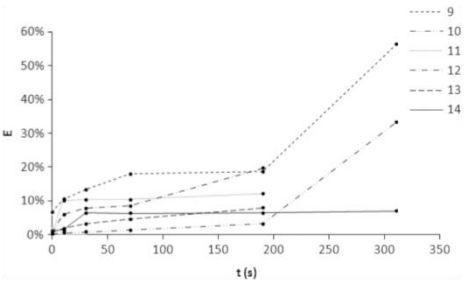


Fig. 9. Descaled surface fraction for specimens with R_a=0.42 μm (specimens No. 9–14).

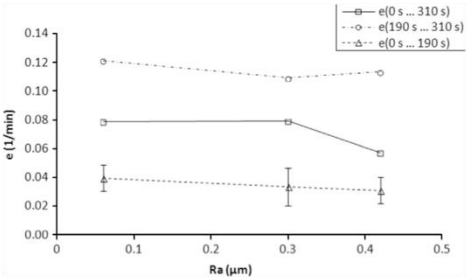


Fig. 10. Mean descaling rate of specimens in different time intervals. Due to the lack of data points after $t=190$ s, standard deviation error bars are only shown for the time interval 0 s…190 s.

experiment, while the corresponding ratio of p_{RMS} was 2.4. The observation that the descaling rate grows faster than the p_{RMS} ratio can be explained by the fact that a certain pressure amplitude threshold must be achieved above which the scale surface erosion can occur. The relatively high experimental data scatter (illustrated by error bars in Fig. 10) can be explained by the fact that the deposit surface of each specimen was unique in its microstructure, resulting in a slightly different temporal development of cavitation damage. The general trends are clearly visible, though.

Apart from the pressure amplitude, the substrate surface roughness (R_a) can also be seen to affect the descaling rate (e). Higher R_a values (i.e. rougher surfaces) reduce the rate and thus efficiency of scale removal as the scale deposits are more firmly attached to the substrate, which is in agreement with the findings of Keysar et al. [24]. Due to reduced cavitation erosion rate, longer times are needed for descaling.

3.3. Specimen edge analysis

In the previous subsection, the descaled specimen surface was characterized by its area. However, as shown in the qualitative analysis subsection, eroded surfaces can feature complex, non-circular geometries, and the surface shape may affect the erosion process. A good measure for the surface shape complexity is the ratio λ of the edge length L to the total area of eroded surface A_d – Eq. (3). Edge length was computed by measuring the length of edge curves. The latter were previously obtained from binary images using Sobel method in Matlab. Also consider Fig. 6c for a

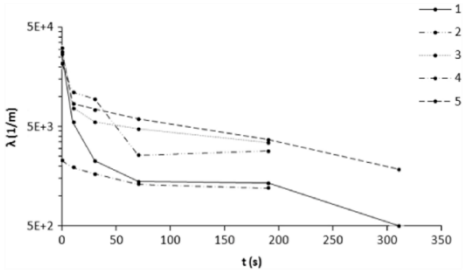


Fig. 11. Edge length to descaled area ratio for specimens with R_a=0.06 μm.

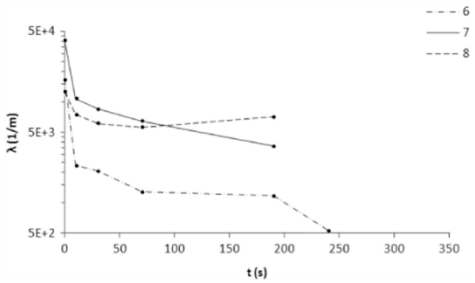


Fig. 12. Edge length to descaled area ratio for specimens with R_a=0.30 μm.

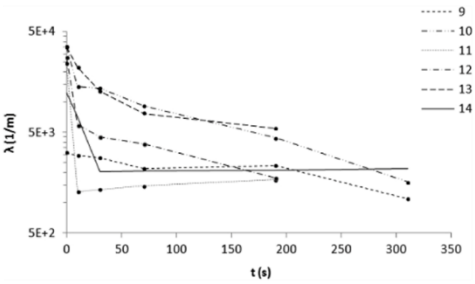


Fig. 13. Edge length to descaled area ratio for specimens with R_a=0.42 μm.

sample edge image.

$$\lambda = \frac{L}{A_d} \tag{3}$$

Figs. 11–13 present the diagrams of λ as a function of time. On all specimens, the highest λ values can be seen to occur immediately after the start of cavitation process when first erosion damage became visible. During the cavitation process, the calcium carbonate deposit is gradually eroded, resulting in both thinning and breakage of scale layers. Due to the erosion, the area of descaled surface increases while the local curvature of its edges decreases. As a result, the edge length to area ratio (λ) is decreased in time for most of the operating regimes used in our experiments.

Lower λ values, along with the reduction of local pressure amplitudes farther from the specimen center (and thus, the sonotrode tip) are likely the main reasons why the descaled surface fraction (E, Figs. 7–9) stabilizes after a certain time, i.e. until t=190 s. Nevertheless, if the amplitude of the pressure pulsations is increased (t > 190 s), the descaling rate increases again and λ resumes to decrease. This again indicates a significant effect of the pressure pulsation amplitude on the scale erosion process.

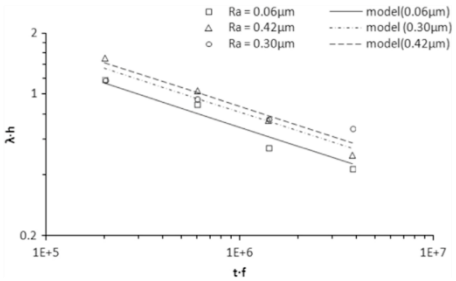


Fig. 14. Multiple regression model for λ. Data points shown are averages for all specimens with the same surface roughness analyzed at a particular time t.

Based on the experimental data, a dimensionless regression model for λ can be proposed assuming the following power law relation:

$$\lambda \cdot h = a_0 (t \cdot f)^{a_1} \left(\frac{R_a}{h}\right)^{a_2} \tag{4}$$

By using a linearized form of Eq. (4) with the least-squares fitting method, we obtain a_0=149, a_1=−0.311, a_2=0.121 and a high coefficient of determination (R^2=0.963). This regression model (see also Fig. 14) suggests that λ decreases with time regardless of the cavitation erosion mechanism. A decrease in λ results in a reduction of the pressure-induced force per unit of edge length, which may partly contribute to a reduction of the descaling rate after a certain time.

4. Conclusions

In this paper, the mechanism of ultrasonic cavitation erosion on metallic specimens covered by calcium carbonate deposits was investigated. After the scale deposition process, the specimens were exposed to acoustic cavitation generated by a sonotrode.

Depending on the scale surface hardness and microstructure, as well as the substrate surface roughness, two different cavitation erosion mechanisms may evolve. If the scale surface is resistant to cracking, the scale layer is eroded gradually (layer by layer) and relatively slowly. The mechanism by breakage of larger scale areas from the specimen surface is predominant for more brittle scale deposits, especially if they contain a substantial amount of local inhomogeneities. Even for the substrate surface roughness as low as 0.3 μm, such scale deposits can be very difficult to remove if the layer is initially very homogeneous, as it is polished and thus further hardened rather than broken away. In such cases, the only efficient measure for scale destruction is to significantly increase the pressure amplitude of the ultrasonic cavitation generator.

With that said, a few measures can be proposed to improve the efficiency of scale deposit prevention and removal. First of all, the surface of heaters and other areas in industrial and household appliances where scale deposits are expected, should have a very fine surface finish (i.e. R_a < 0.1 μm) when possible. Furthermore, the scale deposition process should be controlled in such manner as to produce a relatively inhomogeneous layer. This measure would generate weak spots to induce the breakage mechanism as well as increase the active layer edge length per unit area, thus further intensifying the erosion process. One possible method to achieve this goal is by introducing intermittent ultrasonic cavitation into the liquid near exposed surfaces, which would prevent excessive scale deposition and simplify the cleaning (descaling) process.

References

[1] DOE, EnergySavers: Tips on Saving Money & Energy at Home, US Department of Energy, Office of Energy Efficiency and Renewable Energy (2011) 1–44 http://energy.gov/sites/prod/files/energy_savers.pdf (accessed at 27.02.16).

[2] MarketsandMarkets, Scale Inhibitors Market (2011–2016). ⟨www.marketsandmarkets.com/Market-Reports/water-treatment-342.html⟩, 2012 (accessed at 15.01.16).

[3] D. Hasson, H. Shemer, A. Sher, State of the art of friendly "green" scale control inhibitors: a review article, Ind. Eng. Chem. Res. 50 (12) (2011) 7601–7607.

[4] J.T. Hansen, G.E. Saxon, Improving condenser efficiency with innovative scale removal system technology, in: Proceedings of ASME 2004 Conference, 2004, pp. 19–23.

[5] B. Širok, M. Dular, B. Stoffel, Cavitation, I2 Publishing, Ljubljana, Slovenia, 2006.

[6] C.E. Brennen, Cavitation and Bubble Dynamics, Oxford University Press, New York, Oxford, 1995.

[7] J. MacAdam, S.A. Parsons, Calcium carbonate scale formation and control, Rev. Environ. Sci. Biotechnol. 3 (2) (2004) 159–169.

[8] D. Heath, B. Širok, M. Hočevar, B. Pečnik, The use of the cavitation effect in the mitigation of $CaCO_3$ deposits, Stroj. vestnik – J. Mech. Eng. 59 (4) (2013) 203–215.

[9] A.W. Momber, Cavitation damage to geomaterials in a flowing system, J. Mater. Sci. 38 (4) (2003) 747–757.

[10] D. Grabco, N. Palistrant, O. Shikimaka, R. Zhitaru, V. Rahvalov, D. Zugravescu, Hardness and brittleness of rocks studied by microindentation in combination with the acoustic emission method, in: Proceedings of the 8th European Conference on Nondestructive Testing, 2002, pp. 17–21.

[11] E. Dalas, The effect of ultrasonic field on calcium carbonate scale formation, J. Cryst. Growth 222 (1–2) (2001) 287–292.

[12] W. Benzinger, U. Schygulla, M. Jager, K. Schubert, Anti fouling investigations with ultrasound in a micro-structured heat exchanger, in: Proceedings of the 6th International Heat Exchanger Fouling and Cleaning – Challenges and Opportunities Conference, 2005, pp. 197–201.

[13] H.X. Li, X.I. Huai, J. Cai, Q. Liang, Experimental research on antiscale and scale removal by ultrasonic cavitation, J. Therm. Sci. 18 (1) (2009) 65–73.

[14] N. Kazi, G.G. Duffy, X.D. Chen, Fouling and fouling mitigation on heated metal surfaces, Desalination 288 (2012) 126–134.

[15] A.J. Karabelas, Scale formation in tubular heat exchangers – research priorities, Int. J. Therm. Sci. 41 (7) (2002) 682–692.

[16] H. Elfil, H. Roques, Role of hydrate phases of calcium carbonate on the scaling phenomenon, Desalination 137 (1–3) (2001) 177–186.

[17] K.A. Mørch, Reflections on cavitation nuclei in water, Phys. Fluids 19 (7) (2007) 1–7.

[18] M.N. Davydov, V.K. Kedrinskii, Mathematical simulation of bubbly cluster and spall formation in a liquid at dynamic loading, in: Proceedings of the 5th International Symposium on Cavitation, Osaka, 2003.

[19] M. Dular, O. Coutier-Delgosha, M. Petkovšek, Observations of cavitation erosion pit formation, Ultrason. Sonochem. 20 (4) (2013) 1113–1120.

[20] M. Petkovšek, M. Dular, Simultaneous observation of cavitation structures and cavitation erosion, Wear 300 (1/2) (2013) 55–64.

[21] Gorenje, d.d., Velenje, Slovenia, IQcook. ⟨www.gorenje.com/iqcook/ww/⟩, (accessed at 04.01.16).

[22] L. Črepinšek-Lipuš, A. Hamler, I. Ban, B. Ačko, Permanent magnets for water-scale prevention, Adv. Prod. Eng. Manag. 10 (4) (2015) 209–216.

[23] K. Izumi, S. Takahashi, T. Sawa, Y. Ikenaga, Sludge deposition and scale formation on the surface of the heat transfer tubes in multi-stage flash evaporators, in: Proceedings of the 6th International Symposium on Fresh Water from the Sea, vol. 6, 1978, pp. 201–209.

[24] S. Keysar, R. Semiat, D. Hasson, Y. Yahalom, Effect of surface roughness on the morphology of calcite crystallizing on mild steel, J. Colloid Interface Sci. 162 (1994) 311–319.

[25] A. Osterman, B. Bachert, B. Širok, M. Dular, Time dependant measurements of cavitation damage, Wear 266 (9–10) (2009) 945–951.

[26] B. Pečnik, R. Šturm, M. Hočevar, M. Dular, B. Širok, Cavitation erosion of the calcium carbonate deposits, Int. J. Microstruct. Mater. Prop. (2016), in press http://dx.doi.org/10.1504/IJMMP.2015.074998.

6 Conclusions

In presented doctoral thesis, the effect of the ultrasonic cavitation on calcium carbonate-scaled metallic surfaces has been studied. The thesis has been divided into three main parts. In the introductory part, the literature was overviewed in the field of the ultrasonic cavitation effect on brittle crystalline materials such as the limescale. The following step was very time consuming, as it required the preparation and execution of experiments on two different experimental setups, namely for limescale deposition and for measurements of ultrasonic cavitation effects. In the third step, measurement results were analyzed to determine the correlation between ultrasonic excitation parameters and cavitation erosion effects on the surface of scale deposits.

According to set goals of the thesis, our findings can be summarized to following conclusions:

- On the basis of hydrophone measurements, high-speed camera image analysis, and subsequent computer-aided calculation of pressure pulsations (own open-source software *ADMflow*), a strong correlation has been determined between the flow velocity field and the pressure pulsations during the growth and collapse of cavitation structures. Consequently, our method can be used for non-contact analysis of pressure and velocity conditions in various engineering applications.
- Cavitation erosion intensity has been determined to be proportional to the intensity of pressure fluctuations, generated under the sonotrode.
- A reduction in the roughness of metallic surfaces coated by limescale deposits can increase cavitation erosion effects and thus intensify the scale removal process. It is therefore recommended to keep the surface roughness of elements exposed to scale formations (heaters, critical areas in industrial systems and household appliances) below $R_a = 0.1$ μm whenever possible.
- Scale destruction mechanism is largely dependent on the microstructure of the scale deposit. Local inhomogeneities may intensify the rate of scale erosion.
- Scale deposits can, depending on their surface hardness, presence of local microstructure inhomogeneities and specimen's surface treatment, either be eroded layer by layer, or by breakage of larger scale areas. Regardless of the exact descaling mechanism, the edge length-to-area ratio of descaled surfaces decreases with time, leading to a gradual reduction of descaling efficiency.
- With that said, our research hypothesis has been fully confirmed.

6.1 Future Perspectives

As it was mentioned in the conclusions above, the scale deposition process should be controlled in such manner as to produce a relatively inhomogeneous scale layer. This measure would create weak spots to induce the breakage mechanism as well as increase the active layer edge length per unit area, thus further intensifying the erosion process. One possible method to achieve this goal would be by introducing intermittent ultrasonic cavitation into the liquid near exposed surfaces, which would already weaken the scale structure during the deposition phase and therefore simplify the cleaning (descaling) process. It is desirable to attain a descaling process in which the scale layer would be regularly periodically removed during the device operation, as this would prevent the deterioration of exposed surface functionality and consequent need for overhaul. It would certainly be reasonable to focus further research activites in this direction.

References

Andritsos, N., Karabelas, A. J., Koutsoukos, P. G. (1997). Morphology and Structure of $CaCO_3$ Scale Layers Formed under Isothermal Flow Conditions. *Langmuir*, vol. 13, p. 2873-2879. doi:10.1021/la960960s.

Heath, D., Širok, B., Hočevar, M., Pečnik, B. (2013). The Use of the Cavitation Effect in the Mitigation of $CaCO_3$ Deposits. *Strojniški vestnik - Journal of Mechanical Engineering,* 59(2013)4, 203-215. doi:10.5545/sv-jme.2012.732.

Pečnik, B., Šturm, R., Hočevar, M., Dular, M., Širok, B. (2015). Cavitation erosion of the calcium carbonate deposits. *Int. J. Microstructure and Materials Properties*, Vol. 10, Nos. 5/6. doi: 10.1504/IJMMP.2015.074998.

Pečnik, B., Hočevar, M., Širok, B., Bizjan, B. (2016). Scale deposit removal by means of ultrasonic cavitation. *Wear,* 356-357 (2016) 45-52. doi: 10.1016/j.wear.2016.03.012.

Bibliography

Publications Related to the Thesis

Journal Articles

Heath, D., Širok, B., Hočevar, M., Pečnik, B. (2013). The Use of the Cavitation Effect in the Mitigation of $CaCO_3$ Deposits. *Strojniški vestnik - Journal of Mechanical Engineering,* 59(2013)4, 203-215. doi:10.5545/sv-jme.2012.732.

Pečnik, B., Šturm, R., Hočevar, M., Dular, M., Širok, B. (2015). Cavitation erosion of the calcium carbonate deposits. *Int. J. Microstructure and Materials Properties*, Vol. 10, Nos. 5/6. doi: 10.1504/IJMMP.2015.074998.

Pečnik, B., Hočevar, M., Širok, B., Bizjan, B. (2016). Scale deposit removal by means of ultrasonic cavitation. *Wear,* 356-357 (2016) 45-52. doi: 10.1016/j.wear.2016.03.012.

Biluš, I., Lešnik, L., Bizjan, B., Širok, B., Dular, M., Pečnik, B. (2016). Non-contact Method for Analysis of Cavitating Flows. *Ultrasonics*, under review.

Conference Paper

Širok. B., Biluš. I., Podbevšek. D., Pečnik. B., Bizjan B. (2014). Eksperimentalna analiza ultrazvočno vzbujene kavitacije. *Kuhljevi dnevi 2014*, 14. September 2014, Ljubljana, Slovenia.

Biography

Boštjan Pečnik was born in 1971 in Slovenj Gradec, Slovenia. In 1995 he received the Bachelor of Science degree at the University of Ljubljana, Faculty of mechanical engineering. He has nearly 20 years of experience in the household appliances business in the field of R&D, product management and production. He was the Head of cooking appliances R&D in Gorenje Group from 1997 to 2002. From 2002 to 2003, he was the Head of R&D for small motorized appliances in BSH (Bosch und Siemens Haushaltsgeräte) in Nazarje, Slovenia. At the end of the year 2003, he once again joined the Gorenje Group and was the director of the Cooking appliances until 2006. Since 2006, he has been an Executive Director for R&D of the Gorenje Group.